KERNFORSCHUNGSANLAGE JÜLICH GmbH
Institut für Kernphysik

Application of the Quasiparticle-Random-Phase Approximation in the Region of the Semi-Magic Nucleus $^{146}_{64}Gd_{82}$

by
C. Conci

Jül - Spez - 241
January 1984
ISSN 0343-7639

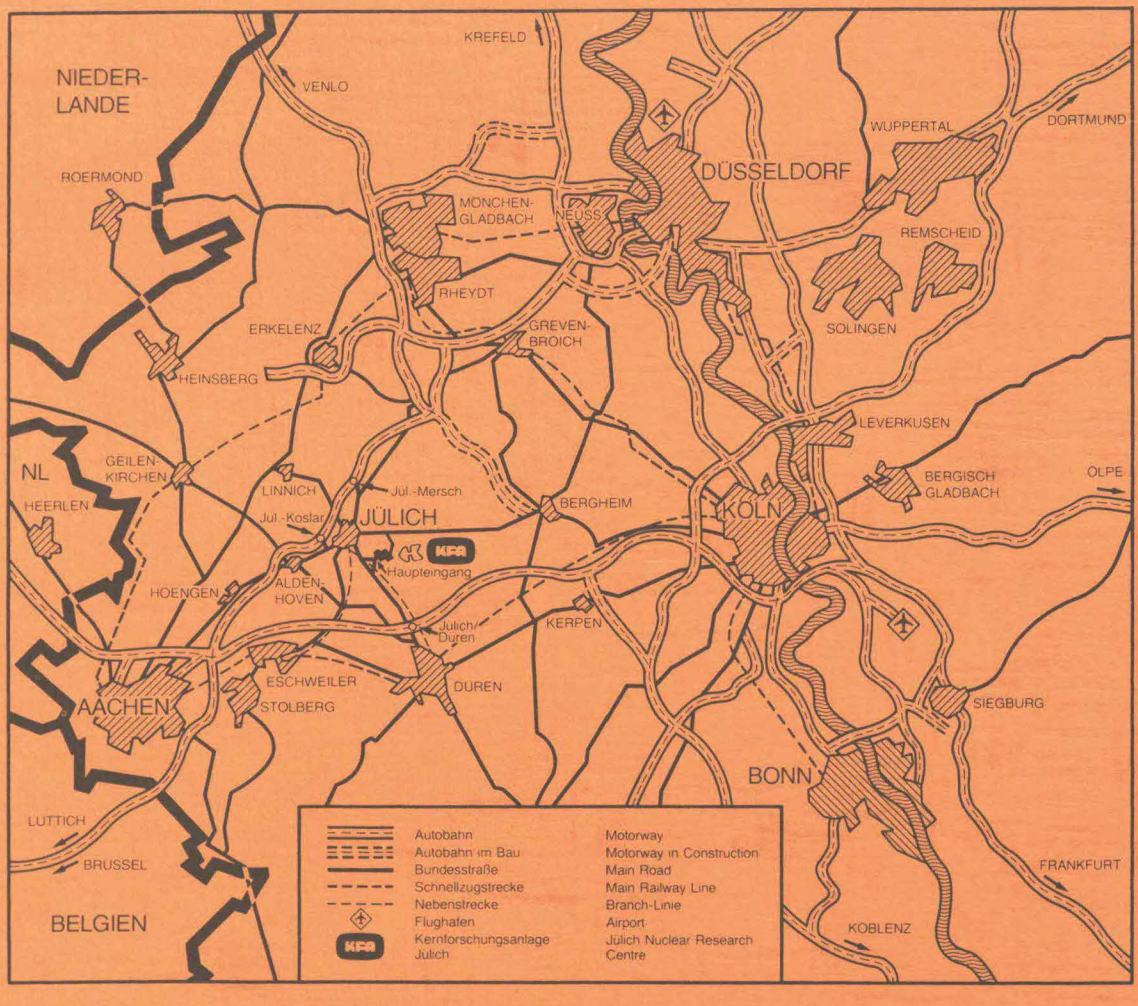

Als Manuskript gedruckt

Berichte der Kernforschungsanlage Jülich – Nr. 241
Institut für Kernphysik Jül-Spez-241

Zu beziehen durch: ZENTRALBIBLIOTHEK der Kernforschungsanlage Jülich GmbH
Postfach 1913 · D-5170 Jülich (Bundesrepublik Deutschland)
Telefon: 02461/610 · Telex: 833556-0 kf d

Application of the Quasiparticle-Random-Phase Approximation in the Region of the Semi-Magic Nucleus $^{146}_{64}Gd_{82}$

by

C. Conci

D 5 (Diss. Uni. Bonn)

Kurzfassung

Die spektroskopischen Eigenschaften der gerade-gerade Isotone mit N=82 und Z=60∿68, insbesondere des Kerns $^{146}_{64}Gd_{82}$, sind innerhalb der Quasiteilchen-Random-Phase-Näherung (QRPA) untersucht worden. Die effektive Teilchen-Loch- und Teilchen-Teilchen- Wechselwirkung werden getrennt betrachtet.

Sowohl in der QRPA- als auch in der BCS-Gleichung haben wir eine dichteabhängige Wechselwirkung der Reichweite Null benutzt.

Für die Teilchen-Loch-Kraft haben wir eine verallgemeinerte Wechselwirkung benutzt, die außer der Landau-Migdalschen Kraft auch explizit die Beiträge des Ein-Boson-Austauschpotentials enthält.

Da dieses die erste Arbeit ist, in der derartige Kräfte benutzt werden, um sowohl elektrische als auch magnetische Kerneigenschaften zu beschreiben, haben wir eine neue Kraftparametrisierung eingeführt. Um sicher zu gehen, daß unsere Parametrisierung in verschiedenen Regionen der Nuklidkarte gilt, haben wir dieselben Rechnungen auch für die Kerne ^{88}Sr und ^{90}Zr durchgeführt.

Dieses sind die ersten Rechnungen, die das ganze Niveauschema von ^{146}Gd bis zu 4 MeV, einschließlich sowohl vorwiegend kollektiver Niveaus als auch der mehr reinen Teilchen-Loch-Hochspin-Anregungen, reproduzieren können.

Innerhalb unseres Formalismus ist es möglich auch die Kerneigenschaften der N=82 gerade-gerade Isotone um ^{146} Gd zu berechnen. Die Resultate für ^{142}Nd, ^{144}Sm, ^{148}Dy und ^{150}Er zeigen eine gute Übereinstimmung mit den experimentellen Daten, jedoch weisen sie, im Gegensatz zu ^{146}Gd, bezüglich der gemessenen Zustände eine systematische Verschiebung der angeregten Niveaus zu höheren Energien auf. Dieser Effekt läßt sich durch die einfache Struktur der effektiven Teilchen-Teilchen-Wechselwirkung (dichteabhängige δ-Kraft) erklären.

Abstract

The spectroscopic properties of the even-even N=82 isotones with Z=60∿68, with special attention to the nucleus $^{146}_{64}Gd_{82}$, have been investigated in the framework of the Quasiparticle Random-Phase Approximation (QRPA). The particle-hole and the particle-particle effective interaction are considered separately.

In the QRPA- as well as in the BCS-equation we have used a density-dependent zero-range interaction. For the particle-hole force we have made use of a generalized interaction which includes, in addition to the zero-range terms of the Landau-Migdal force, also explicitly the contributions of the one-pion and one-rho exchange potential. This being the first work where this kind of force is used to describe both eletric and magnetic nuclear properties, it has been necessary to introduce a new parameterization of the force. To make sure that our parametrization is valid in different regions of the periodic table, we have performed the same kind of calculations also for the nuclei ^{88}Sr and ^{90}Zr. These are the first calculations which can reproduce simultaneously the full level scheme of ^{146}Gd up to 4 MeV including both predominantly collective levels as well as the more pure particle-hole excitations with higher spin.

Within our formalism it has been possible to calculate also the nuclear properties of the even-even N=82 isotones around ^{146}Gd. The results concerning ^{142}Nd, ^{144}Sm, ^{148}Dy and ^{150}Er show a good agreement with the experimental data, however they exhibit, unlike ^{146}Gd, a systematic upward shift of the excited levels with respect to the observed states. We ascribe this effect to the semplicity of our choice for the particle-particle interaction, which is a density-dependent δ-force.

TABLE OF CONTENTS

CHAPTER I

INTRODUCTION

In recent years there have been extensive investigations of the region around $^{146}_{64}Gd_{82}$ because of the apparent doubly-closed shell behaviour of this nucleus.

The first experimental works on ^{146}Gd and the neighbouring nuclei appeared at the beginning of the seventies (Kow72,Kri73), but they suggested the assignment of spin and parity 2^+ to the first excited state at 1579 keV, which led to wrong interpretations of the energy level spectra.

In the following years no special interest was focused on this region of the periodic table, but this changed intensely when P. Kleinheinz (Klz78a) established $J^\pi = 3^-$ for the first excited states, characterizing ^{146}Gd as the only doubly-even nucleus besides ^{208}Pb showing this feature. Furthermore it was found (Klz78b) that the 3^- level in ^{146}Gd has an unusually large E3 transition strength to the ground state, comparable to the corresponding value found in ^{208}Pb and indicating a strong collectivity. The subsequent identification of the first 2^+ state at 1971 keV (Oga78), i.e. 300 keV higher than in any other N=82 nucleus, was interpreted as spectroscopic evidence for a pronounced energy gap in the single-particle spectrum at Z=64 between the $2d_{5/2}$ and the $1h_{11/2}$ proton orbitals.

These conclusions have stimulated a series of systematic nuclear structure studies for the nuclei around ^{146}Gd. The data on the four one-valence-nucleon nuclei ^{145}Eu (Wil71), ^{145}Gd (Pak82), ^{147}Tb (Brd79,Nag81), and ^{147}Gd (Sty81, Pii82) are the principal sources of information on the single-particle energies above and below Z=64 and N=82. Studies of proton and neutron particle-hole excitations in ^{146}Gd (Klz79,Sty81) indicate that the proton and the neu-

tron gaps are about equally large (even though they are smaller than in ^{208}Pb). A number of additional recent experimental investigations of nuclei in the close vicinity of ^{146}Gd have now provided unusually complete nuclear structure information for this region. These new experimental results have greatly increased the interest in these nuclei and gave rise to intense theoretical studies of the nuclear region around Z=64 and N=82.

We give in the following a brief outline of the theoretical studies concerning the A ~ 146 mass region, and particularly the doubly-even nucleus ^{146}Gd.

In an early paper by Goodman (Goo79) it was pointed out that spherical Hartree-Fock-Bogoliubov (HFB) calculations performed for Z=64 and for N=82 even mass nuclei do not produce any proton shell closure in ^{146}Gd.

The same theory, i.e. the HFB theory, was used in (Plo79) to describe the high-spin non-collective configurations in the N=82 region. However, from these calculations only a description of the yrast levels with I $\geq$ 5 of the nucleus ^{146}Gd between 3 and 9 MeV is obtained, while the low-lying collective states cannot be described by this formalism.

In (Døs81) the yrast spectroscopy in the ^{146}Gd region is discussed in the framework of the deformed independent-particle model, with empirically based spherical single-particle energies and pairing correlations treated in the BCS-approximation. The results obtained for the high-spin yrast levels are good, but there are appreciable discrepancies between the measured and the calculated energies in the lower part of the yrast lines, which cannot be reproduced in detail within this model.

Similarly, recent calculations by Dudek et al. (Dud82) also give a satisfactory description of the high-spin states in ^{146}Gd. These calculations are per-

formed optimizing a Woods-Saxon single-particle potential and taking into account pairing correlations for protons.

Also Chasman has carried out a number of theoretical studies on nuclei in the ^{146}Gd region using the projected quasiparticle formalism. In a first paper (Cha80) the proton single-particle level spacings near Z=64 were deduced from the analysis of the low-lying levels in ^{145}Eu and of the ^{146}Gd proton particle-hole states, using the configuration assignment given in the original experimental work (Klz79). From these results high-spin states in ^{144}Sm, ^{146}Gd and ^{148}Dy have been calculated. Subsequently (Cha81,Cha82) also the neutron single-particle spectrum has been obtained and was used, together with the empirical proton single-particle energies, to calculate the excitation energies of aligned states in the Dy isotopes and of high-spin states in other nuclei in the A ~ 150 mass region. In a later work (Cha83) also excitation energies of spherical and deformed high-spin states in ^{147}Gd, E2 transition probabilities for several N=82 isotones as well as the 0^+ excited state spectra in ^{146}Gd and ^{144}Sm have been calculated.

Summarizing we can say that, from the theoretical point of view, there are up to now no calculations which can simultaneously encompass the full level scheme of the nucleus ^{146}Gd, including both the predominantly collective levels as well as the more pure particle-hole excitations with higher spin.

In this thesis we intend to study the spectroscopic properties, viz. the excitation energies and the electric and magnetic transition probabilities, of the spherical even-even N=82 isotones in the rare-earth region between mass numbers A = 142~150, paying particular attention to the nucleus $^{146}_{64}Gd_{82}$. We shall compare our results with the experimental data achieved in the last years. The theory we will use for this study is the Quasiparticle Random-Phase Approxima-

tion (QRPA), which gives the possibility to treat collective and non-collective states of closed subshell nuclei within the same framework. Our choice has been suggested by the fact that, even though there are some similarities between ^{146}Gd and the doubly-magic nucleus ^{208}Pb, there exists however a qualitative difference between them: while the Z=82 and N=126 energy gaps are large enough to make negligible the nuclear pairing effect, the Z=64 gap is significantly smaller and consequently a relatively strong effect of proton pairing is present in the nucleus ^{146}Gd. This is manifest already from the early (^{3}He,d) transfer studies (Wil71) and is discussed in more detail in (Klz79,Blo83a).

Using the well-known normal RPA-approximation, the vibrational excitations in Fermi systems, i.e. systems where the particles occupy the levels below the Fermi energy, while those above are empty, can be described as a superposition of elementary excitations of particle-hole character.

In the more refined theory of Finite Fermi Systems (FFS) (Mig67,Kle70,Spe77) instead of particles and holes one has to deal with quasiparticles and quasiholes (in the Migdal sense), i.e. particles and holes due to the interaction with the other particles and holes are surrounded by a polarization cloud. The resulting equations of motion are formally identical to the RPA, the interaction being replaced by an effective interaction which is assumed to be density-dependent.

In the case of semi-magic nuclei the elementary excitations, due to the smearing out of the Fermi surface, are no longer particles (holes) or quasiparticles (quasiholes) in the Migdal sense, but they are approximately a superposition of particle- and hole-type excitations, the Bogoliubov quasiparticles (Bog58a,Bog58b). The equations derived for this kind of systems are known as

QRPA-equations. They can be obtained either linearizing the equations of motion (Bar60,Bel65) or using the Green's function formalism (Bir68,Kam69). Recently Zawischa et al. (Zaw78) have shown how the QRPA-equations can be renormalized in the Landau-Migdal sense.

The ground state of a closed-subshell nucleus, for which the pairing effect plays a significant role, corresponds to the Bardeen-Cooper-Schrieffer (BCS) ground states and is characterized through the quasiparticle energies and the occupation probabilities of the single orbits.

We shall calculate the BCS-wave functions from a Woods-Saxon potential using a large single-particle basis and assuming pairing correlations between like nucleons only, because we consider single-closed-shell nuclei. The BCS-equations will be solved using a realistic pairing force like a density-dependent δ-force. The same force will be used as residual particle-particle interaction in the solution of the QRPA-equations.

As for the residual particle-hole interaction we will consider, in addition to a density-dependent zero-range force of Migdal type, also explicitly the finite-range contribution due to the one-pion and one-rho exchange potentials.

Up to now the finite-range force has been used only to describe magnetic properties of doubly-magic nuclei (Bäc80,Spe80,Wam80). We will apply it to the description of both electric and magnetic properties of semi-magic nuclei in the framework of the QRPA-theory.

We will first explain in Chapter II the formalism used to describe low-energy spectra of single-closed-shell nuclei, which consists in the application of the QRPA-theory after the solution of the BCS-equations.

In Chapter III we shall present the details of our calculations.

The results of the application of the QRPA-approximation on the study of the spectroscopic properties of the nucleus ^{146}Gd and of the neighbouring N=82 isotones ^{142}Nd, ^{144}Sm, ^{148}Dy and ^{150}Er will be the subject of Chapter IV. In the last part of this chapter the validity of the parametrization of the force, which is proposed for the first time in this work, will be checked for other two single-closed-shell nuclei, i.e. ^{88}Sr and ^{90}Zr.

The conclusions will follow in Chapter V.

CHAPTER II

FORMALISM

2.1 General remarks

In chapter I we have already pointed out the reason why the model we use to describe low energy spectra of single-closed shell nuclei is the QRPA. In the framework of this theory the correlations due to the short-range part of the nucleon-nucleon interaction, the so-called pairing correlations, which become very important when we move away from the closed shells, are taken into account approximately. In fact, the field produced by the pairing force in the BCS-theory plays a role completely analogous to the mean-field in the Hartree-Fock theory. Since there exist rather complete descriptions of the method of dealing with pairing correlations in nuclear systems (Bel59, Kis60, Kis63), we limit ourselves to a brief discussion of the procedure in order to define the various quantities we will use later on. Because we are going to consider single-closed shell nuclei, we take into account the pairing correlations between like nucleons only.

2.2 BCS-approximation

The ground state of an independent particle system, as in the nuclear shell model, corresponds to filling of the single-particle levels with a sharp cut-off at the Fermi energy.

In the presence of the pairing correlations some of the particles are excited from the occupied single-particle levels to the unoccupied ones. The ground state of such a system corresponds to a particle distribution which is contin-

uous across the Fermi surface, while in the normal systems there is a discontinuity (see Fig. 1). The change from a system of independent particles to one where the "new" particles, which we call "quasiparticles" and which are superpositions of particles and holes, is carried out using the Bogoliubov-Valatin transformation (Bog58a, Bog58b, Val58). Here one defines the quasiparticle creation and annihilation operators α^+_α, $\alpha_{\bar\alpha}$ in terms of the corresponding particle operators a^+_α, $a_{\bar\alpha}$:

$$\begin{pmatrix} \alpha^+_\alpha \\ \alpha_{\bar\alpha} \end{pmatrix} = \begin{pmatrix} u_\alpha & -v_\alpha \\ v_\alpha & u_\alpha \end{pmatrix} \begin{pmatrix} a^+_\alpha \\ a_{\bar\alpha} \end{pmatrix} \tag{2.1}$$

where v_α and u_α are real numbers and satisfy the relation:

$$v^2_\alpha + u^2_\alpha = 1 \ , \tag{2.2}$$

thereby preserving the Fermi anticommutation relations:

$$\begin{aligned} \{\alpha_\alpha, \alpha^+_\beta\} &= \delta_{\alpha\beta} \\ \{\alpha_\alpha, \alpha_\beta\} &= \{\alpha^+_\alpha, \alpha^+_\beta\} = 0 \end{aligned} \tag{2.3}$$

The index α indicates the state $|n_\alpha \ell_\alpha j_\alpha m_\alpha>$ and $\bar\alpha$ the time-reversed one:

$$|\bar\alpha> = (-)^{j_\alpha + m_\alpha} |n_\alpha \ell_\alpha j_\alpha -m_\alpha> \tag{2.4}$$

In our notation a Latin subscript (e.g., a) stands for all the quantum numbers of the corresponding Greek subscript (e.g., α), except the z-projection m_α of j_α.

The transition from a system of independent particles to a system of independent quasiparticles corresponds to a change from a system with fixed number of particle N to one where N is no longer a good quantum number. The ground state of the new system, the Bardeen-Cooper-Schrieffer (BCS) quasiparticle vacuum (Bad57), is expressed in terms of a product of quasiparticle states:

$$|BCS> = \prod_{\alpha>0} (u_\alpha + v_\alpha a^+_\alpha a^+_{\bar{\alpha}}) |0> \tag{2.5}$$

where $\alpha>0$ means that the product is carried out only for positive values of angular momentum projection m_α and $|0>$ indicates the bare particle vacuum.

In order to specify the BCS wave functions one needs to know the occupation probabilities v_α and u_α. They are determined by the two BCS-equations (Row70), that for spherical nuclei can be written in the following angular momentum coupled form:

$$\Delta_a = -\frac{1}{4} \sum_b \sqrt{\frac{2j_b+1}{2j_a+1}} F^{pair}_{aabb} \frac{\Delta_b}{\sqrt{(\varepsilon_b-\lambda)^2+\Delta_b^2}} \tag{2.6}$$

$$N = \frac{1}{2} \sum_b (2j_b+1) \left\{1 - \frac{(\varepsilon_b-\lambda)}{\sqrt{(\varepsilon_b-\lambda)^2+\Delta_b^2}}\right\} \tag{2.7}$$

Here λ is the chemical potential, j_a is the total angular momentum, ε_a is the single-particle (shell-model) energy, and Δ_a is the gap parameter. The energy of the quasiparticle is given as:

$$E_a = \sqrt{(\varepsilon_a-\lambda)^2 + \Delta_a^2} \tag{2.8}$$

The equations (2.6) and (2.7) have to be solved simultaneously and the iterative method we use for that is explained in Appendix A.

From the solutions λ and Δ_a, one obtains the occupation coefficients:

$$v_a^2 = \frac{1}{2}\left\{1 - \frac{(\varepsilon_a-\lambda)}{\sqrt{(\varepsilon_a-\lambda)^2+\Delta_a^2}}\right\} \qquad (2.9)$$

$$u_a^2 = \frac{1}{2}\left\{1 + \frac{(\varepsilon_a-\lambda)}{\sqrt{(\varepsilon_a-\lambda)^2+\Delta_a^2}}\right\}$$

These two equations can be combined to the relation:

$$v_a u_a = \frac{\Delta_a}{2E_a} \qquad (2.10)$$

2.3 Density matrix approach

The generalization of the RPA in which the pairing correlations are taken into account is called the quasiparticle RPA (QRPA). Here the elementary excitations of the nucleus are approximated by a superposition of two quasiparticle states.

The corresponding equations can be derived in different ways: Baranger (Bar60) linearized the equations of motion to obtain the QRPA. Birbrair (Bir68) and Kamerdzhiev (Kam69) used the Green's function formalism making explicit the difference between effective particle-particle and particle-hole interaction.

A brief outline of the Green's function formalism (Mig67,Bir68,Zaw78,Sch81) is given in Appendix B. It is shown there that, except for contributions from renormalization, the following transition density matrices result as solution of eigenvalue equations with the particle-particle and particle-hole amplitudes as interaction kernels (eq. (B.10) and Fig. 2):

$$X^{0\mu}_{\alpha\beta} = \langle A,0|a^{+}_{\beta}a_{\alpha}|A,\mu\rangle$$

$$X^{0\mu}_{\bar{\beta}\bar{\alpha}} = \langle A,0|a^{+}_{\bar{\alpha}}a_{\bar{\beta}}|A,\mu\rangle$$

$$\bar{\phi}^{0\mu}_{\alpha\bar{\beta}} = \langle A,0|a_{\bar{\beta}}a_{\alpha}|A+2,\mu\rangle \tilde{=} \langle A-2,0|a_{\bar{\beta}}a_{\alpha}|A,\mu\rangle \qquad (2.11)$$

$$\bar{\phi}^{0\mu}_{\bar{\alpha}\beta} = \langle A+2,0|a^{+}_{\beta}a^{+}_{\bar{\alpha}}|A,\mu\rangle \tilde{=} \langle A,0|a^{+}_{\beta}a^{+}_{\alpha}|A-2,\mu\rangle$$

The matrix elements of the effective particle-hole and particle-particle interaction which enter into eq. (B.10) are represented graphically in Fig. 3.

The matrix elements of the particle-hole interaction F^{ph} and of the particle-particle one F^{pp} are connected in the following way (Boh69, p. 374):

$$F^{ph}_{\alpha\beta\gamma\delta} \hat{=} F^{pp}_{\alpha\delta\beta\gamma} \qquad (2.12)$$

In Appendix C it is shown that using the symmetry properties of F^{ph} and F^{pp} (B.11)-(B.13) and the angular momentum algebra (Ros57), the equations (B.10) for the density matrices, written in the total angular momentum coupled representation, hold exactly the same form.

From now on we will omit the index J, introduced in Appendix C to indicate the total angular momentum coupled representation, by keeping in mind that we are working with coupled quantities.

2.4 Derivation of the QRPA-equations

The QRPA-equations can be simplified by the introduction of the following linear combinations of the density matrices:

$$X^{\pm}_{ab} = \frac{1}{2}\left(X^{0\mu}_{ab} \pm \bar{X}^{0\mu}_{ab}\right) \tag{2.13}$$

$$\phi^{\pm}_{ab} = \frac{1}{2}\left(\phi^{0\mu}_{ab} \pm \bar{\phi}^{0\mu}_{ab}\right) \tag{2.14}$$

where here and in the following all quantities are angular momentum coupled.

In the same way we introduce linear combinations of particle-hole matrix elements:

$$F^{\pm}_{abcd} = \frac{1}{2}\left(F^{ph}_{abcd} \pm (-)^{j_a+j_b+J+1} F^{ph}_{abdc}\right) \tag{2.15}$$

In addition we define:

$$n^{\pm}_{ab} = u_a v_b \pm v_a u_b \tag{2.16}$$

$$\xi^{\pm}_{ab} = u_a u_b \mp v_a v_b \tag{2.17}$$

The equations for the new amplitudes $X^{\pm}_{ab}$ and $\phi^{\pm}_{ab}$ follow from the corresponding equations (B.10) in straightforward way:

$$[(E_a+E_b)^2-\omega^2]X^{\pm}_{ab}$$

$$= -\sum_{c>d}\frac{2}{1+\delta_{cd}}\{(E_a+E_b)(\eta^{\pm}_{ab})^2 F^{ph\pm}_{abcd}X^{\pm}_{cd} + \omega\,\eta^{+}_{ab}\eta^{-}_{ab}F^{ph\mp}_{abcd}X^{\mp}_{cd} \qquad (2.18)$$

$$- (E_a+E_b)\eta^{\pm}_{ab}\xi^{\pm}_{ab}F^{pp}_{abcd}\phi^{\pm}_{cd} - \omega\,\eta^{\pm}_{ab}\xi^{\mp}_{ab}F^{pp}_{abcd}\phi^{\mp}_{cd}\}$$

$$[(E_a+E_b)^2-\omega^2]\phi^{\pm}_{ab}$$

$$= -\sum_{c>d}\frac{2}{1+\delta_{cd}}\{(E_a+E_b)(\xi^{\pm}_{ab})^2F^{pp}_{abcd}\phi^{\pm}_{cd} + \omega\,\xi^{+}_{ab}\xi^{-}_{ab}F^{pp}_{abcd}\phi^{\mp}_{cd} \qquad (2.19)$$

$$- (E_a+E_b)\eta^{\pm}_{ab}\xi^{\pm}_{ab}F^{ph\pm}_{abcd}X^{\pm}_{cd} - \omega\,\eta^{\mp}_{ab}\xi^{\pm}_{ab}F^{ph\mp}_{abcd}X^{\mp}_{cd}\}$$

Dividing eq. (2.18) by $\eta^{\pm}_{ab}\sqrt{1+\delta_{ab}}$ and eq. (2.19) by $\xi^{\pm}_{ab}\sqrt{1+\delta_{ab}}$, one can immediately see that the right hand sides of these equations are pairwise identical but opposite in sign. Therefore only one pair of those equations is independent.

It is convenient to introduce the amplitudes $Z^{\pm}_{ab}$ defined as:

$$Z^{\pm}_{ab} = \frac{X^{\pm}_{ab}}{\eta^{\pm}_{ab}\sqrt{1+\delta_{ab}}} = -\frac{\phi^{\pm}_{ab}}{\xi^{\pm}_{ab}\sqrt{1+\delta_{ab}}} \qquad (2.20)$$

At last we define the particle-hole and the particle-particle effective interactions as:

$$V^{\pm}_{abcd} = 2\,\frac{\eta^{\pm}_{ab}}{\sqrt{1+\delta_{ab}}}\,F^{ph\pm}_{abcd}\,\frac{\eta^{\pm}_{cd}}{\sqrt{1+\delta_{cd}}} \qquad (2.21)$$

$$G^{\pm}_{abcd} = 2 \frac{\xi^{\pm}_{ab}}{\sqrt{1+\delta_{ab}}} F^{pp}_{abcd} \frac{\xi^{\pm}_{cd}}{\sqrt{1+\delta_{cd}}} \tag{2.22}$$

Inserting the relations (2.20)-(2.22) in eq. (2.18), or (2.19) respectively, we obtain the QRPA equations in the usual form (Bir68,Zaw78):

$$(E_a+E_b)Z^{+}_{ab} + \sum_{c>d} (V^{+}_{abcd}+G^{+}_{abcd})Z^{+}_{cd} = \omega\, Z^{-}_{ab} \tag{2.23}$$

$$(E_a+E_b)Z^{-}_{ab} + \sum_{c>d} (V^{-}_{abcd}+G^{-}_{abcd})Z^{-}_{cd} = \omega\, Z^{+}_{ab} \tag{2.24}$$

The normalization condition for the eigenvectors Z^{+}_{ab} and Z^{-}_{ab}, solutions of eqs. (2.23) and (2.24) read (see Appendix D, eq. (D.8)):

$$2 \sum_{a>b} \{(Z^{J+}_{ab})^{*} Z^{J'-}_{ab} + (Z^{J-}_{ab})^{*} Z^{J'+}_{ab}\} = \delta_{JJ'} \tag{2.25}$$

CHAPTER III

NUMERICAL CALCULATIONS

3.1 Single-particle basis

The single-particle wave functions and the corresponding energies are deduced from a one-body potential of the Woods-Saxon type. This potential is composed of a spin-independent central term, a spin-orbit coupling one and, only for protons, a repulsive electrostatic potential V_{Coul}, generated from a uniform charge distribution with radius R_{Coul}:

$$V(r) = - \frac{V_o}{1+e^{(r-R_o)/\alpha_o}} - \lambda_{so} \frac{\hbar^2}{m^2c^2} \frac{\vec{\ell}\cdot\vec{s}}{2r} \frac{d}{dr} \left[\frac{1}{1+e^{(r-R_{so})/\alpha_{so}}}\right] + V_{Coul}(r) \qquad (3.1)$$

where V_{Coul} is defined as:

$$V_{Coul}(r) = \begin{cases} \frac{Ze^2}{2R_{Coul}} \left[3-\left(\frac{r}{R_{Coul}}\right)^2\right] & \text{for } r \leq R_{Coul} \\ \frac{Ze^2}{r} & \text{for } r > R_c \end{cases} \qquad (3.2)$$

V_o is the depth of the potential, α_o and α_{so} are the central and spin-orbit diffuseness parameters, R_o, R_{so} and R_{Coul} are the radii, m is the nucleon mass (average between proton and neutron) and λ_{so} is a positive dimensionless parameter, characterizing the strength of the spin-orbit coupling.

The potential (3.1) gives radial wave functions $R_{n\ell j}(r)$ which depend not only on the orbital angular momentum ℓ but also on the total angular momentum $j = \ell \pm 1/2$.

For numerical reasons we expand the eigenfunctions in terms of harmonic oscillator wave functions $R^{osc}_{n\ell}(r)$ (Blo59,Kle70):

$$R_{n\ell j}(r) = \sum_{m=1}^{M} a_m(n\ell j) R^{osc}_{m\ell}(r) \tag{3.3}$$

where $a_m(n\ell j)$ are the expansion coefficients and:

$$R^{osc}_{n\ell}(r) = \sqrt{\frac{2(n-1)!}{\Gamma(n+\ell+1/2)b^3}} \left(\frac{r}{b}\right)^{\ell} L^{\ell+1/2}_{n-1}\left(\frac{r^2}{b^2}\right) e^{-r^2/2b^2} \tag{3.4}$$

$$= \sqrt{\frac{2}{b^3}(n-1)!\Gamma(n+\ell+1/2)} \sum_{\nu=0}^{n-1} \frac{(-)^{\nu}(r/b)^{2\nu+\ell}}{\Gamma(\nu+\ell+3/2)\nu!(n-\nu-1)!} e^{-r^2/2b^2}$$

with $n = 1,2,3,\ldots$, where $b = \sqrt{\frac{\hbar}{m\omega}}$ is the oscillator constant, $L^{\ell+1/2}_{n-1}$ are the generalized Laguerre polynomials of order (n-1) and Γ the Gamma function.

The coefficients $a_m(n\ell j)$ are determined by diagonalizing the Woods-Saxon Hamiltonian in the oscillator basis. Since this Hamiltonian is already diagonal in ℓ and j, the problem decomposes in diagonalizations within the subspaces of the partial waves (ℓ,j):

$$\sum_{m'=1}^{M_\ell} \langle m\ell j | H_{WS} | m'\ell j \rangle a_{m'}(n\ell j) = \varepsilon_{n\ell j} a_m(n\ell j) \tag{3.5}$$

The dimension of the subspaces necessary for sufficient accuracy is found by comparing the approximate solutions (3.3) with the respective values of the "exact" solutions of the differential equations as e.g. given by Blomqvist and Wahlborn (Blo59).

It turns out that N=15 oscillator shells are sufficient for heavy nuclei (and corresponding fewer for light ones) determining the quantities M_ℓ by:

$$N = 2M_\ell + \ell - 1 \tag{3.6}$$

This method automatically provides also a discretization of the continuum. In (Blo59) the parameters of the potential (3.1) are chosen in order to reproduce the experimental single-particle spectra in the lead region as well as possible.

In the present calculations, once the values of the radii of the considered nucleus A have been "extrapolated" from those of ^{208}Pb using the relation:

$$R(A) = R(208)\ (\frac{A}{208})^{1/3} \tag{3.7}$$

the potential depths are fixed in such a way that the chemical potentials are reproduced.

The chemical potential $\lambda^{\pm}$ can be calculated from the experimentally known separation energies E_0 of the nucleus A and of its odd mass neighbouring nuclei, which are given in the Atomic Mass Table (Wap77), in the following way:

$$\begin{aligned} \lambda_k^+ &= E_0(A+1,K+1) - E_0(A,K) \\ \lambda_k^- &= E_0(A,K) - E_0(A-1,K-1) \end{aligned} \tag{3.8}$$

where the index k indicates proton or neutron and, correspondingly, K is Z or N.

The oscillator constant b is determined from the relation (Bru77):

$$b = 1.00\ A^{1/6}\ \text{fm} \tag{3.9}$$

For the nuclei we are going to consider, we give in Table 1 the values of the Woods-Saxon parameters and of the quantities $\lambda_k = \frac{1}{2}(\lambda_k^+ + \lambda_k^-)$.

For comparison we also show the corresponding values for ^{208}Pb used in (Rik78).

The model space we use in the present calculations includes single-particle levels of three shells above and below the Fermi energy.

The single-particle energies obtained from the Woods-Saxon diagonalization are given in Tables 2, 3, 4 respectively for ^{88}Sr, ^{90}Zr and ^{146}Gd. As far as possible, we use in the present calculation the experimental values.

3.2 The effective interaction

For the solution of the QRPA-equations (2.23) and (2.24) we need to specify the two-body residual interactions F^{ph} and F^{pp}. For F^{ph} we use a generalized particle-hole interaction which includes, in addition to the zero-range terms of the Landau-Migdal theory, also explicitly the contributions of the one-pion and one-rho exchange potential.

The density-dependent zero-range force of Migdal type has the following expression:

$$F^{ph}_{Mig}(\vec{r},\vec{r}') = C_0\{f_0(\rho)+f_0'(\rho)\vec{\tau}\cdot\vec{\tau}'+g_0(\rho)\vec{\sigma}\cdot\vec{\sigma}'+g_0'(\rho)\vec{\sigma}\cdot\vec{\sigma}'\ \vec{\tau}\cdot\vec{\tau}'\}\delta(\vec{r}-\vec{r}') \tag{3.10}$$

where $\vec{\sigma}$ and $\vec{\tau}$ are the spin and isospin operators for the nucleons. C_0 is the inverse of the density of states at the Fermi surface and makes dimensionless the parameters f_0, f_0', g_0 and g_0'. For a noninteracting Fermi gas one gets:

$$C_0 = \frac{\pi^2\hbar^2}{k_F m^*} = \frac{16}{9}\pi r_0^3 \varepsilon_F \text{ MeV fm}^3 \quad \text{with} \quad m^* = \frac{\hbar^2 k}{\partial\varepsilon(k)/\partial k}\Big|_{k=k_F} \tag{3.11}$$

Taking $r_0 = 1.2$ fm and $\varepsilon_F = 40$ MeV one obtains $C_0 = 386$ MeV fm^3. The density dependence of the force parameters is introduced to account for the finite size of the nucleus:

$$f(\rho(r)) = \frac{\rho(r)}{\rho(0)} f^{in} + \left[1 - \frac{\rho(r)}{\rho(0)}\right] f^{ex} \tag{3.12}$$

where $\rho(0)$ is the density at the center of the nucleus and:

$$\rho(r) = \frac{\rho(0)}{1+e^{(r-R)/\alpha}} \tag{3.13}$$

is the density distribution. The radius R and the diffuseness α are of the order of the nuclear radius and of the thickness of the nuclear surface. We take $\alpha = 0.60$ fm and $R = 1.2\ A^{1/3}$ fm.

The Migdal force has been widely and successfully used to calculate low-lying collective spectra within the framework of the RPA-theory (Rin74,Kle70,Spe77). In Table 5 we give the parameters which have been used by Rinker and Speth (Rik78). This force shows strong attraction outside the nucleus and is very weak inside. In this approach only the parameter f_0 depends on the density.

In connection with pion condensation Migdal (Mig74) suggested that the one-pion exchange potential should be included explicitly in the particle-hole an-

satz. Baym and Brown argued (Bay75) that one has to consider also the one-rho exchange potential in order to reduce the strong tensor force of the one-pion exchange.

The finite-range force has been used in the calculation of magnetic properties of nuclei (Spe80) and of isoscalar collective spin states (Wam80) and in the analysis of the Pauli principle sum rule for the Landau parameters (Bäc80).

In the momentum space the one-pion exchange potential is given as:

$$V_{OPEP}(q) = -\frac{4\pi f_\pi^2 \hbar^3}{m_\pi^2 c}\,\vec{\tau}\cdot\vec{\tau}'\,\frac{(\vec{\sigma}_1\cdot\vec{q})(\vec{\sigma}_2\cdot\vec{q})}{q^2+m_\pi^2} \tag{3.14}$$

where q is the momentum transfer, $m_\pi c^2$ =138 MeV is the pion mass and $f_\pi^2 = 0.08$ is the pion-nucleon coupling constant. For the reason mentioned above we also included the contribution due to the exchange of the ρ-meson:

$$V_\rho(q) = -\frac{4\pi f_\rho^2 \hbar^3}{m_\rho^2 c}\,\vec{\tau}\cdot\vec{\tau}'\,\frac{(\vec{\sigma}_1\times\vec{q})(\vec{\sigma}_2\times\vec{q})}{q^2+m_\rho^2} \tag{3.15}$$

with $m_\rho c^2$ = 770 MeV and $f_\rho^2 = 4.86$.

We give in Appendix E the complete expression of the particle-hole interaction F^{ph}, obtained by adding to the density-dependent zero-range force (3.10) the one-pion and one-rho exchange potential (3.14) and (3.15):

$$F^{ph} = F^{ph}_{Mig} + F_\pi + F_\rho \tag{3.16}$$

In the second line of Table 5 we give the set of parameters of the particle-hole force (E.15) used in the actual calculations. We postpone the discussion about them to section 4.3.

Analogously to the zero-range part of the particle-hole interaction, the particle-particle interaction F^{pp} is chosen as a density-dependent δ-force:

$$F^{pp}(\vec{r},\vec{r}') = C_0\, h(\rho)\, \frac{1-P^\sigma}{2}\, \delta(\vec{r}-\vec{r}') \qquad \text{for } T=1$$

$$F^{pp}(\vec{r},\vec{r}') = C_0\, g(\rho)\, \frac{1+P^\sigma}{2}\, \delta(\vec{r}-\vec{r}') \qquad \text{for } T=0 \tag{3.17}$$

where the T=0 case never occurs in our work and where $P^\sigma = \frac{1+\vec{\sigma}\cdot\vec{\sigma}'}{2}$ is the spin-exchange operator.

We choose for the force parameter $h(\rho)$ the same density-dependence as given in (3.12). The matrix elements of a δ-function interaction between particle-particle states are given in Appendix F. The choice of the force parameters h^{in} and h^{ex} will be discussed in the next paragraph.

3.3 Solution of the gap-equation with realistic forces

For solving the QRPA-equations (2.23) and (2.24) we also need the quasiparticle energies E_a and the occupation probabilities v_a and u_a. We have seen in section 2.2 that these quantities follow from the BCS-equations (2.6) and (2.7).

Usually the gap-equation has been solved using a schematic pairing force, the matrix elements of which are constant:

$$F^{pair}_{\alpha\bar{\alpha}\beta\bar{\beta}} = \frac{1}{4} \sum_{\alpha\beta} V^{as}_{\alpha\bar{\alpha}\beta\bar{\beta}}\, a^+_\alpha a^+_{\bar{\alpha}} a_{\bar{\beta}} a_\beta = -G \sum_{\alpha\beta} a^+_\alpha a^+_{\bar{\alpha}} a_{\bar{\beta}} a_\beta \tag{3.18}$$

where G is the so-called pairing constant.

The angular momentum coupled matrix elements are:

$$F^{pair}_{aabb} = -G\sqrt{(2j_a+1)(2j_b+1)} \tag{3.19}$$

and thereby eq. (2.6) gets the form:

$$\Delta = \frac{G}{4}\sum_b (2j_b+1)\frac{\Delta}{\sqrt{(\varepsilon_b-\lambda)^2+\Delta^2}} \tag{3.20}$$

Using this schematic force, the gap Δ is the same for all single-particle levels.

In the actual calculation, however, we use the density-dependent zero-range force defined in eq. (3.17). Since the matrix elements of F^{pair} are no longer constant, the solution of the system of eqs. (2.6) provides us with a gap Δ_a different for every single-particle level a.

The force parameters h^{in} and h^{ex} are fixed for the various regions of the periodic table in such a way that the calculated quasiparticle energies agree with the experimental ones. For comparison we also perform the calculations using the schematic pairing force (3.19). In Table 6 we give the values of the parameters h^{in} and h^{ex}, which we have chosen for our calculations and the corresponding values of the pairing constant G. The comparison between experimental values and calculated ones is done for the quantities $\delta_{p,n}$ obtained from the chemical potentials λ_k^+ and λ_k^- (3.8) in the following way:

$$\begin{aligned}\delta_p &= \lambda_p^+ - \lambda_p^- \\ \delta_n &= \lambda_n^+ - \lambda_n^-\end{aligned} \tag{3.21}$$

where p(n) stands for proton (neutron).

The gap-equation is solved in a model space which includes three shells below and three above the Fermi surface. The values we obtain for the gaps Δ_a and the corresponding quasiparticle energies $E_a = \sqrt{(\varepsilon_a-\lambda)^2+\Delta_a^2}$ are given for ^{88}Sr, ^{90}Zr and ^{146}Gd in Tables 7, 8, 9 and the comparison with the experimental values is shown in Figs. 4, 5, 6.

We used in the QRPA-equations the same particle-particle interaction as we used for the gap-equation. This guarantees that the spurious 0^+ states are at zero energy.

3.4 Transition probabilities

All the quantities which enter in the solution of the QRPA-equations (2.23) and (2.24) now are specified.

Rewriting those equations in the form (D.3):

$$C^+Z^+ = \omega Z^- \tag{3.22}$$

$$C^-Z^- = \omega Z^+ \tag{3.23}$$

one gets the final form:

$$(C^-C^+)Z^+ = \omega^2 Z^+ \tag{3.24}$$

The dimension of the matrix (C^-C^+) is determined by the number of two-quasiparticle configurations, which is the sum of the particle-hole, particle-par-

ticle and hole-hole configurations, that contribute to the excited state J^{π}. It is obvious that one gets very large dimensions (for the 2^+ in ^{146}Gd they are: 322x322). As the particle-particle and the hole-hole pairs are important only close to the Fermi energy, we reduce the dimensions by neglecting all the particle-particle and hole-hole configurations which have two-quasiparticle energy $(E_a+E_b) > 10$ MeV (for the 2^+ in ^{146}Gd the dimensions become 170x170).

The diagonalization of the real matrix (C^-C^+) is carried out using a routine of the IMSL-library, which computes the eigenvalues ω^2 and the eigenvectors Z^+. Z^- can be immediately calculated using (3.22).

The reduced transition matrix elements of a one-body operator O^J is given by:

$$\langle J\|O^J\|0\rangle = - \sum_{a\geq b} \{(Z^+_{ab}+Z^-_{ab})^*+(-)^J(Z^+_{ab}-Z^-_{ab})^*\}(O^J)_{ab}(u_a v_b+\tau v_a u_b) \qquad (3.25)$$

The parameter τ is +1 for electric and -1 for magnetic operators.

The exact expressions of the single-particle matrix elements $(O^J)_{ab}$ for the electric and the magnetic case are given in Appendix G.

The total probability of a transition of multipolarity J follows as:

$$B(O^J;J\to 0) = \frac{1}{2J+1} |\langle J\|O^J\|0\rangle|^2 \qquad (3.26)$$

CHAPTER IV

RESULTS AND DISCUSSION

4.1 General remarks

In the first part of this chapter we will present the results obtained in the framework of the QRPA-theory for the nucleus $^{146}_{64}Gd_{82}$ and for the neighbouring even-even N=82 isotones $^{142}_{60}Nd$, $^{144}_{62}Sm$, $^{148}_{66}Dy$, $^{150}_{68}Er$.

We have already explained in Chapter I the reason why these nuclei have attracted great interest in the past years and why we address our attempts to them.

The calculations are carried out in the following way: first of all we choose the single-particle basis and the parameters of the pairing force as explained in sections 3.1 and 3.3. Then we solve the gap-equations (2.6) for the open shell nucleons (we are considering single-closed shell nuclei). This provides us with the quasiparticle energies, which, together with the particle-hole and the particle-particle effective interaction (see section 3.2), are the quantities we need for the QRPA-equations (2.23) and (2.24). The eigenvalue ω corresponds to the energy of the J^π excited state and the eigenvectors Z^+_{ab}, Z^-_{ab} are directly connected with the wave function of a given state J^π. Inserting them into eq. (3.25) we can calculate the electric and magnetic transition probability from the excited state J^π to the ground state.

The particle-hole force which we use in our calculation should be a "universal force", in the sense that the parameters should not change with the mass number A and the multipolarity of a given state, respectively.

The force parameters shown in Table 5 have been used for $^{146}_{64}Gd_{82}$, as well as for $^{88}_{38}Sr_{50}$ and $^{90}_{40}Zr_{50}$, which will be discussed in section 4.6.

Furthermore we have to mention that with the same force we have calculated also the properties of the low-lying states in ^{208}Pb. The fact that the corresponding results are quite satisfactory is an additional confirmation of the validity of our parametrization of the force.

4.2 On the choice of the empirical single-particle energies in the ^{146}Gd region

The calculated energies of low-lying collective states of a nucleus like ^{146}Gd are expected to be very sensitive to the unperturbed particle-hole energies. In magic nuclei the theoretical single-particle energies derived from a Woods-Saxon potential agree in general quite well with the experimental ones. In semi-magic nuclei, however, the situation is more complicated. Basically there are two main effects which have to be considered and which act in opposite directions.

First of all the relatively small energy gap between subshells enhances the importance of pairing effects (to demonstrate this is one of the main aims of this work). This leads to a widening of the shell gap, compared to a Woods-Saxon result.

Secondly, the relatively small shell gap leads to very low-lying collective states (e.g. 3^- and 2^+ in ^{146}Gd which are made up mainly by proton particle-hole configurations). These low-lying states of the even-even nucleus couple especially with the neutron particle and hole states of the neighbouring odd

mass nuclei, thereby lowering their respective energies. Therefore the neutron shell gap, which, because of the excellent shell closure (N=82) is very large in Woods-Saxon calculation (4.2 MeV), is reduced considerably. To calculate these effects in a fully consistent way is beyond the scope of the present work and would require the application of a much more sophisticated theory (as e.g. proposed in (Kle82)).

Qualitatively, however, it is clear that the combined effect of the pairing force and particle-(hole-) phonon coupling tends to make the proton and neutron gaps equal.

As a pragmatic choice, we decided to use calculated (Woods-Saxon plus BCS) values for the proton particle and hole energies near the Fermi energy. As we have discussed above, the quasiparticle energies based on these Woods-Saxon single-particle energies are in close agreement with the discovered quasiparticle energies in the odd-Z nuclei. For the neutrons we use partly empirical (as far as known and marked in Table 4) and partly calculated values. Our QRPA-results seem to justify our choice.

The empirical single-particle energies for the nucleus ^{146}Gd are given in Fig. 6 and Table 4 respectively for protons and neutrons. It may be useful to illustrate how they were derived from the experimental data.

One can obtain the magnitude of the Z=64 and N=82 energy gaps from the difference of the separation energies S_p and S_n (Klz79):

$$\delta_p = S_p(^{146}_{64}\mathrm{Gd}) - S_p(^{147}_{65}\mathrm{Tb}) = 3.38\ \mathrm{MeV} \qquad (4.1)$$

$$\delta_n = S_n(^{146}_{64}\mathrm{Gd}) - S_n(^{147}_{65}\mathrm{Gd}) = 3.68\ \mathrm{MeV} \qquad (4.2)$$

The separation energies which enter the previous relations are obtained from the ground state masses of the five relevant nuclei ^{145}Eu, ^{145,146,147}Gd and ^{147}Tb. Two of these masses, namely ^{145}Eu and ^{147}Gd, are known experimentally (Wap77), whereas the three other values have been extrapolated from mass formulas.

Recently Blomqvist et al. (Blo81, Blo83a) have derived the ground state masses of ^{146}Gd, ^{147,148}Tb, ^{148,149,150}Dy, ^{150,151,152}Er from a shell model analysis of high spin states in the very neutron deficient nuclei above ^{146}Gd.

Using these newly derived semiempirical values, the values of the energy gaps given in (4.1) and in (4.2) do not change very much.

Furthermore from β-decay studies of Tb isotopes, Styczen et al. (Sty81) have interpreted the 3423 keV 3^- level in ^{146}Gd as $\nu f_{7/2}\text{-}d_{3/2}^{-1}$, which is the lowest neutron particle-hole excitation in this nucleus.

Because its energy should be equal to the N=82 gap at Z=64, except for small contributions of collective or nucleon-nucleon interactions, they conclude that the N=82 single-particle energy gap has to be less than 4 MeV, in agreement with the value given in (4.2).

The single-particle energy separations above and below the gaps are taken as the experimental excitation energies in the four neighbouring odd-mass nuclei. These might differ from the true single-particle energies in cases where the observed levels are not pure single-particle states but rather quasiparticle states. The experimental information about the four odd mass nuclei around ^{146}Gd can be found in the following papers: ^{145}Eu (Wil71,Led78), ^{147}Tb (Brd79,Nag81), ^{145}Gd (Pak82) and ^{147}Gd (Klz79,Klz82,Pii82).

The empirical low-energy excitation spectra of these four nuclei are shown in Fig. 7. The predominantly single-particle levels are labelled.

The proton and neutron single-particle states corresponding to Z=64 and N=82 have been recently discussed from the theoretical point of view by Chasman in (Cha80,Cha81,Cha82).

4.3 On the parametrization of the (δ+π+ρ) particle-hole force

The results we will present and discuss in the remaining part of this chapter are obtained in the framework of the QRPA-theory using for the particle-particle interaction a density-dependent δ-force and a generalized particle-hole interaction which includes in addition to a density-dependent δ-force also the finite-range contribution due to the one-pion and one-rho exchange potentials (see section 3.2).

We give the parameters for the particle-particle interaction as discussed in section 3.3 in Table 6, and the set of parameters for the particle-hole interaction in Table 5.

At this point it is necessary to spend some words about the parametrization of the particle-hole force.

Up to now the finite-range force has been used only to describe magnetic properties of the nucleus (Bäc80,Spe80,Wam80) and therefore only the values of the spin-dependent parameters g_0 and g_0' have been determined.

In the first paper about meson-exchange potential applied to nuclear structure calculations (Spe80), the values used for g_0 and g_0' were:

$$g_0 = 0.70$$
$$g_0' = 0.75 \qquad (4.3)$$

Very recent Brueckner G-matrix calculations (Nak83) based on one-boson exchange potential give for the isoscalar spin-dependent parameter g_0 a value which is around 0.12.

Moreover in a study about the influence of the spin-dependent nuclear interaction on the recently identified 1^+ state in ^{208}Pb at 5.845 MeV, Toki et al. (Tok83) found that the isoscalar interaction strength would be in the range:

$$\frac{1}{7} g_0' < g_0 < \frac{1}{2} g_0' \qquad (4.4)$$

which is in agreement with the results of Nakayama et al. (Nak83).

In accordance with these findings, we choose the following values for the parameters g_0 and g_0':

$$g_0 = 0.1$$
$$g_0' = 0.7 \qquad (4.5)$$

Once the parameters g_0 and g_0' are fixed, we adjust the values of $(f_0^{in}-f_0^{ex})$ and of f_0^{ex} in order to reproduce the observed energies and transition probabilities of the 3^- and 2^+ first excited states in the nucleus ^{146}Gd which are discussed in the next paragraph. We obtained:

$$f_0^{ex} = -1.75$$
$$f_0^{in}-f_0^{ex} = 1.95 \qquad (4.6)$$

4.4 The nucleus $^{146}_{64}Gd_{82}$

In the nucleus ^{146}Gd fourteen protons are added to the closed proton case tin (Z=50) and they fill the $1g_{7/2}$ and $2d_{5/2}$ levels which differ only little in energy. The three remaining levels of the 50 Z<82 major shell, i.e. $1h_{11/2}$, $3s_{1/2}$ and $2d_{3/2}$, are separated from the previous two by an energy gap of ~ 3.4 MeV (see Fig. 6). For the neutrons the energy gap between the completely filled shell and the next empty one at N=82 is ~ 3.7 MeV (see Table 4).

Since the $\pi 1h_{11/2}$ level lies closer above the Z=64 gap than the neutron high-j levels above the N=82 gap, one expects that proton particle-hole excitations will form the yrast states of ^{146}Gd.

Moreover, observing the proton and the neutron energies in Fig. 6 and Table 4, one concludes that proton particle-hole excitations of the type $\pi 1h_{11/2}\text{-}2d_{5/2}^{-1}$ and $\pi 1h_{11/2}\text{-}1g_{7/2}^{-1}$ most likely give rise to the negative parity yrast levels up to J=9.

The measured ^{146}Gd yrast states are in full accordance with these expectations, and so are the calculations which we present in Table 10 and which we will discuss in the following.

At this point we have to emphasize once more that these are the first calculations which can reproduce simultaneously the full level scheme of ^{146}Gd up to ~ 4 MeV including both predominantly collective levels as well as the more particle-hole-like excitations with higher spin.

In the following we compare the experimental excitation energies and in three cases also the transition probabilities with our theoretical results. In all cases the agreement between theory and experiment is good.

We begin by discussing the first 3^- level and then continue upwards in Table 10. In two different measurements (Klz78b,Klz82) the half-life of the first 3^- level was found to be (1.06±0.12)ns and (1.06±0.06)ns, corresponding to an E3-transition probability of:

$$B(E3;3^- \rightarrow 0^+) = (4.7 \pm 0.2) \cdot 10^4 \ e^2 \ fm^6 \qquad (4.7)$$

The calculated B(E3) value, which we give in Table 10, corresponds to the inverse transition: $0^+ \rightarrow 3^-$ and therefore has to be divided by 2J+1 = 7, giving a value of $5.19 \times 10^4 \ e^2 fm^6$, which is in good agreement with the experimental result (4.7).

Transforming the B(E3) transition probability (4.7) into Weisskopf units, one obtains a value of (37±2)W.u., which is very close to that one obtained for the corresponding transition in ^{208}Pb (Spr83).

This fact indicates that, analogously to ^{208}Pb, the first 3^- state in ^{146}Gd is characterized by a strong collectivity. This is confirmed from our results of Table 10, where one can see that a mixture of many particle-hole excitations contributes to the $3^-_{(1)}$ state, as one expects for a collective vibration.

The main contribution is given from the proton particle-hole configuration $\pi 1h_{11/2}{}^{-2}d_{5/2}^{-1}$, with unperturbed energy ε_{2qp} = 3428 keV and amplitude X = 0.73, while the $\pi 1h_{11/2}{}^{-1}g_{7/2}^{-1}$ configuration, which is also nearby in energy (ε_{2qp} = 3658 keV) gives only a small contribution (X = 0.15), because it involves a spinflip process.

The second excited 3^- state, at 3423 keV, has been interpreted, in a ß-decay study of the Tb isotopes (Sty81), as the lowest neutron particle-hole excita-

tion. This is in accord with the calculated results which show that the main contribution to the $3^-_{(2)}$ is given from the $\nu 2f_{7/2}\text{-}3s^{-1}_{1/2}$ and $\nu 2f_{7/2}\text{-}2d^{-1}_{3/2}$ neutron particle-hole configurations.

The first 2^+ quadrupole excitation contains mostly proton particle-hole configurations of $(3s_{1/2}\text{-}2d^{-1}_{5/2})$ and $(2d_{3/2}\text{-}1g^{-1}_{9/2})$ character.

Although the calculation suggests that the largest individual amplitude arises from the $(\nu 2f_{7/2}\text{-}1h^{-1}_{11/2})$ neutron particle-hole excitation, which contributes 25 % to the state. Despite the high multiplicity of this configuration, this result is somewhat surprising, since the unperturbed $(\nu 2f_{7/2}\text{-}1h^{-1}_{11/2})$ energy lies ~ 1 MeV higher than the lowest proton particle-hole 2^+ excitations. Since, however, we include a pairing factor in the force for the protons (see eqs. (2.21) and (2.22)), their calculated contributions to the collective 2^+ state appear correspondingly reduced.

In addition, the calculations suggest that the two-hole configuration $(\pi 2d_{5/2})^{-2}$ gives a contribution of 12 % to this state.

In a $^{144}Sm(\alpha,2n)^{146}Gd$ in-beam γ-experiment, an upper limit of 10^{-12} sec has been placed on the half-life of the 1972 keV $2^+_{(1)}$ state (Oga78) by considering the stopping time of the recoiling Gd ions in Sm.

From the calculated B(E2)-value in Table 10 we get:

$$B(E2;2^+\rightarrow 0^+) = \frac{0.448\times 10^4}{5}\, e^2fm^4 = 0.896\times 10^3\, e^2fm^4 \qquad (4.8)$$

The corresponding decay rate per sec (Boh69, p. 382) is:

$$T(E2) = 1.22\times 10^9 \times 1.97^5 \times 0.896\times 10^3/\text{sec} = 3.24\times 10^{-13}/\text{sec} \qquad (4.9)$$

and finally the half-life:

$$T_{1/2} = \frac{\ell n 2}{T(E2)} = 0.2\times10^{-13} \text{ sec} \qquad (4.10)$$

which is in agreement with the upper limit given above.

In a recent experimental (p,t) study on pairing monopole and quadrupole vibrations in the nuclei ^{146}Gd and ^{144}Sm (Fly83) a higher lying 2^+ level has been identified at 3378 keV. Since this reaction populates neutron two-particle-two-hole excitations, this level cannot be identified with any of the calculated 2^+ levels of Table 11.

Through the observation of the $E0(0^+_{(2)}\rightarrow 0^+_{(1)})$ transition following the reaction ^{144}Sm $(^3$He,n$)^{146}$Gd, Julin et al. (Jul80) established the existence of the $0^+_{(2)}$ state in ^{146}Gd at 2165(4) keV. The measured half-life 375(40)ps corresponds to a dimensionless monopole strength of 0.0122(13). The excitation energy we calculated for the first proton pairing vibrational monopole state is 2524 keV with a corresponding strength of 0.0117 in very good agreement with experiment.

The calculation gives the lowest, rather collective, 4^+ level at 2466 keV, with the dominant proton two-hole configuration $(\pi 2d_{5/2})^{-2}$. In experiment, a $J<4$ level has been observed (Fly83) at 2612 keV. This level could correspond to the calculated 4^+_1 state.

The following five calculated negative parity levels, 5^-, 7^-, 4^-, 6^- and $8^-_{(1)}$, are all predominantly members of the $(\pi 1h_{11/2}{}^{-2}d_{5/2}^{-1})$ configurations.

To the first one, the 5^- level, this configuration contributes 59 %. However, also many other configurations are significant.

For the other four levels the contribution of the $(\pi 1h_{11/2}\text{-}2d^{-1}_{5/2})$ configuration is larger than 85 % and the importance of the configuration mixing is much less than in the 5^- case.

The $8^-_{(2)}$ and the 9^- levels are the two highest-spin members of the $(\pi 1h_{11/2}\text{-}1g^{-1}_{7/2})$ proton particle-hole configuration. The results show that the $8^-_{(2)}$ is mixed with the close lying $8^-_{(1)}$, while the 9^- has a pure configuration, because no states with the same spin and parity are expected nearby.

Since there are no particle-hole configurations which can couple to J=10 and positive parity below 7 MeV, the observed 3865 keV 10^+ state is formed from the proton two-particle configuration $(\pi 1h_{11/2})^2$.

The configuration assignment for the ^{146}Gd high-spin states with seniority 2 proposed by our calculation agrees with those made originally (Klz79). However, as we have pointed out above, the present calculation is the first one which includes both the collective excitations as well as the states of higher spin which are more purely of two-quasiparticle character.

The schemes of Fig. 8 indicate that the calculated level sequence agrees with the experimental one up to 9^-, but the levels from 5^- up to 9^- lie 300-400 keV higher than the experimental ones. We argue that these energy shifts are due to the fact that in the present calculations the residual Coulomb interaction has not been included.

Recently, RPA-calculations have been performed for the low-energy spectrum of ^{208}Pb by taking into account the contribution of the Coulomb interaction (Co'83). Those calculations show that the Coulomb force leads to an attractive particle-hole interaction and that the order of magnitude of this effect can be estimated to be around 200-300 keV. The results obtained for ^{208}Pb indicate

also that for rather collective states the energy shift due to the Coulomb interaction is very small, because the full effect is spread out over all the particle-hole components.

Considering that the Coulomb interaction is proportional to R^{-1}, one can estimate for ^{146}Gd a value of 230-340 keV. Based on more qualitative considerations, a similar energy correction was taken into account in (Klz79). Applying the previous conclusions to the level scheme b of ^{146}Gd in Fig. 8, we see that the agreement with the experimental one improves significantly.

The situation is just the opposite for the $(\pi 1h_{11/2})^2$ two-particle 10^+ state, which turns out to lie lower than the experimental one.

In this case the Coulomb force is repulsive, because the main configuration is of particle-particle structure (Blo83b). Therefore this state will be pushed up above the 10^+ state, which is just the effect needed.

4.5 The neighbouring even-even nuclei ^{142}Nd, ^{144}Sm, ^{148}Dy and ^{150}Er

Within the formalism exposed in chapter II, it is possible to calculate also the spectroscopic properties of the even-even N=82 isotones around ^{146}Gd, changing only the proton number.

We only have to add or to take away two or four protons and to solve again the BCS- and the QRPA-equations (2.6), (2.7), (2.23) and (2.24) for the corresponding particle number.

In Fig. 9 it is shown how the occupation probabilities v^2 and the quasiparticle energies E change by increasing the proton number from Z=60 in

^{142}Nd to Z=68 in ^{150}Er for fixed neutron number N=82. Here we did not change the single-particle energies.

Our calculated quasiparticle energy sequences are in reasonable agreement with the sequence of the observed single-particle states in the odd-Z N=82 isotones (Wil71,Nag81). The quasiparticle level sequence, which in ^{142}Nd is $d_{5/2}$-$g_{7/2}$-$h_{11/2}$-$s_{1/2}$-$d_{3/2}$ is reversed in ^{150}Er to $s_{1/2}$-$h_{11/2}$-$d_{3/2}$-$d_{5/2}$-$g_{7/2}$. This can be interpreted as a support for the good closure of the Z=64 subshell.

The results obtained for the two- and four-proton-hole nuclei $^{144}_{62}Sm_{82}$ and $^{142}_{60}Nd_{82}$ and for the two- and four-proton-particle nuclei $^{148}_{66}Dy_{82}$ and $^{150}_{68}Er_{82}$ are given in Tables 12, 13, 14, 15.

The nuclei ^{142}Nd and ^{144}Sm have four and two protons less in the $2d_{5/2}$-$1g_{7/2}$ subshell with respect to the doubly closed nucleus ^{146}Gd. The main configurations which will contribute to the yrast levels are the proton two-hole configurations $(\pi 2d_{5/2})^{-2}$, $(\pi 1g_{7/2})^{-2}$ and $(\pi 2d_{5/2}\text{-}1g_{7/2})^{-2}$. In both nuclei they give rise to the sequence of positive parity states: 2^+, 4^+, 6^+. For these states the agreement with the experimental values taken from (Led78,Tul78, Pen79) is less than 300 keV. Again, as found in ^{146}Gd and discussed there, the largest contribution to the 2^+ states appears to be a neutron particle-hole excitation across N=82, which probably is not very realistic, but in the calculation arises from the reduction of the force due to pairing. For the states with negative parity the energy differences between the experimental values and the corresponding calculated ones are of the same order of magnitude.

In the ^{142}Nd the only negative parity state which has been measured experimentally is the 3^- at 2084 keV with a B(E3) value of 6.3×10^4 e^2fm^6 (Tul78). For

this state we calculate an energy of 2501 keV and a B(E3) value of 2.0×10^4 $e^2 fm^6$.

The sequence of negative parity states with spin 3 to 9 in ^{144}Sm, which has been investigated a few years ago (Pen79), is analogous to that one discussed in ^{146}Gd and is quite well reproduced in our calculations.

In both nuclei the proton monopole pairing vibration state $0^+_{(2)}$ is reproduced, particularly well in ^{144}Sm.

More than ten years ago Waroquier and Heyde (War71) performed shell-model calculations for the nuclei ^{142}Nd and ^{144}Sm using a surface delta interaction and a Gaussian force as residual interaction. Our calculated positive parity level energies are not vastly different from theirs. Of the negative parity states they calculate only the 3^-, find it however 1 MeV too high.

In contrast to these early calculations we have now also calculated the negative parity states up to $J^\pi = 9^-$ and find good agreement with experiment for those, including the 3^- octupole state.

A few years ago P. Daly et al. (Dal80) investigated the two proton nucleus $^{148}_{66}Dy_{82}$ by γ-ray and conversion electron measurement in (α,xn) and $(^{16}O,xn)$ reactions on enriched ^{152}Gd and ^{136}Ce targets and established the level scheme up to 4 MeV for this nucleus. Since the $1h_{11/2}$, $3s_{1/2}$ and $2d_{3/2}$ proton orbitals lie close together and are the only orbitals between the Z=64 and the Z=82 energy gaps, one expects that excitations involving the $\pi 1h_{11/2}$ level would form the complete sequence of the yrast states in ^{148}Dy.

Looking at the results given in Table 14, we can see that the $(\pi 1h_{11/2})^2$ two-particle configuration contributes to all the positive parity states 2^+, 4^+,

6^+, 8^+, 10^+, and that the 10^+ is the fully aligned $(\pi 1h_{11/2})^2$ state. As in ^{146}Gd, the main contribution to the 3^- originates from the $(\pi 1h_{11/2}\text{-}2d_{5/2}^{-1})$ configuration, which involves the promotion of a proton across the Z=64 gap. Because the Fermi surface in ^{148}Dy is shifted upwards with respect to ^{146}Gd, the 3^- level is expected higher in that nucleus than in ^{146}Gd; this trend is reproduced in our calculations.

For the ^{148}Dy 5^- and 7^- states Daly et al. (Dal80) have proposed, on account of their 150-300 keV lowered energies as compared to ^{146}Gd, that these ^{148}Dy levels are predominant two-particle states of $(\pi 1h_{11/2}\text{-}3s_{1/2})^2$ and $(\pi 1h_{11/2}\text{-}2d_{3/2})^2$ proton excitations. In our calculation these configurations also contribute to the ^{148}Dy 5^- and 7^- states, but in both cases the calculated main amplitude is still $(\pi 1h_{11/2}\text{-}2d_{5/2}^{-1})$, which is also reflected in the much more similar excitation energies calculated for Dy and Gd.

Very recently two different groups (Hel82,Nol82) have determined the yrast states of the nucleus $^{150}_{68}Er_{82}$ up to 3 MeV.

Based on the $(\pi h_{11/2})^2$ two-body matrix elements as observed in ^{148}Dy, the positive parity spectrum of ^{150}Er up to $J^\pi = 10^+$ has been described quite well in (Law81) as the sequence of the $(\pi 1h_{11/2})^4$ seniority two configuration. For these ν=2 states our theory is equally well applicable, without resorting directly to the measured ^{148}Dy level energies.

As one would expect, the 10^+ to 8^+ and 8^+ to 6^+ spacings agree well with experiment (and Lawson's empirical shell-model calculation), which is in accordance with the experience that the fully and nearly fully aligned members of a j^2 multiplet are well reproduced by a δ-force, as we use for the particle-particle interaction. On the other hand, we calculate the 10^+ to 2^+ and 10^+ to 0^+

spacings about 300 to 400 keV larger than experiment, which corresponds to an overestimated collectivity for these levels. This is again apparent from the 2^+ components listed in Table 15, where a possibly unrealistic neutron particle-hole contribution is significant.

We have seen that in ^{148}Dy the 3^- lies higher than in ^{146}Gd, because the Fermi surface is shifted upwards by adding two protons. This tendency continues in the four valence-proton nucleus ^{150}Er, where the octupole vibration has still a dominant $(\pi 1h_{11/2}\text{-}2d_{5/2}^{-1})$ component.

In the discussion about the nucleus ^{148}Dy it has already been remarked that the 5^- and the 7^- levels tend to change their structure with respect to ^{146}Gd. The increase of the $(\pi 1h_{11/2}\text{-}2d_{3/2})^2$ and $(\pi 1h_{11/2}\text{-}3s_{1/2})^2$ contributions to these levels in ^{150}Er expected for the further increase of the occupation probability, corresponding to four valence protons, is apparent from Table 15. In fact, it turns out that in ^{150}Er the main configuration which contributes to the 5^- is the two-particle excitation $(\pi 1h_{11/2}\text{-}3s_{1/2})^2$ and that of the 7^- state is the $(\pi 1h_{11/2}\text{-}2d_{3/2})^2$ one.

Looking at Fig. 10 we can have a complete overview of the results concerning the five N=82 isotones, which we have discussed on the previous pages, viz. $^{142}_{60}$Nd, $^{144}_{62}$Sm, $^{146}_{64}$Gd, $^{148}_{66}$Dy and $^{150}_{68}$Er. Apart from ^{146}Gd, where the agreement between the experimental and the theoretical values is very good (see section 4.4), one immediately observes that the calculated energy levels for all other nuclei lie systematically between 100 and 600 keV too high.

Our interpretation of this result is the following: In the nucleus ^{146}Gd the excitations are mainly of particle-hole type (see Table 10), while in the neighbouring nuclei, because of the added valence particles (or holes), the

main contributions to the excited states are of particle-particle (or hole-hole) character (see Tables 12, 13, 14 and 15). If one considers our choice for the nucleon-nucleon residual interaction (see section 3.2), one sees that, while for the particle-hole interaction we take into account, in addition to a density-dependent zero-range force, also the contributions of the one-pion and one-rho exchange potential, for the particle-particle interaction we use a much simpler force, viz. a density-dependent δ-force. The simplicity of our choice for the particle-particle interaction appears not to impair the results for ^{146}Gd because most of the states there are dominantly of particle-hole structure. The nuclei ^{142}Nd, ^{144}Sm, ^{148}Dy and ^{150}Er however seem to demand a more realistic particle-particle force to reproduce their level energies which are more strongly dominated by particle-particle configurations.

Another possible interpretation to explain why the calculated level energies are too high might be the presence of some kind of pre-deformation in the nuclei with 2 or 4 valence protons, which is of course not considered in our calculations.

This beginning of deformation would make the nucleus softer than the closed ^{146}Gd nucleus and thereby explain the lowering of the excitation energies. However up to now there seem to be no experimental indications of any kind of deformation effects for these even-even N=82 isotones.

4.6 The nuclei $^{88}_{38}Sr_{50}$ and $^{90}_{40}Zr_{50}$

In the first part of this chapter we have already explained that the QRPA-calculations performed for ^{88}Sr and ^{90}Zr have been carried out in order to reconsider the parametrization of the force given in Table 5, which has been pro-

posed for the first time in the present work and has been fitted to ^{146}Gd.

The nuclei ^{88}Sr and ^{90}Zr, which have been widely investigated both from experimental and from theoretical point of view (see (Koc75,Bun76,All72,Akk82) and references given there) show, as ^{146}Gd, the characteristic of semi-magicity.

In the following we will comment very briefly on the results concerning these two nuclei having a closed subshell for protons, respectively at Z=38 and Z=40, and a closed shell for neutrons at N=50.

The single-particle energies we used for them are given respectively in Table 2 and 3, and the solution of the BCS-equations in Table 7 and 8.

In ^{146}Gd the proton shell between Z=50 and Z=82 is only partially occupied and is given by four positive parity subshells $1g_{7/2}$, $2d_{5/2}$, $3s_{1/2}$ and $2d_{3/2}$, and by the $1h_{11/2}$ subshell which has negative parity and has the highest spin in this shell.

Analogously in ^{88}Sr and ^{90}Zr the partially occupied shell between Z=28 and Z=50 is made up by three negative parity states, $1f_{5/2}$, $2p_{3/2}$ and $2p_{1/2}$, and by the positive parity state $1g_{9/2}$.

Using the force given in Table 5 we reproduce very well the sequence of positive parity states in ^{90}Zr: 2^+, 4^+, 6^+ and 8^+, which are all components of the $(\pi 1g_{9/2})^2$ multiplet. The only particle-hole configuration which gives a large contribution to the first 2^+ state, whose calculated excitation energy is equal to 2234 keV (E_{exp} = 2187 keV), is the neutron $(\nu 2d_{5/2}\text{-}1g_{9/2}^{-1})$ excitation. The other main configurations which contribute to this state are mainly of two-particle (two-hole) type, e.g. $(\pi 1f_{5/2}^{-1}\text{-}2p_{1/2}^{-1})$, $(\pi 2p_{1/2}^{-1}\text{-}2p_{3/2}^{-1})$ and $(\pi 1g_{9/2})^2$.

This last characteristic is present also in the following two quadrupole excitations, which lie respectively at 3309 keV (E_{calc} = 3375 keV) and 3843 keV (E_{calc} = 3914 keV). Equally good results are obtained for the corresponding states in ^{88}Sr. For this nucleus also the experimental value of the $B(E2,0^+_{(1)}\rightarrow 2^+_{(1)}) = 0.114\times10^4\ e^2fm^4$ is available and it is very close to our calculated value of $0.132\times10^4\ e^2fm^4$.

From our calculations it turns out that the two low-lying negative parity states, the 5^- at 2319 keV and the 3^- at 2750 keV, in ^{90}Zr are both members of the $(\pi 1g_{9/2}\text{-}2p^{-1}_{3/2})$ proton configuration, which has a two-quasiparticle energy equal to 3754 keV. However the main contribution to the 5^- state is given by the $(\pi 1g_{9/2}\text{-}2p^{-1}_{1/2})$ configuration, which lies lower in energy (3195 keV) and which cannot couple to J=3, giving rise to the lowering of the 5^- with respect to the 3^-.

Finally we would like to comment on the 3486 keV 1^+ state in ^{88}Sr. From our calculations it turns out that this state is almost completely (~ 90 %) the proton spin-flip configuration $(\pi 2p_{1/2}\text{-}2p^{-1}_{3/2})$ with a small admixture (~ 9 %) of the $(\pi 1f_{5/2}\text{-}2p_{3/2})^{-2}$ two-hole configuration. In addition we obtain an excitation energy of 3361 keV and a $B(M1,0^+\rightarrow 1^+) = 0.32\ \mu_N^2$. This value is smaller than half the experimental value, which is equal to $0.92\pm0.15\ \mu_N^2$ (Met71).

We interpret the reduction of the theoretical B(M1)-value with respect to the experimental one as mainly due to the effect of the pairing coefficients $\gamma = (u_a v_b - v_a u_b)$, which enter the matrix elements of the magnetic multipole operator (3.25). The value of this coefficient for the main configuration $(\pi 2p_{1/2}\text{-}2p^{-1}_{3/2})$ can be easily calculated from the occupation probabilities given in Table 7, obtaining a value of 0.41. It means that the transition matrix element of the $(\pi 2p_{1/2}\text{-}2p^{-1}_{3/2})$ configuration is reduced by a factor of

0.41 and that the corresponding reduction of the B(M1) value is of the order of $0.41^2 = 0.17$. We check this assumption calculating the B(M1) value by taking into account only the particle-hole configuration $(\pi 2p_{1/2}\text{-}2p_{3/2}^{-1})$ for two different values of γ: 0.41 (with) and 1 (without pairing correlations). The obtained B(M1) values were respectively equal to 0.61 μ_N^2 and 3.56 μ_N^2, giving a reduction factor of exactly 0.17. This is only a rough estimate of the reduction effect due to the pairing coefficients, but the situation is much more complicated when we use the full configuration space.

Recently L.T. van der Bijl et al. (Bij82), discussing the electron scattering form factor of the 1^+ in ^{88}Sr, have reported that calculations performed in the two broken pair scheme give a B(M1) value equal to 1.91 μ_N^2, which is twice the experimental value. They argue that non-nucleonic degrees of freedom like Δ-hole polarization are needed to explain the reduction of the M1-strength at low q. Unfortunately we did not have the possibility to compare in detail our calculations with those quoted in (Bij82).

It is clear that the understanding of the structure of the 1^+ in ^{88}Sr requires a deeper analysis, but this is something which goes beyond the aim of this work.

4.7 Octupole vibration and pairing correlations

Before concluding the exposition of the work, we would like to discuss an important point concerning the calculation of the octupole vibrational state, and more in general of the collective states with negative parity (e.g. the 5^- level), in semi-magic nuclei.

In fact one of the difficulties encountered in carrying out our calculations was the failure to reproduce simultaneously the first 2^+ and 3^- levels in semi-magic nuclei. Once the energy and the B(E2) value of the 2^+ of ^{146}Gd was reproduced, the 3^- came out more than 1 MeV higher than the experimental level, with a too small B(E3) value.

Looking through the literature, we discovered that this problem does frequently arise, but it is never discussed in detail. In most of the studies on nuclear structure calculations for even-even semi-magic nuclei the problem is avoided by considering only positive parity states.

In those cases where both positive and negative parity states are considred, the calculations are carried out either using a force depending on the multipolarity, like the quadrupole-quadrupole and the octupole-octupole interaction, which then are adjusted separately (Yos62,Vej66), or considering a more universal force, like Migdal's force, but taking different values of the force parameters for different multipolarity (Bir70).

In shell-model calculations for the doubly even single-closed-shell nuclei with N=82, Waroquier et al. (War71) ascribed the too high energy of the 3^- level to the too small configuration space (they consider only one major oscillator shell).

We disagree with this conclusion because, even though using a very large configuration space (see Table 4), we obtain for the 3^- in ^{146}Gd an energy of 2747 keV, i.e. 1168 keV higher than the corresponding experimental value.

We will discuss in the following the origin of this limitation of the calculations and consider possible measures for improvement.

We give in Fig. 11 a schematic picture of the proton and neutron quasiparticle levels near the Fermi surface for the nucleus ^{146}Gd. One can immediately see that the only 0$\hbar\omega$ configuration which contributes strongly to the 3^- is the $(\pi 1h_{11/2}\text{-}2d_{5/2}^{-1})$. The $(\pi 1h_{11/2}\text{-}2g_{7/2}^{-1})$ configuration, which lies very close in energy, is disfavoured because of the spin-flip. All the other configurations which contribute to the collective 3^- level are of the type 1$\hbar\omega$, 2$\hbar\omega$ and higher (see discussion in section 4.4) and therefore they are less significant.

If one now considers the quantities which enter in the QRPA-equations (2.23) and (2.24), one can see that, besides the quasiparticle energies, there are the matrix elements of the particle-hole interaction $F^{ph^{\pm}}_{abcd}$, which are multiplied with the pairing coefficients $\gamma_1^{\pm} = (u_a v_b \pm v_a u_b)(u_c v_d \pm v_c u_d)$, and the particle-particle matrix elements F^{pp}_{abcd} with the factors $\gamma_2^{\pm} = (u_a u_b \mp v_a v_b)(u_c u_d \mp v_c v_d)$. In the diagonal case of $ab \equiv cd \equiv h_{11/2}\text{-}d_{5/2}^{-1}$ we have:

$$\gamma_1^+ = 0.998 \qquad \gamma_1^- = 0.465$$

$$\gamma_2^+ = 0.057 \qquad \gamma_2^- = 0.885 \tag{4.11}$$

It means that the matrix elements of the particle-hole interaction for configurations near the Fermi surface are cut in half due to the pairing coefficients. On the other hand one expects that the particle-particle force will be strong enough to compensate this reduction effect, as it happens for the 2^+.

Looking again at the results of Fig. 10, one can observe that the main configurations contributing to the 3^-, besides the $(\pi h_{11/2}\text{-}2d_{5/2}^{-1})$ are neutron par-

ticle-hole excitations, which are not affected by the particle-particle force, because the coefficients $\gamma_2^{\pm}$ vanish for pure particle-hole configuration.

For this reason the excitation energy of the 3^- turns out to be higher than the experimental value. The reduction of the matrix elements of the particle-hole force due to the pairing correlations can be corrected artificially by removing the smearing out of the proton Fermi surface, i.e. by taking:

$$\begin{aligned} u_a &= 0 \qquad v_a = 1 \quad \text{for hole-like states} \\ u_a &= 1 \qquad v_a = 0 \quad \text{for particle-like states} \end{aligned} \tag{4.12}$$

In this way we have brought down the energy of the 3^- in ^{146}Gd to the experimental value and we have reproduced also very well the B(E3) value (see section 4.4).

The same problem has earlier been recognized by Baranger in a paper about BCS-treatment of pairing correlations applied to heavy spherical nuclei (Bar60). He argued that in the case of a 3^- oscillation "pairing correlations are not so important here, because the large spacing between shells already plays the role of an energy gap. Then one can use the equations of section 3 (corresponding to our QRPA-equations), but set u equal 1 for a particle and to 0 for a hole".

CHAPTER V

CONCLUSIONS AND OUTLOOK

Motivated by the recent active research on the nucleus $^{146}_{64}Gd_{82}$ and on the nuclei of the surrounding region, we have investigated the spectroscopic properties, i.e. the excitation energies and the electric and magnetic transition probabilities, of the even-even N=82 isotones with Z = 60~68, paying special attention to the nucleus ^{146}Gd.

The calculations have been performed in the framework of the QRPA-theory, with a large single-particle configuration space obtained using a one-body potential of Woods-Saxon type and solving the BCS-equations only in the case of open shell nucleons.

The particle-hole and the particle-particle effective interaction are considered separately.

In the QRPA- as well as in the gap-equation we have used a density-dependent zero-range interaction. The corresponding strength has been determined by reproducing, after solving the BCS-equations, the experimental quasiparticle energies. In this way the spurious 0^+ states are obtained at zero energy.

For the particle-hole force we have made use of a generalized interaction which includes, in addition to the zero-range terms of the Landau-Migdal force, also explicitly the contributions of the one-pion and one-rho exchange potential. This being the first work where this kind of force is used to describe both electric and magnetic nuclear properties, it has been necessary to introduce a new parametrization of the force. For the isovector parameters our values are in agreement with earlier assignment. We have adjusted the values

of the isoscalar parameters in order to reproduce the observed energies and transition probabilities of the 3^- and 2^+ first excited states in the nucleus ^{146}Gd.

To make sure that our parametrization is valid in different regions of the periodic table, using the same force we have performed QRPA-calcualtions for other two semi-magic nuclei, i.e. ^{88}Sr and ^{90}Zr, as well as RPA-calculations for the low-energy levels of the doubly-magic nucleus ^{208}Pb.

We have to emphasize once more that these are the first calculations which can reproduce simultaneously the full level scheme of ^{146}Gd up to 4 MeV including both predominantly collective levels as well as the more pure particle-hole excitations with higher spin.

The results presented for the nucleus ^{146}Gd are in very good agreement with experiment.

Within our formalism it has been possible to calculate also the nuclear properties of the even-even N=82 isotones around ^{146}Gd, changing only the proton number. The results concerning the nuclei ^{142}Nd, ^{144}Sm, ^{148}Dy and ^{150}Er show a good agreement with the experimental data. However they exhibit, unlike ^{146}Gd, a systematic upward shift of the excited levels with respect to the observed states.

We ascribe this effect to the simplicity of our choice for the particle-particle interaction, which is a density-dependent δ-force.

This choice doesn't impair the results for ^{146}Gd, because here most of the states are dominantly of particle-hole structure. However, in the neighbouring nuclei, because of the added valence particles (or holes), the energy levels

are more strongly dominated by particle-particle (or hole-hole) configurations and therefore their description demands a more realistic particle-particle interaction.

The introduction of a finite-range term also in the particle-particle force will be one of the first tasks which we intend to face in the future.

Furthermore it seems that the method applied here can be extended, without requiring additional information, to the odd mass nuclei adjacent the closed ones, thereby giving the possibility to investigate more fully this region of the periodic table.

Appendix A

Scheme for the solution of the BCS-equations

In order to solve the BCS-equations (2.6) and (2.7):

$$\Delta_a = -\frac{1}{4}\sum_b \sqrt{\frac{2j_b+1}{2j_a+1}}\, F^{pair}_{aabb}\, \frac{\Delta_b}{\sqrt{(\varepsilon_b-\lambda)^2+\Delta_b^2}} \tag{2.6}$$

$$N = \sum_b (2j_b+1)v_b^2 = \frac{1}{2}\sum_b (2j_b+1)\left\{1 - \frac{(\varepsilon_b-\lambda)}{\sqrt{(\varepsilon_b-\lambda)^2+\Delta_b^2}}\right\} \tag{2.7}$$

with

$$v_a u_a = \frac{\Delta_a}{2\sqrt{(\varepsilon_a-\lambda)^2+\Delta_a^2}} \tag{2.10}$$

we start with the single-particle wave function ψ_a and the corresponding energy ε_a obtained from our Woods-Saxon diagonalization.

The initial values of v_a^2 and u_a^2 are estimated from the particle distribution of Fermi type:

$$v_a^2 = \frac{1}{1+e^{(\varepsilon_a+E_F)/\hbar\omega}} \tag{A.1}$$

$$u_a^2 = 1 - v_a^2$$

where E_F is the Fermi energy in the shell model single-particle basis. This permits us to calculate the initial value of Δ_a from (2.6) and (2.10):

$$\Delta_a = -\frac{1}{2}\sum_b \sqrt{\frac{2j_b+1}{2j_a+1}}\, F^{pair}_{aabb}\, u_b v_b \tag{A.2}$$

\fter this, the simultaneous solution of the gap-equation (2.6) and of the)article number equation (2.7) is carried out through two iterative processes:

|) with the initial value of Δ_a (A.2), N is calculated from (2.7) by varying the chemical potential λ, until N equals the particle number of the actual nucleus.

i) with the value of λ fixed in the previous step, we perform the iterative solution of (2.6).

With this aim we rewrite the system of equations (2.6) in terms of the new variables X_a defined as:

$$X_a = \frac{\Delta_a}{\sqrt{(\varepsilon_a-\lambda)^2+\Delta_a^2}} \tag{A.3}$$

By using the iterative method of Kantorowitsch (Col68, p. 25), we are left with the solution of a linear system of equation, whose solutions are the changes $\delta X_a^{(I)}$ of $X_a^{(I)}$ in the iteration step number I resulting in $X_a^{(I+1)} = X_a^{(I)} + \delta X_a^{(I)}$:

$$\sum_b A_{ab}^{(I)} Y_b^{(I)} = B_a^{(I)} \tag{A.4}$$

where

$$A_{ab}^{(I)} = \frac{|\varepsilon_b-\lambda|}{[1-(X_b^{(I)})^2]^{3/2}}\,\delta_{ba} + \frac{1}{4}\sqrt{\frac{2j_b+1}{2j_a+1}}\,F_{aabb}^{pair}$$

$$B_a^{(I)} = -\frac{|\varepsilon_a-\lambda|}{\sqrt{1-(X_a^{(I)})^2}}\,X_a^{(I)} - \frac{1}{4}\sum_b \sqrt{\frac{2j_b+1}{2j_a+1}}\,F_{aabb}^{pair}\,X_b^{(I)} \tag{A.5}$$

$$Y_b^{(I)} = \delta\, X_b^{(I)}$$

and δ_{ba} is the Kronecker symbol and (I) indicates the iteration number.

From (A.3) we obtain:

$$\Delta_a^{(I+1)} = \frac{(\varepsilon_a-\lambda)^2(\chi_a^{(I+1)})^2}{1-(\chi_a^{(I+1)})^2} \qquad (A.6)$$

at the end of every interaction I, new values of v_a^2 are calculated using the (A.6).

The iterative process is stopped when the following convergency condition is reached:

$$\frac{1}{N}\sum_b (2j_b+1)\left|(v_b^{(I+1)})^2 - (v_b^{(I)})^2\right| < \varepsilon \qquad (A.7)$$

where ε is a sufficiently small number.

Steps i) and ii) are repeated until one obtains stationary values for λ and Δ_a. Then the occupation probabilities v_a^2 are calculated using (2.9) and the quasiparticle energies are obtained from (2.8).

Appendix B

Green's function formalism for deriving the QRPA-equations

The one-particle Green's function is defined (Noz64,Fet71) in the following way:

$$G_{\alpha\beta}(t_\alpha,t_\beta) = -i\langle A,0|\,T\{a_\alpha(t_\alpha)a^+_\beta(t_\beta)\}\,|A,0\rangle \qquad (B.1)$$

where $a_\alpha(t_\alpha)$, $a^+_\beta(t_\beta)$ are the annihilation and creation operators in the Heisenberg representation, T is the Wick time-ordering operator and $|A,0\rangle$ is the exact ground state of the A-particle system.

The Fourier transform $G_{\alpha\beta}(\omega)$ of (B.1) is defined through:

$$G_{\alpha\beta}(t_\alpha,t_\beta) = \frac{1}{2\pi}\int_{-\infty}^{+\infty} d\omega\; e^{-i\omega(t_\alpha-t_\beta)}\; G_{\alpha\beta}(\omega) \qquad (B.2)$$

The Green's function for one-hole can be described as the time-reversed of the one-particle Green's function:

$$G_{\bar\beta\bar\alpha}(t_\alpha,t_\beta) = -i\langle A,0|\,T\{a_{\bar\beta}(t_\beta)a^+_{\bar\alpha}(t_\alpha)\}\,|A,0\rangle = i\langle A,0|\,T\{a^+_{\bar\alpha}(t_\alpha)a_{\bar\beta}(t_\beta)\}\,|A,0\rangle \qquad (B.3)$$

At this point one has to consider the fact that in superfluid nuclei the particle-particle interaction gives rise to the Cooper pairs, that means to bound states of two quasiparticles with zero total angular momentum. If an external field is applied to the system, the quasiparticle pairs with non-zero total angular momentum can form Cooper pairs, transferring their momentum to the external field. Therefore, besides the propagation of one particle and of one hole with a Cooper pair, described respectively by $G_{\alpha\beta}$ and $G_{\bar\beta\bar\alpha}$, one has to

take into account the process of creation and destruction of Cooper pairs in the external field. This is done by introducing the "anomalous" Green's functions $F_{\alpha\bar{\beta}}$ and $\bar{F}_{\bar{\alpha}\beta}$ (Gor58), which don't conserve the particle number:

$$F_{\alpha\bar{\beta}}(t_\alpha,t_\beta) = -i\langle A,0|T\{a_\alpha(t_\alpha)a_{\bar{\beta}}(t_\beta)\}|A+2,0\rangle \tag{B.4}$$

$$\bar{F}_{\bar{\alpha}\beta}(t_\alpha,t_\beta) = -i\langle A+2,0|T\{a^+_{\bar{\alpha}}(t_\alpha)a^+_\beta(t_\beta)\}|A,0\rangle \tag{B.5}$$

$F_{\alpha\bar{\beta}}$ describes a transition from the particle state to the hole plus Cooper pair state and $\bar{F}_{\bar{\alpha}\beta}$ the opposite one.

In analogy to normal systems (Spe77) we introduce the generalized Green's function $G^{0\mu}_{\alpha\beta}$:

$$G^{0\mu}_{\alpha\beta}(t_\alpha,t_\beta) = -i\langle A,0|t\{a_\alpha(t_\alpha)a^+_\beta(t_\beta)\}|A,\mu\rangle \tag{B.6}$$

and likewise for $G_{\bar{\beta}\bar{\alpha}}$, $F_{\alpha\bar{\beta}}$ and $\bar{F}_{\bar{\alpha}\beta}$, where $|A,\mu\rangle$ indicates the excited state μ of the A-nucleons system.

Performing the perturbative expansion (Noz64) of the generalized Green's functions considering both effective interactios, particle-particle F^{pp} and particle-hole F^{ph}, one obtains the following coupled system of equations (Zaw78):

$$G^{0\mu}_{\alpha\beta} = \frac{1}{2\pi i}\{G_{\alpha\alpha'}G_{\beta\beta'}\sum_{\gamma\delta}\int d\omega' F^{ph}_{\alpha'\delta\beta'\gamma}G^{0\mu}_{\gamma\delta} + F_{\alpha\bar{\alpha}}G_{\beta'\beta}\sum_{\gamma\delta}\int d\omega' F^{pp}_{\bar{\gamma}\delta\bar{\alpha}\beta'}\bar{F}^{0\mu}_{\bar{\gamma}\delta}$$

$$+ G_{\alpha\alpha'}\bar{F}_{\beta'\beta}\sum_{\gamma\delta}\int d\omega' F^{pp}_{\alpha\bar{\beta}\gamma\bar{\delta}}F^{0\mu}_{\gamma\bar{\delta}} - F_{\alpha\bar{\alpha}}\bar{F}_{\bar{\beta}\beta}\sum_{\gamma\delta}\int d\omega' F^{ph}_{\bar{\beta}\gamma\bar{\alpha}\delta}G^{0\mu}_{\bar{\delta}\bar{\gamma}}\} \tag{B.7}$$

$$G^{o\mu}_{\bar{\beta}\bar{\alpha}} = \frac{1}{2\pi i}\{G_{\bar{\beta}\bar{\beta}'}\, G_{\bar{\alpha}'\bar{\alpha}} \sum_{\gamma\delta} \int d\omega'\, F^{ph}_{\bar{\beta}'\bar{\gamma}\bar{\alpha}'\bar{\delta}}\, G^{o\mu}_{\bar{\delta}\bar{\gamma}} + G_{\beta\bar{\beta}}\, G_{\bar{\alpha}'\bar{\alpha}} \sum_{\gamma\delta} \int d\omega'\, F^{pp}_{\delta\bar{\gamma}\beta\bar{\alpha}'}\, \bar{F}_{\bar{\gamma}\delta}$$

$$+ G_{\bar{\beta}\bar{\beta}'}\, \bar{F}_{\bar{\alpha}\alpha} \sum_{\gamma\delta} \int d\omega'\, F^{pp}_{\bar{\beta}'\alpha\bar{\delta}\gamma}\, F^{o\mu}_{\gamma\bar{\delta}} - F_{\beta\bar{\beta}}\, \bar{F}_{\bar{\alpha}\alpha} \sum_{\gamma\delta} \int d\omega'\, F^{ph}_{\delta\alpha\gamma\beta}\, G^{o\mu}_{\gamma\delta}\}$$

$$F^{o\mu}_{\alpha\bar{\beta}} = \frac{1}{2\pi i}\{-G_{\alpha\alpha'} G_{\bar{\beta}\bar{\beta}'} \sum_{\gamma\delta} \int d\omega'\, F^{pp}_{\alpha'\bar{\beta}'\gamma\bar{\delta}}\, F^{o\mu}_{\gamma\bar{\delta}} + G_{\alpha\alpha'} F_{\beta\bar{\beta}} \sum_{\gamma\delta} \int d\omega'\, F^{ph}_{\alpha'\delta\beta\gamma}\, G^{o\mu}_{\gamma\delta}$$

$$+ F_{\alpha\bar{\alpha}}\, G_{\bar{\beta}\bar{\beta}'} \sum_{\gamma\delta} \int d\omega'\, F^{ph}_{\bar{\beta}'\bar{\gamma}\alpha\bar{\delta}}\, G^{o\mu}_{\bar{\delta}\bar{\gamma}} + F_{\alpha\bar{\alpha}}\, F_{\beta\bar{\beta}} \sum_{\gamma\delta} \int d\omega'\, F^{pp}_{\bar{\gamma}\delta\bar{\alpha}\beta}\, \bar{F}^{o\mu}_{\gamma\delta}\} \qquad \text{(B.7)}$$

$$\bar{F}^{o\mu}_{\bar{\alpha}\beta} = \frac{1}{2\pi i}\{-G_{\bar{\alpha}'\bar{\alpha}}\, G_{\beta'\beta} \sum_{\gamma\delta} \int d\omega'\, F^{pp}_{\bar{\gamma}\delta\bar{\alpha}'\beta'}\, \bar{F}^{o\mu}_{\bar{\gamma}\delta} + \bar{F}_{\bar{\alpha}\alpha}\, G_{\beta'\beta} \sum_{\gamma\delta} \int d\omega'\, F^{ph}_{\alpha\delta\beta'\gamma}\, G^{o\mu}_{\gamma\delta}$$

$$+ G_{\bar{\alpha}'\bar{\alpha}}\, \bar{F}_{\beta\bar{\beta}} \sum_{\gamma\delta} \int d\omega'\, F^{ph}_{\bar{\gamma}\bar{\beta}\bar{\delta}\bar{\alpha}'}\, G^{o\mu}_{\bar{\delta}\bar{\gamma}} + \bar{F}_{\bar{\alpha}\alpha}\, \bar{F}_{\bar{\beta}\beta} \sum_{\gamma\delta} \int d\omega'\, F^{pp}_{\alpha\bar{\beta}\gamma\bar{\delta}}\, F^{o\mu}_{\gamma\bar{\delta}}\}$$

The graphical representation of the system (B.7) using the usual Feynman rules is given in Fig. 2.

Expressing the transition matrix elements in terms of the generalized Green's functions as follows:

$$X^{o\mu}_{\alpha\beta} = -i\, G^{o\mu}_{\alpha\beta}(t_\alpha \to t_\beta) = \frac{1}{2\pi i} \int d\omega\, G^{o\mu}_{\alpha\beta}(\omega)$$

$$X^{o\mu}_{\bar{\beta}\bar{\alpha}} = -i\, G^{o\mu}_{\bar{\beta}\bar{\alpha}}(t_\alpha \to t_\beta) = \frac{1}{2\pi i} \int d\omega\, G^{o\mu}_{\bar{\beta}\bar{\alpha}}(\omega) \qquad \text{(B.8)}$$

$$\phi^{o\mu}_{\alpha\bar{\beta}} = -i\, F^{o\mu}_{\alpha\bar{\beta}}(t_\alpha \to t_\beta) = \frac{1}{2\pi i} \int d\omega\, F^{o\mu}_{\alpha\bar{\beta}}(\omega)$$

$$\bar{\phi}^{o\mu}_{\bar{\alpha}\beta} = -i\, \bar{F}^{o\mu}_{\bar{\alpha}\beta}(t_\alpha \to t_\beta) = \frac{1}{2\pi i} \int d\omega\, \bar{F}^{o\mu}_{\bar{\alpha}\beta}(\omega)\ , \qquad \text{(B.9)}$$

transforming the Green's functions into the Lehman's representation, taking their analytical expression given by Gor'kov (Gor58) and rewriting all the previous quantities for the operators defined in (2.1), one obtains finally the following system of equations for the quasiparticle density matrix elements (Zaw78,Sch81):

$$
\begin{aligned}
X^{0\mu}_{\alpha\beta} = - \sum_{\gamma\delta} \{ & \left(\frac{u^2_\alpha v^2_\beta}{E_\alpha + E_\beta - \omega} + \frac{u^2_\beta v^2_\alpha}{E_\alpha + E_\beta + \omega}\right) F^{ph}_{\alpha\beta\gamma\delta} X^{0\mu}_{\gamma\delta} \\
& + \frac{\Delta_\alpha}{2E_\alpha} \left(\frac{v^2_\beta}{E_\alpha + E_\beta - \omega} - \frac{u^2_\beta}{E_\alpha + E_\beta + \omega}\right) F^{pp}_{\bar{\gamma}\delta\bar{\alpha}\beta} \bar{\phi}^{0\mu}_{\bar{\gamma}\delta} \\
& - \frac{\Delta_\beta}{2E_\beta} \left(\frac{u^2_\alpha}{E_\alpha + E_\beta - \omega} - \frac{v^2_\alpha}{E_\alpha + E_\beta + \omega}\right) F^{pp}_{\alpha\bar{\beta}\gamma\bar{\delta}} \bar{\phi}^{0\mu}_{\gamma\bar{\delta}} \\
& + \frac{\Delta_\alpha \Delta_\beta}{4E_\alpha E_\beta} \left(\frac{1}{E_\alpha + E_\beta - \omega} + \frac{1}{E_\alpha + E_\beta + \omega}\right) F^{pp}_{\bar{\beta}\alpha\bar{\delta}\gamma} X^{0\mu}_{\bar{\delta}\bar{\gamma}} \} \\
X^{0\mu}_{\bar{\beta}\bar{\alpha}} = - \sum_{\gamma\delta} \{ & \left(\frac{u^2_\beta v^2_\alpha}{E_\alpha + E_\beta - \omega} + \frac{u^2_\alpha v^2_\beta}{E_\alpha + E_\beta + \omega}\right) F^{ph}_{\bar{\beta}\alpha\bar{\delta}\gamma} X^{0\mu}_{\bar{\delta}\bar{\gamma}} \\
& + \frac{\Delta_\beta}{2E_\beta} \left(\frac{v^2_\alpha}{E_\alpha + E_\beta - \omega} - \frac{u^2_\alpha}{E_\alpha + E_\beta + \omega}\right) F^{pp}_{\delta\bar{\gamma}\beta\bar{\alpha}} \bar{\phi}^{0\mu}_{\bar{\gamma}\delta} \\
& - \frac{\Delta_\alpha}{2E_\alpha} \left(\frac{u^2_\beta}{E_\alpha + E_\beta - \omega} - \frac{v^2_\beta}{E_\alpha + E_\beta + \omega}\right) F^{pp}_{\bar{\beta}\alpha\bar{\delta}\gamma} \phi^{0\mu}_{\gamma\bar{\delta}}
\end{aligned}
\qquad \text{(B.10)}
$$

$$+\frac{\Delta_\alpha\Delta_\beta}{4E_\alpha E_\beta}\left(\frac{1}{E_\alpha+E_\beta-\omega}+\frac{1}{E_\alpha+E_\beta+\omega}\right)F^{ph}_{\delta\gamma\beta\alpha}X^{o\mu}_{\gamma\delta}\Big\}$$

$$\phi^{o\mu}_{\alpha\bar{\beta}} = -\sum_{\gamma\delta}\Big\{\left(\frac{u^2_\alpha u^2_\beta}{E_\alpha+E_\beta-\omega}+\frac{v^2_\alpha v^2_\beta}{E_\alpha+E_\beta+\omega}\right)F^{pp}_{\alpha\bar{\beta}\gamma\bar{\delta}}\phi^{o\mu}_{\gamma\bar{\delta}}$$

$$-\frac{\Delta_\beta}{2E_\beta}\left(\frac{u^2_\alpha}{E_\alpha+E_\beta-\omega}-\frac{v^2_\alpha}{E_\alpha+E_\beta+\omega}\right)F^{ph}_{\alpha\beta\gamma\delta}X^{o\mu}_{\gamma\delta}$$

$$-\frac{\Delta_\alpha}{2E_\alpha}\left(\frac{u^2_\beta}{E_\alpha+E_\beta-\omega}-\frac{v^2_\beta}{E_\alpha+E_\beta+\omega}\right)F^{ph}_{\bar{\gamma}\bar{\delta}\bar{\alpha}\bar{\beta}}X^{o\mu}_{\bar{\delta}\bar{\gamma}}$$

$$-\frac{\Delta_\alpha\Delta_\beta}{4E_\alpha E_\beta}\left(\frac{1}{E_\alpha+E_\beta-\omega}+\frac{1}{E_\alpha+E_\beta+\omega}\right)F^{pp}_{\bar{\gamma}\delta\bar{\alpha}\beta}\bar{\phi}^{o\mu}_{\bar{\gamma}\delta}\Big\}$$

$$\bar{\phi}^{o\mu}_{\bar{\alpha}\beta} = -\sum_{\gamma\delta}\Big\{\left(\frac{v^2_\alpha v^2_\beta}{E_\alpha+E_\beta-\omega}+\frac{u^2_\alpha u^2_\beta}{E_\alpha+E_\beta+\omega}\right)F^{pp}_{\bar{\gamma}\delta\bar{\alpha}\beta}\bar{\phi}^{o\mu}_{\bar{\gamma}\delta}$$

$$+\frac{\Delta_\alpha}{2E_\alpha}\left(\frac{v^2_\beta}{E_\alpha+E_\beta-\omega}-\frac{u^2_\beta}{E_\alpha+E_\beta+\omega}\right)F^{ph}_{\alpha\beta\gamma\delta}X^{o\mu}_{\gamma\delta}$$

$$+\frac{\Delta_\beta}{2E_\beta}\left(\frac{v^2_\alpha}{E_\alpha+E_\beta-\omega}-\frac{u^2_\alpha}{E_\alpha+E_\beta+\omega}\right)F^{ph}_{\bar{\gamma}\bar{\delta}\bar{\alpha}\bar{\beta}}X^{o\mu}_{\bar{\delta}\bar{\gamma}}$$

$$-\frac{\Delta_\alpha\Delta_\beta}{4E_\alpha E_\beta}\left(\frac{1}{E_\alpha+E_\beta-\omega}+\frac{1}{E_\alpha+E_\beta+\omega}\right)F^{pp}_{\alpha\bar{\beta}\gamma\bar{\delta}}\phi^{o\mu}_{\gamma\bar{\delta}}\Big\} \qquad (B.10)$$

If the particle-particle interaction F^{pp} is Hermitian and invariant under time-reversal operation, the following relations are valid:

$$F^{pp}_{\bar{\alpha}\bar{\beta}\bar{\gamma}\bar{\delta}} = F^{pp}_{\gamma\delta\alpha\beta} \tag{B.11}$$

and

$$F^{pp}_{\alpha\beta\gamma\delta} = F^{pp}_{\beta\alpha\delta\gamma} \tag{B.12}$$

From the relations (2.12), (B.11) and (B.12) it follows immediately:

$$\begin{aligned} F^{ph}_{\alpha\beta\gamma\delta} &= F^{pp}_{\alpha\delta\beta\gamma} = F^{pp}_{\bar{\beta}\bar{\gamma}\bar{\alpha}\bar{\delta}} = F^{ph}_{\bar{\beta}\bar{\alpha}\bar{\delta}\bar{\gamma}} \\ F^{ph}_{\alpha\beta\gamma\delta} &= F^{pp}_{\bar{\beta}\bar{\gamma}\bar{\alpha}\bar{\delta}} = F^{pp}_{\bar{\gamma}\bar{\beta}\bar{\delta}\bar{\alpha}} = F^{ph}_{\bar{\gamma}\bar{\delta}\bar{\alpha}\bar{\beta}} \end{aligned} \tag{B.13}$$

Appendix C

Angular momentum coupling representation of the transition density matrices

Our intention in the following is to couple the equations given at the end of Appendix B to total angular momentum J.

In the jj-coupling scheme the particle-hole and the particle-particle coupling reads:

$$|ab^{-1},JM\rangle = \sum_{m_\alpha m_\beta} (-)^{j_\beta - m_\beta} \langle j_\alpha m_\alpha j_\beta -m_\beta | JM\rangle |\alpha\beta^{-1}\rangle$$

$$= \sum_{m_\alpha m_\beta} \langle j_\alpha m_\alpha j_\beta m_\beta | JM\rangle |\alpha\beta^{-1}\rangle \qquad (C.1)$$

$$|ab,JM\rangle = \frac{1}{\sqrt{1+\delta_{ab}}} \sum_{m_\alpha m_\beta} \langle j_\alpha m_\alpha j_\beta m_\beta | JM\rangle |\alpha\beta\rangle \qquad (C.2)$$

where M is the projection of the total angular momentum J and $|\alpha\beta^{-1}\rangle = a^+_\alpha a_\beta |0\rangle = a^+_{j_\alpha m_\alpha} a_{j_\beta m_\beta} |0\rangle$ indicates a particle-hole state and $|\alpha\beta\rangle = a^+_\alpha a^+_\beta |0\rangle$ indicates a particle-particle one. The difference between Latin and Greek indices is explained in section 2.2. In order to apply the coupling defined above to the density matrices (2.11), we write them in such a way that the ground state is on the right hand side.

$$\chi^{0\mu}_{\alpha\beta} = \langle 0|a^+_\beta a_\alpha|\mu\rangle = \langle\mu|a^+_\alpha a_\beta|0\rangle^*$$

$$\chi^{0\mu}_{\bar\beta\bar\alpha} = \langle 0|a^+_{\bar\alpha} a_{\bar\beta}|\mu\rangle = \langle\mu|a^+_{\bar\beta} a_{\bar\alpha}|0\rangle^* \qquad (C.3)$$

$$\phi^{o\mu}_{\alpha\bar{\beta}} = \langle 0|a_{\bar{\beta}}a_{\alpha}|\mu\rangle = \langle\mu|a^{+}_{\alpha}a^{+}_{\bar{\beta}}|0\rangle^{*}$$

$$\bar{\phi}^{o\mu}_{\bar{\alpha}\beta} = \langle 0|a^{+}_{\beta}a^{+}_{\bar{\alpha}}|\mu\rangle = \langle\mu|a_{\bar{\alpha}}a_{\beta}|0\rangle^{*} \qquad (C.4)$$

By writing down explicitly the time-reversed states in the particle-hole coupling (C.1), it turns out that:

$$(a^{+}_{\bar{\beta}}a_{\bar{\alpha}}|0\rangle)_{JM} = \sum_{m_\alpha m_\beta} (-)^{j_\beta - m_\beta}\langle j_\alpha m_\alpha j_\beta - m_\beta|JM\rangle(-)^{j_\alpha+m_\alpha}(-)^{j_\beta+m_\beta}\, a^{+}_{j_\beta - m_\beta}a_{j_\alpha m_\alpha}|0\rangle$$

$$= \sum_{m_\alpha m_\beta} (-)^{j_\beta - m_\beta}(-)^{j_\alpha+j_\beta+J}\langle j_\beta - m_\beta j_\alpha m_\alpha|JM\rangle(-)^{j_\alpha+m_\alpha}(-)^{j_\beta+m_\beta}\, a^{+}_{j_\beta - m_\beta}a_{j_\alpha m_\alpha}|0\rangle$$

$$= \sum_{m_\alpha m_\beta} (-)^{j_\alpha - m_\alpha}(-)^{j_\alpha+j_\beta+J+1}\langle j_\beta m_\beta j_\alpha - m_\alpha|JM\rangle a^{+}_{j_\beta m_\beta}a_{j_\alpha m_\alpha}|0\rangle$$

$$= (-)^{j_\alpha+j_\beta+J+1}\,(a^{+}_{\beta}a_{\alpha}|0\rangle)_{JM} \qquad (C.5)$$

This means that the quantities $\chi^{o\mu}_{\bar{\beta}\alpha}$ and $\chi^{o\mu}_{\beta\alpha}$ in the coupled representation differ only by the relative phase $(-)^{j_\alpha+j_\beta+J+1}$.

Combining together the relations (C.1), (C.3) and (C.5), it follows that the expressions for the coupled particle-hole amplitudes $\chi^{o\mu,J}_{ab}$ and $\chi^{-o\mu,J}_{ab}$ are:

$$\chi^{o\mu,J}_{ab} = \sum_{m_\alpha m_\beta} (-)^{j_\beta - m_\beta}\langle j_\alpha m_\alpha j_\beta - m_\beta|JM\rangle\langle\mu\, a^{+}_{\alpha}a_{\beta}|0\rangle^{*} \qquad (C.6)$$

$$\chi^{-o\mu,J}_{ab} = (-)^{j_\alpha+j_\beta+J+1}\,\chi^{o\mu,J}_{ba} \qquad (C.7)$$

For the particle-particle amplitudes, using (C.4) we have:

$$\phi_{ab}^{o\mu,J} = \frac{1}{\sqrt{1+\delta_{ab}}} \sum_{m_\alpha m_\beta} (-)^{j_\beta - m_\beta} \langle j_\alpha m_\alpha j_\beta - m_\beta | JM \rangle \; \phi^{o\mu}_{\alpha\bar{\beta}}$$

$$= - \frac{1}{\sqrt{1+\delta_{ab}}} \sum_{m_\alpha m_\beta} \langle j_\alpha m_\alpha j_\beta m_\beta | JM \rangle \langle \mu | a_\alpha^+ a_\beta^+ | 0 \rangle^* \qquad (C.8)$$

$$\bar{\phi}_{ab}^{o\mu,J} = \frac{1}{\sqrt{1+\delta_{ab}}} \sum_{m_\alpha m_\beta} (-)^{j_\alpha + m_\alpha} (-)^{j_\beta - m_\beta} \langle j_\alpha m_\alpha j_\beta m_\beta | JM \rangle$$

$$\cdot \langle \mu | a_{j_\alpha - m_\alpha} a_{j_\beta - m_\beta} | 0 \rangle^* \qquad (C.9)$$

It is easy to verify that in this case:

$$\phi_{ba}^{o\mu,J} = (-)^{j_b + j_b + J + 1} \; \phi_{ab}^{o\mu,J} \qquad (C.10)$$

From (C.7) and (C.10) and using the definitions (2.13) and (2.14) one can see that the following symmetry relations are verified:

$$X_{ba}^{J\pm} = \pm (-)^{j_a + j_b + J + 1} \; X_{ab}^{J\pm}$$

$$\phi_{ba}^{J\pm} = (-)^{j_a + j_b + J + 1} \; \phi_{ab}^{J\pm} \qquad (C.11)$$

The coupling between the interaction and the amplitudes, which appear in eq. (B.10) is carried out by inserting the unity in the form:

$$\sum_{m_\gamma' m_\delta'} \sum_{JM} (-)^{j_\delta - m_\delta} \langle j_\gamma m_\gamma j_\delta - m_\delta | JM \rangle \; (-)^{j_\delta - m_\delta'} \langle j_\gamma m_\gamma' j_\delta - m_\delta' | JM \rangle = 1 \qquad (C.12)$$

Then, using (C.6), we can write:

$$\sum_{m_\gamma m_\delta} F^{ph}_{\alpha\beta\gamma\delta} X^{o\mu}_{\gamma\delta} = \sum_{m'_\gamma m'_\delta} \sum_{JM} F^{ph}_{\alpha\beta\gamma\delta} (-)^{j_\delta - m_\delta} \langle j_\gamma m_\gamma j_\delta - m_\delta | JM \rangle \tag{C.13}$$

$$\cdot (-)^{j_\delta - m'_\delta} \langle j_\gamma m'_\gamma j_\delta - m'_\delta | JM \rangle X^{o\mu}_{j_\gamma m'_\gamma j_\delta m'_\delta} = F^{ph}_{abcd,J} X^{o\mu,J}_{cd}$$

where we have defined the "right-side" coupling of the interaction in the following way:

$$F^{ph}_{abcd,J} = \sum_{m_\gamma m_\delta} (-)^{j_\delta - m_\delta} \langle j_\gamma m_\gamma j_\delta - m_\delta | JM \rangle F^{ph}_{\alpha\beta\gamma\delta} \tag{C.14}$$

Taking into account the relation (C.7), we can write also:

$$\sum_{m_\gamma m_\delta} F^{ph}_{\alpha\beta\gamma\delta} X^{o\mu}_{\bar{\delta}\bar{\gamma}} = (-)^{j_c + j_d + J + 1} F^{ph}_{abcd,J} X^{o\mu,J}_{dc} = F^{ph}_{abcd,J} \bar{X}^{o\mu,J}_{cd} \tag{C.15}$$

The coupling of the particle-particle amplitudes and interaction can be carried out in the same way.

Finally, performing also the "left-side" coupling, we obtain a system of equations, which looks like (B.10), except that in the present case the quantities are coupled.

Appendix D

An equivalent way of writing the QRPA-equations

For sake of completeness we outline here how to transform the QRPA-equations (2.23) and (2.24) ,obtained using the Green's function formalism, into the characteristic form they assume in the equations of motion treatment (Row70). First of all we define:

$$C^{\pm}_{abcd} = (E_a+E_b)\delta_{ac}\delta_{bd} + V^{\pm}_{abcd} + G^{\pm}_{abcd} \tag{D.1}$$

and thereby the eqs. (2.23) and (2.24) become:

$$\begin{aligned} \sum_{c>d} C^{+}_{abcd}\, Z^{+}_{cd} &= \omega\, Z^{-}_{ab} \\ \sum_{c>d} C^{-}_{abcd}\, Z^{-}_{cd} &= \omega\, Z^{+}_{ab} \end{aligned} \tag{D.2}$$

or, in matrix form:

$$\begin{pmatrix} C^{+} & -\omega \\ -\omega & C^{-} \end{pmatrix} \begin{pmatrix} Z^{+} \\ Z^{-} \end{pmatrix} = 0 \tag{D.3}$$

It is straightforward now, by introducing the new quantities:

$$\begin{aligned} A_{abcd} &= \tfrac{1}{2}\,(C^{+}_{abcd}+C^{-}_{abcd}) \\ B_{abcd} &= \tfrac{1}{2}\,(C^{+}_{abcd}-C^{-}_{abcd}) \end{aligned} \tag{D.4}$$

and:

$$X_{ab} = Z^{+}_{ab} + Z^{-}_{ab}$$

$$Y_{ab} = Z^{+}_{ab} - Z^{-}_{ab} \tag{D.5}$$

to write down the QRPA-equations (2.23) and (2.24) in the "RPA-like" form:

$$\begin{pmatrix} A & B \\ -B & -A \end{pmatrix} \begin{pmatrix} X \\ Y \end{pmatrix} = \omega \begin{pmatrix} X \\ Y \end{pmatrix} \tag{D.6}$$

The normalization of X and Y can be derived from the quasiboson structure of the RPA-excitations (Row70):

$$\sum_{a \geq b} \left(X^{J*}_{ab} X^{J'}_{ab} - Y^{J*}_{ab} Y^{J'}_{ab} \right) = \delta_{JJ'} \tag{D.7}$$

Using the transformations (D.5), we obtain the following condition for the amplitudes Z^{+}_{ab} and Z^{-}_{ab}:

$$2 \sum_{a \geq b} \left\{ \left(Z^{J^{+}}_{ab}\right)^{*} Z^{J'^{-}}_{ab} + \left(Z^{J^{-}}_{ab}\right)^{*} Z^{J'^{+}}_{ab} \right\} = \delta_{JJ'} \tag{D.8}$$

Appendix E

Explicit form of the particle-hole interaction

Our total particle-hole interaction is:

$$F^{ph} = F^{ph}_{Mig} + F_\pi + F_\rho \tag{E.1}$$

To write down explicitly F_π and F_ρ we have to start from the expressions of the one-pion and one-rho exchange potential (3.14) and (3.15).

By adding and subtracting the term:

$$-\frac{4\pi f_\pi^2 \hbar^3}{3m_\pi^2 c}\frac{q^2}{q^2+m_\pi^2}\vec{\tau}\cdot\vec{\tau}'\vec{\sigma}\cdot\vec{\sigma}' = -\frac{4\pi f_\pi^2 \hbar^3}{3m_\pi^2 c}\{\vec{\tau}\cdot\vec{\tau}'\vec{\sigma}\cdot\vec{\sigma}' - \frac{m_\pi^2}{q^2+m_\pi^2}\vec{\tau}\cdot\vec{\tau}'\,\vec{\sigma}\cdot\vec{\sigma}'\} \tag{E.2}$$

on the right hand side of (3.14) we obtain:

$$V_{OPEP}(q) = -\frac{4\pi f_\pi^2 \hbar^3}{m_\pi^2 c}\vec{\tau}\cdot\vec{\tau}'\{\frac{(\vec{\sigma}\cdot\vec{q})(\vec{\sigma}'\cdot\vec{q})-1/3\vec{\sigma}\cdot\vec{\sigma}'q^2}{q^2+m_\pi^2} + \frac{1}{3}\vec{\sigma}\cdot\vec{\sigma}' - \frac{1}{3}\frac{m_\pi^2}{q^2+m_\pi^2}\vec{\sigma}\cdot\vec{\sigma}'\} \tag{E.3}$$

In the previous expression the first term corresponds to the usual tensor force, the second one, after a Fourier transformation into the r-space, is a δ -function and therefore it is lumped into the delta part of our force and finally the third term is the central Yukawa part.

The Fourier transformation of (E.3), neglecting the second term, gives:

$$V_{OPEP}(\vec{r}) = \frac{\hbar^3}{c} f_\pi^2 m_\pi^2 \vec{\tau}\cdot\vec{\tau}'\{(\frac{1}{3m_\pi r} + \frac{1}{(m_\pi r)^2} + \frac{1}{(m_\pi r)^3})\, e^{-m_\pi r} S_{12} + \frac{1}{3}\vec{\sigma}\cdot\vec{\sigma}'\,\frac{e^{-m_\pi r}}{m_\pi r}\} \tag{E.4}$$

with:

$$S_{12} = 3(\vec{\sigma}\cdot\hat{r})(\vec{\sigma}'\cdot\hat{r}) - \vec{\sigma}\cdot\vec{\sigma}' \qquad (E.5)$$

where $\hat{r}$ is the unit vector $\frac{\vec{r}}{|\vec{r}|}$.

To write the expression (3.15) for $V_\rho(q)$ in the same way we first have to use the Lagrangian identity for vector products:

$$(\vec{\sigma}\times\vec{q})(\vec{\sigma}'\times\vec{q}) = (\vec{\sigma}\cdot\vec{\sigma}')q^2 - (\vec{\sigma}\cdot\vec{q})(\vec{\sigma}'\cdot\vec{q}) \qquad (E.6)$$

and:

$$(\vec{\sigma}\cdot\vec{\sigma}')q^2 = \frac{1}{3}(\vec{\sigma}\cdot\vec{\sigma}')q^2 + \frac{2}{3}(\vec{\sigma}\cdot\vec{\sigma}') - \frac{2}{3}\frac{m_\rho^2}{q^2+m_\rho^2}\vec{\sigma}\cdot\vec{\sigma}' \qquad (E.7)$$

Thereby we can write:

$$V_\rho(q) = -\frac{4\pi f_\rho^2 \hbar^3}{m_\rho^2 c}\vec{\tau}\cdot\vec{\tau}'\left\{-\frac{(\vec{\sigma}\cdot\vec{q})(\vec{\sigma}'\cdot\vec{q}) - 1/3\vec{\sigma}\cdot\vec{\sigma}'q^2}{q^2+m_\rho^2} + \frac{2}{3}\vec{\sigma}\cdot\vec{\sigma}' - \frac{2}{3}\frac{m_\rho^2}{q^2+m_\rho^2}\vec{\sigma}\cdot\vec{\sigma}'\right\} \qquad (E.8)$$

which differs from the corresponding expression (E.4) of $V_{OPEP}(q)$ in the sign of the first term and by the factor 2 in the second and third term.

The Fourier transformation of (E.8), after dropping the second term, is:

$$V_\rho(\vec{r}) = \frac{\hbar^3}{c} f_\rho^2 m_\rho^2 \vec{\tau}\cdot\vec{\tau}'\left\{-\left(\frac{1}{3m_\rho r} + \frac{1}{(m_\rho r)^2} + \frac{1}{(m_\rho r)^3}\right) e^{-m_\rho r} S_{12} + \frac{2}{3}\vec{\sigma}\cdot\vec{\sigma}'\frac{e^{-m_\rho r}}{m_\rho r}\right\} \qquad (E.9)$$

By definition, the parameters of the Landau-Migdal force F^{ph}_{Mig} contain all contributions to the effective particle-hole force in the Landau limit q=0. Since V_{OPEP} and V_ρ also contribute to these parameters one has to reduce their contributions from the Migdal parameters, to avoid double counting.

The corrections we have to introduce in the parameters of the Migdal force originate from two contributions. The first comes from the direct term of V_{OPEP} and V_ρ and "corrects" only in the $\vec{\sigma}\cdot\vec{\sigma}'$ $\vec{\tau}\cdot\vec{\tau}'$ channel and is determined from (E.3) and (E.8) putting q=0:

$$V_{OPEP}(0) = \frac{4\pi f_\pi^2 \hbar^3}{m_\pi^2 c} \frac{1}{3} \vec{\tau}\cdot\vec{\tau}' \; \vec{\sigma}\cdot\vec{\sigma}' \tag{E.10}$$

$$V_\rho(0) = \frac{4\pi f_\rho^2 \hbar^3}{m_\rho^2 c} \frac{2}{3} \vec{\tau}\cdot\vec{\tau}' \; \vec{\sigma}\cdot\vec{\sigma}' \tag{E.11}$$

The second correction is due to the Pauli exchange terms, which are obtained using the exchange operator $P_{exch} = -P^x P^\sigma P^\tau$ and gives contributions in all channels.

Using the results of an infinite Fermi system (Bro77), one obtains the following relationship for all parameters of meson exchange forces and all orders ℓ of Landau's expansion:

$$F_\ell^{exch} = -(2\ell+1) \frac{m_m^2}{2k_F^2} Q_\ell \left(1 + \frac{m_m^2}{2k_F^2}\right) (\sigma\tau)_{exch} F^{dir} \tag{E.12}$$

where m_m is the meson mass, Q_ℓ are the Legendre functions of the second kind and:

$$(\sigma\tau)_{exch} = \frac{1}{4} \{-9+3\vec{\sigma}\cdot\vec{\sigma}' + 3\vec{\tau}\cdot\vec{\tau}' - \vec{\sigma}\cdot\vec{\sigma}' \; \vec{\tau}\cdot\vec{\tau}'\} \tag{E.13}$$

indicates the exchange matrix element of $\vec{\sigma}\cdot\vec{\sigma}'$ $\vec{\tau}\cdot\vec{\tau}'$ and has been obtained using the property:

$$\langle\vec{\sigma}\cdot\vec{\sigma}'\rangle_{exch}\langle\vec{\tau}\cdot\vec{\tau}'\rangle_{exch} = -\left\langle\frac{3-\vec{\sigma}\cdot\vec{\sigma}'}{2}\,\frac{3-\vec{\tau}\cdot\vec{\tau}'}{2}\right\rangle_{dir} \tag{E.14}$$

By adding to F^{ph}_{Mig} the correction due to the direct and exchange terms of the finite range force, the final explicit form of (E.1) is:

$$\begin{aligned}
C_o^{-1}F^{ph}(\vec{r},\vec{r}') = {} & \left[\left(f_o^{ex}-\frac{9}{4}\left(g_{o\pi}'^{exch}+g_{o\rho}'^{exch}\right)\right)+\left(f_o'+\frac{3}{4}\left(g_{o\pi}'^{exch}+g_{o\rho}'^{exch}\right)\right)\vec{\tau}\cdot\vec{\tau}'\right. \\
& + \left(g_o+\frac{3}{4}\left(g_{o\pi}'^{exch}+g_{o\rho}'^{exch}\right)\right)\vec{\sigma}\cdot\vec{\sigma}' \\
& + \left(g_o'-g_{o\pi}'^{dir}-g_{o\rho}'^{dir}-\frac{1}{4}\left(g_{o\pi}'^{exch}+g_{o\rho}'^{exch}\right)\right)\vec{\sigma}\cdot\vec{\sigma}'\,\vec{\tau}\cdot\vec{\tau}' \\
& \left.+ \left(f_o^{in}-f_o^{ex}\right)\frac{1}{1+e^{(r-R)/\alpha}}\right]\delta(\vec{r}-\vec{r}') \\
& + g_{o\pi}'^{dir}\,\frac{\mu_\pi^3}{4\pi}\left[h_2^{(1)}(im_\pi r)e^{-m_\pi r}S_{12}+\vec{\sigma}\cdot\vec{\sigma}',\ \frac{e^{-m_\pi r}}{m_\pi r}\right]\vec{\tau}\cdot\vec{\tau}' \\
& + g_{o\rho}'^{dir}\,\frac{\mu_\rho^3}{4\pi}\left[-\frac{1}{2\gamma}\,h_2^{(1)}(im_\rho r)e^{-m_\rho r}S_{12}+\vec{\sigma}\cdot\vec{\sigma}',\ \frac{e^{-m_\rho r}}{m_\rho r}\right]\vec{\tau}\cdot\vec{\tau}' \\
& - g_{o\pi}'^{dir}\,\frac{\mu_\pi^3}{4\pi}\,V^{exch}_{OPEP}(\vec{r}_1,\vec{r}_2) - g_{o\rho}'^{dir}\,\frac{\mu_\rho^3}{4\pi}\,V^{exch}_{\rho}(\vec{r}_1,\vec{r}_2)
\end{aligned} \tag{E.15}$$

where $g_{o\pi}'^{dir}$, $g_{o\rho}'^{dir}$ are determined from (E.10) and (E.11) and $g_{o\pi}^{exch}$, $g_{o\rho}^{exch}$, etc. are given from (E.12).

The part in brackets on the right hand side of (E.15) is the zero-range part of the particle-hole interaction and the second and third terms give the one-pion and one-rho exchange potentials in coordinate space, $h_2^{(1)}$ being Hankel's

function of the first kind. The presence of a factor $\mu_{\pi,\rho}^3/4\pi$, where $\mu_\pi = m_\pi c/\hbar$ is the inverse Compton wavelength, allows the normalization of the corresponding central parts to a δ-function, in the limit of infinite heavy meson masses. The factor $\gamma = 0.4$ is introduced in the one-rho exchange part in order to take into account correlations due to the short-range repulsion and the factor 2 refers to the relative double strength of the scalar part of the rho-exchange force compared to the pion exchange. The parameters $g'^{dir}_{o\pi}$ and $g'^{dir}_{o\rho}$ are determined by the coupling constants f_π^2 and f_ρ^2. From (E.10), (E.11) and (E.15) follows:

$$g'^{dir}_{o\pi} = C_o^{-1} \frac{4\pi}{3} \frac{f_\pi^2}{m_\pi^2} \frac{\hbar^3}{c} \tag{E.16}$$

$$g'^{dir}_{o\rho} = C_o^{-1} 2\gamma \frac{4\pi}{3} \frac{f_\rho^2}{m_\rho^2} \frac{\hbar^3}{c} \tag{E.17}$$

where $C_o = \frac{\pi^2\hbar^2}{k_F m^*}$ was introduced in order to make the Migdal force parameters dimensionless (see section 3.2). Choosing $k_F = 1.36$ fm^{-1} we obtain:

$$g'^{dir}_{o\pi} = 0.35$$

$$g'^{dir}_{o\rho} = 0.55 \tag{E.18}$$

Appendix F

Matrix elements of the particle-particle δ-function interaction

The angular part of the matrix elements of a spin-independent δ-function interaction between particle-particle states has the form:

$$\langle(\ell_1 j_1,\ell_2 j_2)J\,|\,\delta(\Omega-\Omega')\,|\,(\ell_3 j_3,\ell_4 j_4)J\rangle$$

$$= \frac{1}{2\pi}(-)^{\ell_1+j_1+1/2}(-)^{\ell_3+j_3+1/2}\sqrt{(j_1+1/2)(j_2+1/2)(j_3+1/2)(j_4+1/2)} \qquad (F.1)$$

$$\cdot\left\{\begin{pmatrix} j_1 & j_2 & J \\ 1/2 & -1/2 & 0\end{pmatrix}\begin{pmatrix} j_3 & j_4 & J \\ 1/2 & -1/2 & 0\end{pmatrix}+(-)^{\ell_1+\ell_3}(-)^{j_2+j_4+1}\begin{pmatrix} j_1 & j_2 & J \\ 1/2 & 1/2 & -1\end{pmatrix}\begin{pmatrix} j_3 & j_4 & J \\ 1/2 & 1/2 & -1\end{pmatrix}\right\}$$

Taking into account also the spin-exchange operator P^σ, we have the following expression:

$$\langle(\ell_1 j_1,\ell_2 j_2)J\,|\,P^\sigma\delta(\Omega-\Omega')\,|\,(\ell_3 j_3,\ell_4 j_4)J\rangle$$

$$= \frac{1}{2\pi}(-)^{\ell_1+j_1+1/2}(-)^{\ell_3+j_3+1/2}\sqrt{(j_1+1/2)(j_2+1/2)(j_3+1/2)(j_4+1/2)}$$

$$\cdot\left\{(-)^{\ell_1+\ell_2}(-)^{J+1}\begin{pmatrix} j_1 & j_2 & J \\ 1/2 & -1/2 & 0\end{pmatrix}\begin{pmatrix} j_3 & j_4 & J \\ 1/2 & -1/2 & 0\end{pmatrix}\right. \qquad (F.2)$$

$$\left.+(-)^{\ell_1+\ell_3}(-)^{j_2+j_4+1}\begin{pmatrix} j_1 & j_2 & J \\ 1/2 & 1/2 & -1\end{pmatrix}\begin{pmatrix} j_3 & j_4 & J \\ 1/2 & 1/2 & -1\end{pmatrix}\right\}$$

The form of the antisymmetrized particle-particle force used in the present calculations is given in eq. (3.17). From the previous matrix elements one can immediately see that the particle-particle interaction doesn't give any contribution in case of unnatural parity states.

Appendix G

Reduced matrix elements of the electric and magnetic multipole operator

The reduced matrix elements of the electric multipole operator $\hat{E}^J$ are (Rin73):

$$(\hat{E}^J)_{ab} = \langle a \| \hat{E}^J \| b \rangle = (-)^{j_a - 1/2} \sqrt{\frac{(2j_a+1)(2j_b+1)(2J+1)}{4\pi}} \begin{pmatrix} j_a & J & j_b \\ -1/2 & 0 & 1/2 \end{pmatrix}$$

$$\cdot \frac{1}{2} \left[1+(-)^{\ell_a+\ell_b+J}\right] e^J \int_0^\infty R_a(r) R_b(r) r^{J+2} dr \qquad (G.1)$$

The reduced matrix elements of the magnetic multipole operator $\hat{M}^J$ are (Bau73):

$$(\hat{M}^J)_{ab} = \langle a \| \hat{M}^J \| b \rangle = \frac{e\hbar}{2m_p c} \langle a \| \left(\frac{2}{J+1} \tilde{g}\vec{\ell} + \tilde{\mu}\vec{\sigma}\right) \cdot \vec{\nabla}(r^J Y_J) + \sqrt{\frac{3}{4\pi}} r^2 (Y_2 \cdot \vec{\sigma})_1 \tau_3 \delta_{J1} \| b \rangle$$

$$= \frac{e\hbar}{2m_p c} \left[1+(-)^{\ell_a+\ell_b+J-1}\right] R^{J-1}_{a,b} \sqrt{\frac{2J+1}{\pi}} \begin{pmatrix} j_b & j_a & J \\ 1/2 & 1/2 & -1 \end{pmatrix}$$

$$\cdot \sqrt{(2j_a+1)(2j_b+1)}\,(-)^{j_a-1/2} \left[\tilde{\mu} + \frac{\tilde{g}}{J+1} \left\{J+1+(j_b+1/2)(-)^{j_b+\ell_b-1/2}\right.\right. \qquad (G.2)$$

$$\left.\left. + (j_a+1/2)(-)^{j_a+\ell_a-1/2}\right\}\right] + \frac{e\hbar}{2m_p c} R^2_{ab} \sqrt{(2j_a+1)(2j_b+1)} \cdot \left\{(-)^{j_b+1/2} \begin{pmatrix} j_a & j_b & 1 \\ 1/2 & 1/2 & 0 \end{pmatrix}\right.$$

$$\left. + (-)^{\ell_a} \sqrt{1/2} \begin{pmatrix} j_a & j_b & 1 \\ 1/2 & 1/2 & -1 \end{pmatrix}\right\} \delta_{J1}\, \tau_3$$

where τ_3 is the z-component of the isospin vector, $R^{(n)}_{a,b} = \int_0^\infty R_a(r) r^n R_b(r) r^2 dr$ and the last term is the correction term due to the mesonic current effect.

ACKNOWLEDGEMENT

First of all I would like to express my gratitude to Professor Josef Speth for the suggestion of the subject and for the discussions of the physical problem.

I have to thank Vilmar Klemt for his help and advice in all the phases of the work and for the friendly assistence during my stay in the theory group.

Special thank is due to Peter Kleinheinz for many valuable discussions and for the careful reading of part of the manuscript.

For useful discussions on the problems encountered in carrying out the present work I want to thank Jan Blomqvist and Jan Styczen.

My special tribute to Dietrich Zawischa for helping me in the approach to the theory.

My best thanks to Madda Heese for her patient and careful typing of the manuscript.

My sincere thanks to Ewald Brökel, who helped me in several ways, particularly in overcoming my problems with the computer and in drawing the figures.

I wish to thank my colleagues of the theory group who gave me the possibility to work in a very friendly environment.

Finally I thank the Kernforschungsanlage Jülich for the financial support.

REFERENCES

Akk82 J.N.L. Akkermans and K. Allaart, Z. Phys. A304 (1982) 245

All72 K. Allaart and E. Boeker, Nucl. Phys. A198 (1972) 33

Bäc80 S.O. Bäckman, G.E. Brown, V. Klemt and J. Speth, Nucl. Phys. A345 (1980) 202

Bad57 J. Bardeen, L.N. Cooper and J.R. Schrieffer, Phy. Rev. 108 (1957) 1175

Bar60 M. Baranger, Phys. Rev. 120 (1960) 957

Bau73 R. Bauer, J. Speth, V. Klemt, P. Ring, E. Werner and T. Yamazaki, Nucl. Phys. A209 (1973) 535

Bay75 G. Baym and G.E. Brown, Nucl. Phys. A247 (1975) 395

Bel59 S.T. Belyaev, Mat. Fys. Medd. Dan. Vid. Selsk. 31, No. 11 (1959)

Bel65 S.T. Belyaev, Nucl. Phys. 64 (1965) 17.

Bij82 L.T. van der Bijl, H.P. Blok, R. Frey, D. Meuer, A. Richter and P.K.A. de Witt Huberts, Z. Phys. A305 (1982) 231

Bir68 B.L. Birbrair, Nucl. Phys. A108 (1968) 449

Bir70 B.L. Birbrair, K.I. Erokhina and I.Kh. Lemberg, Nucl. Phys. A145 (1970) 129

Blo59 J. Blomqvist and S. Wahlborn, Arkiv for Fysik 16, No. 46 (1959) 545

Blo81 J. Blomqvist, P. Kleinheinz, R. Broda and P.J. Daly, Proc. 4th Int. Conf. on Nuclei far from Stability, Helsingør (1981), edited by P.G. Hansen and G.B. Nielsen (CERN, Geneva, 1981) p. 545

Blo83a J. Blomqvist, P. Kleinheinz and P.J. Daly, Z. Phys. A312 (1983) 27

Blo83b J. Blomqvist, private communication

Bog58a N.N. Bogoliubov, J.E.T.P. (U.S.S.R.) 34 (1958) 58 and 73

Bog58b N.N. Bogoliubov, Nuovo Cimento 7 (1958) 794

Boh69 A. Bohr and B.R. Mottelson, "Nuclear Structure", Vol. I, W.A. Benjamin, New York (1969)

Brd79 R. Broda, M. Behar, P. Kleinheinz, P.J. Daly and J. Blomqvist, Z. Phys. A293 (1979) 135

Bro77 G.E. Brown, S.O. Bäckman, E. Oset and W. Weise, Nucl. Phys. A286 (1977) 191

Bru77 P.J. Brussaard and P.W.M. Glaudemans, "Shell-Model Applications in Nuclear Spectroscopy", North-Holland, Amsterdam (1977)

Bun76 R.L. Bunting and J.J. Kaushaar, Nucl. Data Sheets 18 (1976) 87

Cha80 R.R. Chasman, Phys. Rev. C21, No. 1 (1980) 456

Cha81 R.R. Chasman, Phys. Lett. 102B, No. 4 (1981) 229

Cha82 R.R. Chasman, Phys. Lett. 108B, No. 4,5 (1982) 251

Cha83 R.R. Chasman, Phys. Rev. C28, No. 3 (1983) 1374

Col68 L. Collatz, "Funktionalanalysis und numerische Mathematik", Springer Verlag, Berlin (1968)

Co'83 G. Co', J. Heisenberg, S. Krewald and J. Speth, preprint

Dal80 P.J. Daly, P. Kleinheinz, R. Broda, S. Lunardi, H. Backe and J. Blomqvist, Z. Phys. A298 (1980) 173

Døs81 T. Døssing, K. Neergard and H. Sagawa, Phys. Scr. 24 (1981) 258

Dud82 J. Dudek, Z. Szymanski, T. Werner, A. Faessler and C. Lima, Phys. Rev. C26, No. 4 (1982) 1712

Fet71 A.L. Fetter and J.D. Walecka, "Quantum Theory of Many-Particle Systems", McGraw-Hill, New York (1971)

Fly83 E.R. Flynn, J. van der Plicht, J.B. Wilhelmi, L.G. Mann, G.L. Struble and R.G. Lanier, Phys. Rev. C28, No. 1 (1983) 97

Goo79 A.L. Goodman, Nucl. Phys. A331 (1979) 401

Gor58 L.P. Gor'kov, J.E.T.P. (U.S.S.R.) 34 (1958) 735

Hel82 H. Helppi, Y.H. Chung, P.J. Daly, S.R. Faber, A. Pakkanen, I. Ahmad, P. Chowdhury, Z.W. Grabowki, T.L. Khoo, R.D. Lawson and J. Blomqvist, Phys. Lett. 115B (1982) 11

Isa82 V.I. Isakov, S.A. Artamonov and L.A. Sliv, Sov. J. Nucl. Phys. 35 (1982) 173

Jul80 R. Julin, J. Kantele, M. Luontama, A. Passoja, P. Kleinheinz and J. Blomqvist, Phys. Lett. 94B, No. 2 (1980) 123

Kam69 S.P. Kamerdzhiev, Sov. J. of Nucl. Phys. 9 (1969) 190

Kis60 L.S. Kisslinger and R.A. Sorensen, Mat. Fys. Medd. Dan. Vid. Selsk. 32, No. 1 (1960)

Kis63 L.S. Kisslinger and R.A. Sorensen, Rev. Mod. Phys. 35 (1963) 853

Kle70 V. Klemt, "Anwendung der Quasiteilchenmethode auf einige Probleme von ug-Kernen in der Nachbarschaft von ^{208}Pb", Dissertation, TH München (1970)

Kle82 V. Klemt, J. Phys. G8 (1982) 1547

Klz78a P. Kleinheinz, S. Lunardi, M. Ogawa and M.R. Maier, Z. Phys. A284 (1978) 351

Klz78b P. Kleinheinz, M. Ogawa, R. Broda, P.J. Daly, D. Haenni, H. Beuscher and A. Kleinrahm, Z. Phys. A286 (1978) 27

Klz79 P. Kleinheinz, R. Broda, P.J. Daly, S. Lunardi, M. Ogawa and J. Blomqvist, Z. Phys. A290 (1979) 279

Klz82 P. Kleinheinz, J. Styczen, M. Piiparinen, J. Blomqvist and M. Kortelahti, Phys. Rev. Lett. 48, No. 21 (1982) 1457

Klz83 P. Kleinheinz, private communication

Koc75 D.C. Kocher, Nucl. Data Sheets 16 (1975) 55

Kow72 J. Kownacki, H. Ryde, V.O. Sergejev and Z. Sujkowski, Nucl. Phys. A196 (1972) 498.

Kri73 K. Krien, F. Djalali, R.A. Naumann, H. Hübel and E.H. Spejewski, Phys. Rev. C7 (1973) 2484

Law81 R.D. Lawson, Z. Phys. A303 (1981) 51

Led78 C.M. Lederer and V.S. Shirley, "Table of Isotopes", 7th edition, J. Wiley, New York (1978)

Met71 R.F. Metzger, Nucl. Phys. A173 (1971) 141

Mig67 A.B. Migdal, "Theory of Finite Fermi Systems and Application to Atomic Nuclei", J. Wiley, New York (1967)

Mig74 A.B. Migdal, O.A. Markin and I.I. Mishustin, J.E.T.P. (U.S.S.R.) 39 (1974) 212

Nag81 Y. Nagai, J. Styczen, M. Piiparinen, P. Kleinheinz, D. Bazzacco, P.v. Brentano, K.O. Zell and J. Blomqvist, Phys. Rev. Lett. 47, No. 18 (1981) 1259

Nak83 K. Nakayama, S. Krewald, J. Speth and W.G. Love, to be published

Nol82 E. Nolte, G. Colombo, S.Z. Gui, G. Korschinek, W. Schollmeier, P. Kubik, S. Gustavsson, R. Geier and H. Morinaga, Z. Phys. A306 (1982) 211

Noz64 P. Nozières, "Theory of Interacting Fermi Systems", W.A. Benjamin, New York (1964)

Oga78 M. Ogawa, R. Broda, K. Zell, P.J. Daly and P. Kleinheinz, Phys. Rev. Lett. 41, No. 5 (1978) 289

Pak82 A. Pakkanen, J. Muhonen, M. Piiparinen and J. Blomqvist, Nucl. Phys. A373 (1982) 237

Pen79 R. Pengo, S. Lunardi, R. Tischler, Y. Nagai, R. Broda and P. Kleinheinz, Proc. Symp. on High-Spin Phenomena in Nuclei", Argonne Nat. Lab., Argonne, Illinois (1979) p. 385

Pii82 M. Piiparinen, T. Komppa, R. Komu, A. Pakkanen and J. Blomqvist, Z. Phys. A309 (1982) 87

Plo79 M. Ploszajczak and A. Faessler, Proc. Symp. on High-Spin Phenomena in Nuclei, Argonne Nat. Lab., Argonne, Illinois (1979) p. 551

Rik78 G.A. Rinker and J. Speth, Nucl. Phys. A306 (1978) 360

Rin73 P. Ring, R. Bauer and J. Speth, Nucl. Phys. A206 (1973) 97

Rin74 P. Ring and J. Speth, Nucl. Phys. A235 (1974) 315

Ros57 M.E. Rose, "Elementary Theory of Angular Momentum", J. Wiley, New York (1957)

Row70 D.J. Rowe, "Nuclear Collective Motion", Methuen and Co. Ltd., London (1970)

Sch81 M. Schöttler, "Theoretische Untersuchung des odd-even staggering der Isotopieverschiebung des rms-Ladungsradius der Atomkerne", Diplomarbeit, TU Hannover (1981)

Spe77 J. Speth, E. Werner and W. Wild, Phys. Rep. 33C (1977) 127

Spe80 J. Speth, V. Klemt, J. Wambach and G.E. Brown, Nucl. Phys. A343 (1980) 382

Spr83 R.H. Spear, W.J. Vermeer, M.T. Esat, J.A. Kuehner, A.M. Baxter and S. Hinds, Phys. Lett. 128B, No. 1,2 (1983) 29

Sty81 J. Styczen, P. Kleinheinz, M. Piiparinen and J. Blomqvist, Proc. 4th Int. Conf. on Nuclei far from Stability, Helsingør (1981), edited by P.G. Hansen and G.B. Nielsen (CERN, Geneva, 1981) p. 548

Tok83 H. Toki, G.F. Bertsch and D. Cha, Phys. ev. C28, No. 3 (1983) 1398

Tul78 J.K. Tuli, Nucl. Data Sheets 25 (1978) 53

Val58 J.G. Valatin, Nuovo Cimento 7 (1958) 794

Vej66 C.J. Veje, Mat. Fys. Medd. Dan. Vid. Selsk. 35, No. 1 (1966)

Wam80 J. Wambach, A.D. Jackson and J. Speth, Nucl. Phys. A348 (1980) 221

Wap77 A.H. Wapstra and K. Bos, Atom. Dat. and Nucl. Dat. Tabl. 19 (1977) 177

War71 M. Waroquier and K. Heyde, Nucl. Phys. A164 (1971) 113

Wil71 B.H. Wildenthal, E. Newman and R.L. Auble, Phys. Rev. C3, No. 3 (1971) 1199

Yos62 S. Yoshida, Nucl. Phys. 38 (1962) 380

Zaw78 D. Zawischa, J. Speth and D. Pal, Nucl. Phys. A311 (1978) 445

TABLE CAPTIONS

Table 1: The parameters of the Woods-Saxon potential, defined in (3.1), are given for ^{88}Sr, ^{90}Zr and ^{146}Gd. For comparison we include also the corresponding values for ^{208}Pb, taken from (Rik 78). The potential depths V_0 are fixed in order to reproduce the quantities λ_{exp} obtained from the Atomic Mass Table (Wap77) as explained in section 3.1. $b = \sqrt{\frac{\hbar}{m\omega}}$ is the oscillator constant.

Table 2: Single-particle eneregies for ^{88}Sr calculated with the Woods-Saxon potential given in Table 1. The energies marked with (*) are taken from experiment (Isa82). These states also define the configuration space.

Table 3: Single-particle energies for ^{90}Zr. For the explanation see Table 2.

Table 4: Single-particle energies for ^{146}Gd. The experimental energies (*) are taken from (Sty81,Pii82,Klz83).

Table 5: In the first line we write the parametrization of the Migdal-force used in (Rik78). In the second line we give the set of parameters which are applied in the present QRPA-calculations, where in addition to the zero-range force also the finite-range is considered.

Table 6: Choice of the parameters h^{in} and h^{ex} of the particle-particle force (3.17) in order to reproduce the separation energy differences $\delta_p^{(exp)}$. The corresponding values of the pairing constant G are given in the fourth column. $\delta_p^{(1)}$ and $\delta_p^{(2)}$ indicate the proton separation energy differences calculated using respectively the δ-pairing force and the schematic one. The experimental values $\delta_p^{(exp)}$ are taken from a) (Wap77) and b) (Klz79).

Table 7: The BCS-equations (2.6) and (2.7) have been solved in ^{88}Sr for all the levels given in this table, using the pairing force given in the first two columns of Table 6. Since we are using a pairing force which has no constant matrix elements, the energy gaps Δ_a are different for each level. v_a^2 are the occupation probabilities which correspond to the particle distribution of Fig. 1b. The energies $\varepsilon_{(qp)a}$ are obtained from the quasiparticle energies E_a through the relation: $\varepsilon_{(qp)a} = \pm E_a + \lambda$, where the positive sign is taken if the corresponding single-particle state a is a particle state and the negative sign for a hole state.

Table 8: Solution of the BCS-equations for proton states in ^{90}Zr. For explanation see Table 7.

Table 9: Solution of the BCS-equations for proton states in ^{146}Gd. For explanation see Table 7.

Table 10: The experimental excitation energies E_{exp} (keV), the calculated ones E_{th} (keV), the corresponding differences $(E_{exp}-E_{th})$ (keV) and the electric and magnetic transition probabilities B are tabulated for the low-lying states up to ~ 4 MeV of the nucleus ^{146}Gd. ε_{2qp} indicates the energy of the corresponding two-quasiparticle configuration, which is equal to (E_a+E_b), where E_a is the quasiparticle energy of the orbit a obtained from (2.8). X and Y are the forward and backward amplitudes, which are related to the QRPA-eigenfunctions through the relation (D.5). The B-values are given in the following units:

- B(EJ) in: e fm^{2J}
- B(MJ) in: $(n\ m)^2$ $fm^{2(J-1)}10^{2J}$.

The electric monopole strength B(E0) is dimensionless. The experimental values are taken from:

a) (Klz79)

b) (Sty81)

c) (Fly83)

d) (Jul80).

Table 11: Calculated excitation energies and transition probabilities of the first five quadrupole vibrational states of ^{146}Gd. For explanation see Table 10.

Table 12: The same of Table 10 for the four-proton-hole nucleus $^{142}_{60}Nd_{82}$. The experimental values are taken from (Tul78).

Table 13: The same of Table 10 for the two-proton-hole nucleus $^{144}_{62}Sm_{82}$. The experimental values are taken from a) (Led78), b) (Pen79).

Table 14: The same of Table 10 for the two-proton-particle nucleus $^{148}_{66}Dy_{82}$. The experimental values are taken from (Dal80).

Table 15: The same of Table 10 for the four-proton-particle nucleus $^{150}_{68}Er_{82}$. The experimental values are taken from a) (Hel82), b) (Nol82).

Table 1: Woods-Saxon parameters

		V_o (MeV)	α_o (fm)	R_o (fm)	λ_{so}	α_{so} (fm)	R_{so} (fm)	R_{Coul} (fm)	b (fm)	λ (MeV)	λ_{exp} (MeV)
$^{88}_{38}Sr_{50}$	p	57.0	0.67	5.60	32.0	0.67	5.41	5.56	2.109	-8.94	-8.84
	n	50.5	0.67	5.41	32.0	0.67	5.22	-		-8.99	-8.74
$^{90}_{40}Zr_{50}$	p	56.8	0.67	5.64	32.0	0.67	5.45	5.60	2.117	-7.43	-6.76
	n	51.1	0.67	5.45	32.0	0.67	5.26	-		-9.79	-9.59
$^{146}_{64}Gd_{82}$	p	57.3	0.79	6.63	27.0	0.59	6.40	6.58	2.295	-3.66	-3.57
	n	48.0	0.66	6.40	32.0	0.64	6.19	-		-8.01	-9.21
$^{208}_{82}Pb_{126}$	p	60.40	0.79	7.46	20.25	0.59	7.20	7.41	2.440	-5.47	-5.91
	n	44.32	0.66	7.46	24.87	0.64	6.96	-		-5.66	-5.61

Table 2: Single-particle energies for ^{88}Sr

orbit	energy (MeV)	
	proton	neutron
$1s_{1/2}$	-35.90	-42.48
$1p_{3/2}$	-29.93	-35.74
$1p_{1/2}$	-28.35	-34.23
$1d_{5/2}$	-23.05	-28.21
$1d_{3/2}$	-19.60	-24.88
$2s_{1/2}$	-19.01	-24.64
$1f_{7/2}$	-15.45	-20.04
$1f_{5/2}$	-10.25	-13.10*
$2p_{3/2}$	-9.66	-12.33*
$2p_{1/2}$	-8.22	-11.47*
$1g_{9/2}$	-7.26	-11.09*
$2d_{5/2}$	-1.63	-6.41*
$3s_{1/2}$	0.57	-5.57*
$1g_{7/2}$	1.09	-3.81*
$1h_{11/2}$	1.42	-2.23*
$2d_{3/2}$	1.69	-4.23*
$2f_{7/2}$	6.38	1.32
$3p_{3/2}$	7.25	1.52
$3p_{1/2}$	8.16	2.27
$2f_{5/2}$	9.88	4.17
$4s_{1/2}$	10.41	4.66
$1i_{13/2}$	10.45	6.97
$3d_{5/2}$		5.24
$3d_{3/2}$		5.90
$1h_{9/2}$		7.22

Table 3: Single-particle energies for ^{90}Zr

orbit	energy (MeV)	
	proton	neutron
$1s_{1/2}$	-35.21	-43.17
$1p_{3/2}$	-29.35	-36.48
$1p_{1/2}$	-27.81	-34.99
$1d_{5/2}$	-22.57	-28.99
$1d_{3/2}$	-19.19	-25.70
$2s_{1/2}$	-18.55	-25.43
$1f_{7/2}$	-15.07	-20.86
$1f_{5/2}$	- 9.89	-14.00*
$2p_{3/2}$	- 9.38	-13.19*
$2p_{1/2}$	-7.88	-12.54*
$1g_{9/2}$	-6.98	-11.95*
$2d_{5/2}$	-1.34	-7.22*
$3s_{1/2}$	0.86	-5.56*
$1g_{7/2}$	1.24	-4.45*
$1h_{11/2}$	1.61	-3.15*
$2d_{3/2}$	1.93	-4.46*
$2f_{7/2}$	6.61	0.73
$3p_{3/2}$	7.51	1.13
$3p_{1/2}$	8.42	1.94
$2f_{5/2}$	10.09	3.76
$1i_{13/2}$	10.56	6.12
$4s_{1/2}$	10.66	4.43
$3d_{5/2}$		5.02
$3d_{3/2}$		5.68
$1h_{9/2}$		6.50

Table 4: Single-particle energies for ^{146}Gd

orbit	energy (MeV)	
	proton	neutron
$1s_{1/2}$	-32.07	-42.34
$1p_{3/2}$	-27.48	-37.24
$1p_{1/2}$	-26.77	-36.42
$1d_{5/2}$	-22.06	-31.39
$1d_{3/2}$	-20.33	-29.45
$2s_{1/2}$	-18.98	-28.52
$1f_{7/2}$	-16.01	-24.92
$1f_{5/2}$	-12.83	-21.44
$2p_{3/2}$	-11.90	-20.87
$2p_{1/2}$	-10.60	-19.52
$1g_{9/2}$	- 9.46	-17.91
$1g_{7/2}$	- 4.70	-11.06*
$2d_{5/2}$	-4.46	-10.81*
$1h_{11/2}$	-2.85	-10.52*
$3s_{1/2}$	-2.55	-9.79*
$2d_{3/2}$	-2.30	-9.82*
$2f_{7/2}$	2.54	-6.29*
$1h_{9/2}$	4.55	-4.89*
$3p_{3/2}$	4.65	-5.14*
$1i_{13/2}$	4.85	-4.24*
$3p_{1/2}$	5.69	-4.44*
$2f_{5/2}$	5.80	-4.39*
$2g_{9/2}$	9.52	1.97
$3d_{5/2}$	10.37	2.30
$4s_{1/2}$	10.39	2.10
$3d_{3/2}$	11.28	3.15
$1j_{15/2}$	12.51	5.62
$2g_{7/2}$	12.70	4.98
$1i_{11/2}$	13.81	6.52
$4p_{3/2}$		5.47
$4p_{1/2}$		5.81
$3f_{7/2}$		6.26
$3f_{5/2}$		7.02
$2h_{11/2}$		7.85

Table 5: Parameters of the particle-hole force

ph-force	$f_0^{in}-f_0^{ex}$	f_0^{ex}	f_0'	g_0	g_0'
δ-force	2.65	-2.45	1.50	0.553	0.697
$(\delta+\pi+\rho)$	1.95	-1.75	1.50	0.1	0.7

Table 6: Parametrization of the particle-particle (and pairing) force

nucleus	$h^{in}-h^{ex}$	h^{ex}	C_0 (MeV fm^3)	G (MeV)	$\delta_p^{(1)}$ (MeV)	$\delta_p^{(2)}$ (MeV)	$\delta_p^{(exp)}$ (MeV)
^{88}Sr	2.50	-3.20	386	18	3.48	3.21	3.53[a]
^{90}Zr	2.35	-3.008	386	18	3.19	3.15	3.20[a]
^{146}Gd	2.60	-3.328	386	19	3.35	3.41	3.38[b]

Table 7: BCS-solution for proton states in ^{88}Sr

orbit a	$\varepsilon_{(sp)a}$ (MeV)	$\varepsilon_{(qp)a}$ (MeV)	Δ_a (MeV)	v_a^2
$1s_{1/2}$	-35.90	-35.93	1.44	0.9993
$1p_{9/2}$	-29.93	-29.98	1.55	0.9986
$1p_{1/2}$	-28.35	-28.41	1.52	0.9985
$1d_{5/2}$	-23.05	-23.15	1.66	0.9966
$1d_{3/2}$	-19.60	-19.72	1.62	0.9944
$2s_{1/2}$	-19.01	-19.14	1.63	0.9937
$1f_{7/2}$	-15.45	-15.68	1.74	0.9833
$1f_{5/2}$	-10.25	-11.07	1.70	0.8121
$2p_{3/2}$	-9.66	-10.64	1.57	0.7188
$2p_{1/2}$	-8.22	-7.16	1.59	0.3039
$1g_{9/2}$	-7.26	-6.49	1.76	0.1600
$2d_{5/2}$	-1.63	-1.51	1.33	0.0082
$3s_{1/2}$	0.57	0.64	1.11	0.0034
$1g_{7/2}$	1.09	1.24	1.71	0.0072
$1h_{11/2}$	1.42	1.56	1.71	0.0067
$2d_{3/2}$	1.69	1.77	1.31	0.0038
$2f_{7/2}$	6.38	6.41	0.97	0.0010
$3p_{3/2}$	7.25	7.26	0.64	0.0004
$3p_{1/2}$	8.16	8.17	0.54	0.0003
$2f_{5/2}$	9.88	9.89	0.71	0.0004
$4s_{1/2}$	10.41	10.42	0.30	0.0001
$1i_{13/2}$	10.45	10.52	1.55	0.0016

Table 8: BCS-solution for proton states in ^{90}Zr

orbit a	$\varepsilon_{(sp)a}$ (MeV)	$\varepsilon_{(qp)a}$ (MeV)	Δ_a (MeV)	v_a^2
$1s_{1/2}$	-35.21	-35.24	1.19	0.9995
$1p_{3/2}$	-29.35	-29.39	1.31	0.9991
$1p_{1/2}$	-27.81	-27.85	1.28	0.9990
$1d_{5/2}$	-22.57	-22.64	1.42	0.9976
$1d_{3/2}$	-19.19	-19.27	1.38	0.9963
$2s_{1/2}$	-18.55	-18.64	1.38	0.9958
$1f_{7/2}$	-15.07	-15.23	1.50	0.9891
$1f_{5/2}$	-9.89	-10.39	1.45	0.8959
$2p_{3/2}$	-9.38	-9.92	1.33	0.8589
$2p_{1/2}$	-7.88	-9.36	1.36	0.4546
$1g_{9/2}$	-6.98	-6.17	1.52	0.2202
$2d_{5/2}$	-1.34	-1.25	1.13	0.0071
$3s_{1/2}$	0.86	0.91	0.94	0.0028
$1g_{7/2}$	1.24	1.36	1.48	0.0063
$1h_{11/2}$	1.61	1.73	1.48	0.0058
$2d_{3/2}$	1.93	2.00	1.12	0.0031
$2f_{7/2}$	6.61	6.63	0.83	0.0008
$3p_{3/2}$	7.51	7.52	0.54	0.0003
$3p_{1/2}$	8.42	8.43	0.46	0.0002
$2f_{5/2}$	10.09	10.10	0.62	0.0003
$1i_{13/2}$	10.56	10.61	1.35	0.0013
$4s_{1/2}$	10.66	10.66	0.25	0.0001

Table 9: BCS-solution for proton states in ^{146}Gd

orbit a	$\varepsilon_{(sp)a}$ (MeV)	$\varepsilon_{(qp)a}$ (MeV)	Δ_a (MeV)	v_a^2
$1d_{5/2}$	-22.06	-22.11	1.43	0.9985
$1d_{3/2}$	-20.33	-20.38	1.39	0.9982
$2s_{1/2}$	-18.98	-19.04	1.37	0.9980
$1f_{7/2}$	-16.01	-16.10	1.53	0.9961
$1f_{5/2}$	-12.83	-12.94	1.47	0.9935
$2p_{3/2}$	-11.90	-12.03	1.43	0.9924
$2p_{1/2}$	-10.60	-10.75	1.43	0.9892
$1g_{9/2}$	-9.46	-9.68	1.49	0.9811
$1g_{7/2}$	-4.70	-5.59	1.54	0.7467
$2d_{5/2}$	-4.46	-5.36	1.40	0.7068
$1h_{11/2}$	-2.85	-2.01	1.62	0.2424
$3s_{1/2}$	-2.55	-1.93	1.29	0.1485
$2d_{3/2}$	-2.30	-1.74	1.41	0.1331
$2f_{7/2}$	2.54	2.67	1.26	0.0094
$1h_{9/2}$	4.55	4.70	1.57	0.0086
$3p_{3/2}$	4.65	4.71	1.00	0.0035
$1i_{13/2}$	4.85	5.00	1.61	0.0084
$3p_{1/2}$	5.69	5.74	0.97	0.0026
$2f_{5/2}$	5.80	5.88	1.24	0.0041
$2g_{9/2}$	9.52	9.56	1.00	0.0014
$3d_{5/2}$	10.37	10.39	0.60	0.0005
$4s_{1/2}$	10.39	10.40	0.47	0.0003
$3d_{3/2}$	11.28	11.29	0.50	0.0003
$1j_{15/2}$	12.51	12.58	1.52	0.0023
$2g_{7/2}$	12.70	12.72	0.77	0.0006

Table 10: Excitation energies and transition probabilities of the low-lying states in $^{146}_{64}Gd_{82}$

J^π	E_{exp} (keV)	E_{th} (keV)	$E_{exp}-E_{th}$ (keV)	B-value ($0^+ \to J^\pi$)	main config.	ε_{2qp} (keV)	X	Y
3_1^-	1579[a]	1555	24	0.363×10^6	$\pi 1h_{11/2}-2d_{5/2}^{-1}$	3428	0.7342	-0.2849
					$\nu 1h_{9/2}-2d_{3/2}^{-1}$	4930	0.3777	-0.1847
					$\nu 2f_{7/2}-3s_{1/2}^{-1}$	3500	0.2903	-0.1075
					$\nu 1i_{13/2}-1h_{11/2}^{-1}$	6280	0.2250	-0.1204
3_2^-	3423[b]	3561	-138	0.212×10^3	$\nu 2f_{7/2}-3s_{1/2}^{-1}$	3500	0.8086	0.0161
					$\nu 2f_{7/2}-2d_{3/2}^{-1}$	3530	0.5522	-0.0055
					$\pi 1h_{11/2}-2d_{5/2}^{-1}$	3428	-0.1122	0.0016
2^+	1972[a]	1968	4	0.448×10^4	$\nu 2f_{7/2}-1h_{11/2}^{-1}$	4230	0.5340	0.1837
					$\pi 2d_{3/2}-1g_{7/2}^{-1}$	3846	0.5074	0.1338
					$\pi 3s_{1/2}-2d_{5/2}^{-1}$	3349	0.3752	0.0785
					$(\pi 2d_{5/2})^{-2}$	3070	0.3463	0.0546
0_2^+	2165[d]	2524	-359	0.0117	$(\pi 1h_{11/2})^{-2}$	3786	-0.7006	0.1792
					$(\pi 1g_{7/2})^{-2}$	3530	0.5207	-0.1699
					$(\pi 2d_{5/2})^{-2}$	3070	0.5149	-0.1710
≤ 4	2612[c]	4^+:2466	146	0.856×10^7	$\pi 3s_{1/2}-1g_{7/2}^{-1}$	3579	0.4253	0.0665
					$\pi 2d_{3/2}-2d_{5/2}^{-1}$	3616	-0.3796	-0.0694
					$\pi 1g_{7/2}^{-1}-2d_{5/2}^{-1}$	3300	-0.3794	-0.0461
					$\nu 2f_{7/2}-1h_{11/2}^{-1}$	4230	-0.3647	-0.0885
					$(\pi 2d_{5/2})^{-2}$	3070	-0.3369	-0.0271
5^-	2658[a]	2845	-187	0.287×10^9	$\pi 1h_{11/2}-2d_{5/2}^{-1}$	3428	0.7655	-0.0714
					$\nu 2f_{7/2}-2d_{3/2}^{-1}$	3530	-0.3798	0.0532
7^-	2982[a]	3379	-397	0.136×10^{12}	$\pi 1h_{11/2}-2d_{5/2}^{-1}$	3428	-0.9874	0.0068
4^-	2996[c]	3435	-439	0.890×10^6	$\pi 1h_{11/2}-2d_{5/2}^{-1}$	3428	0.9850	-0.0031
6^-	3099[c]	3468	-369	0.664×10^{10}	$\pi 1h_{11/2}-2d_{5/2}^{-1}$	3428	-0.9703	0.0064
8_1^-	3183[a]	3590	-407	0.360×10^{14}	$\pi 1h_{11/2}-2d_{5/2}^{-1}$	3428	-0.9151	0.0203
					$\pi 1h_{11/2}-1g_{7/2}^{-1}$	3658	0.4025	0.0045
8_2^-	3294[a]	3672	-378	0.760×10^{13}	$\pi 1h_{11/2}-1g_{7/2}^{-1}$	3658	0.9137	-0.0073
					$\pi 1h_{11/2}-2d_{5/2}^{-1}$	3428	0.4023	-0.0168
9^-	3429[a]	3825	-396	0.439×10^{15}	$\pi 1h_{11/2}-1g_{7/2}^{-1}$	3658	-0.9945	0.0528
10^+	3865[a]	3763	102	0.522×10^{16}	$(\pi 1h_{11/2})^2$	3786	0.9912	-0.0015

Table 11: Quadrupole vibrational states in $^{146}_{64}Gd_{82}$

J^π	E_{th} (keV) $(0^+ \to J^\pi)$	B-value	main config.	ε_{2qp} (keV)	X	Y
2_1^+	1968	0.448×10^4	$\nu 2f_{7/2}\text{-}1h_{11/2}^{-1}$	4230	0.5340	0.1837
			$\pi 2d_{3/2}\text{-}1g_{7/2}^{-1}$	3846	0.5074	0.1338
			$\pi 3s_{1/2}\text{-}2d_{5/2}^{-1}$	3349	0.3752	0.0785
			$(\pi 2d_{5/2})^{-2}$	3070	0.3463	0.0546
2_2^+	3161	0.419×10^2	$(\pi 2d_{5/2})^{-2}$	3070	-0.9211	0.0296
			$\pi 3s_{1/2}\text{-}2d_{5/2}^{-1}$	3349	0.2916	0.0168
2_3^+	3371	0.183	$(\pi 1g_{7/2}\text{-}2d_{5/2})^{-2}$	3300	0.7014	-0.0022
			$(\pi 1g_{7/2})^{-2}$	3530	-0.4932	0.0188
2_4^+	3403	0.614×10^2	$(\pi 1h_{11/2})^2$	3786	-0.5300	0.0125
			$(\pi 1g_{7/2})^{-2}$	3530	0.4852	-0.0221
2_5^+	3505	0.462×10^2	$\pi 3s_{1/2}\text{-}2d_{5/2}^{-1}$	3349	0.7531	-0.0286
			$(\pi 1g_{7/2})^{-2}$	3530	-0.4815	-0.0061

Table 12: Excitation energies and transition probabilities of the low-lying states in $^{142}_{60}Nd_{82}$

J^π	E_{exp} [a] (keV)	E_{th} (keV)	$E_{exp}-E_{th}$ (keV)	B-value ($0^+ \to J^\pi$)	main config.	ε_{2qp} (keV)	X	Y
2^+	1576	2019	-443	0.321×10^4	$(\pi 2d_{5/2})^{-2}$	2655	-0.5465	-0.0437
					$\nu 2f_{7/2}\text{-}1h_{11/2}^{-1}$	4230	-0.4607	-0.1533
					$\pi 2d_{3/2}\text{-}1g_{7/2}^{-1}$	3994	-0.4021	-0.0996
					$\pi 1g_{7/2}^{-1}\text{-}2d_{5/2}^{-1}$	2819	-0.3230	-0.0444
(3^-)	2084	2501	-417	0.140×10^6	$\pi 1h_{11/2}\text{-}2d_{5/2}^{-1}$	3515	-0.7173	0.1032
					$\nu 2f_{7/2}\text{-}3s_{1/2}^{-1}$	3500	-0.3083	0.0480
(4^+)	2100	2329	-229	0.555×10^7	$\pi 1g_{7/2}^{-1}\text{-}2d_{5/2}^{-1}$	2819	0.5614	0.0416
					$(\pi 2d_{5/2})^{-2}$	2655	0.5354	0.0219
(6^+)	2210	2509	-299	0.585×10^{10}	$\pi 1g_{7/2}^{-1}\text{-}2d_{5/2}^{-1}$	2819	-0.9223	-0.0287
					$(\pi 1g_{7/2})^{-2}$	2983	-0.2249	-0.0130
0^+	2217	2492	-275	0.176	$(\pi 2d_{5/2})^{-2}$	2655	-0.6230	0.2227
					$(\pi 1h_{11/2})^{2}$	4375	0.6138	-0.1174
					$(\pi 1g_{7/2})^{-2}$	2983	-0.5675	0.2283
2^+	2385	2852	-467	0.852×10^2	$(\pi 2d_{5/2})^{-2}$	2655	0.7670	-0.0358
					$(\pi 1g_{7/2})^{-2}$	2983	-0.4526	-0.0017
					$\pi 1g_{7/2}^{-1}\text{-}2d_{5/2}^{-1}$	2819	-0.3833	-0.0062
2^+	2583	2937	-354	0.677×10^2	$\pi 1g_{7/2}^{-1}\text{-}2d_{5/2}^{-1}$	2819	-0.7697	0.0140
					$(\pi 1g_{7/2})^{-2}$	2983	0.6233	-0.0163

Table 13: Excitation energies and transition probabilities of the low-lying states in $^{144}_{62}Sm_{82}$

J^π	E_{exp} (keV)	E_{th} (keV)	$E_{exp}-E_{th}$ (keV)	B-value ($0^+ \to J^\pi$)	main config.	ε_{2qp} (keV)	X	Y
2^+	1660[a]	1998	-338	0.388×10^4	$\nu 2f_{7/2}\text{-}1h_{11/2}^{-1}$	4230	0.5041	0.1699
					$\pi 2d_{5/2}^{-1}\text{-}1g_{9/2}^{-1}$	3903	0.4651	0.1180
					$(\pi 2d_{5/2})^{-2}$	2822	0.4553	0.0513
					$\pi 3s_{1/2}\text{-}2d_{5/2}^{-1}$	3419	0.3406	0.0672
3^-	1810[a]	2021	-211	0.228×10^6	$\pi 1h_{11/2}\text{-}2d_{5/2}^{-1}$	3444	-0.7202	0.1835
					$\nu 2f_{7/2}\text{-}3s_{1/2}^{-1}$	3500	-0.2888	0.0733
4^+	2190[a]	2399	-209	0.711×10^7	$\pi 1g_{7/2}^{-1}\text{-}2d_{5/2}^{-1}$	3024	-0.4866	-0.0453
					$(\pi 2d_{5/2})^{-2}$	2822	-0.4591	-0.0252
					$\pi 3s_{1/2}\text{-}1g_{7/2}^{-1}$	3620	0.3487	0.0583
6^+	2323[a]	2703	-383	0.593×10^3	$\pi 1g_{7/2}^{-1}\text{-}2d_{5/2}^{-1}$	3024	-0.9182	-0.0286
					$(\pi 1g_{7/2})^{-2}$	3226	-0.2028	-0.0125
2^+	2424[a]	2989	-565	0.923×10^2	$(\pi 2d_{5/2})^{-2}$	2822	-0.8675	0.0372
					$\pi 3s_{1/2}\text{-}2d_{5/2}^{-1}$	3419	0.2506	0.0207
					$(\pi 1g_{7/2})^{-2}$	3226	0.2460	0.0087
					$\pi 1g_{7/2}^{-1}\text{-}2d_{5/2}^{-1}$	3024	0.2424	-0.0010
0^+	2479[a]	2507	-28	0.069	$(\pi 1h_{11/2})^2$	4065	-0.6591	0.1467
					$(\pi 2d_{5/2})^{-2}$	2822	0.5727	-0.1994
					$(\pi 1g_{7/2})^{-2}$	3226	0.5477	-0.2005
4^+	2588[a]	2938	-350	0.221×10^6	$(\pi 2d_{5/2})^{-2}$	2822	0.8714	-0.0225
					$\pi 1g_{7/2}^{-1}\text{-}2d_{5/2}^{-1}$	3024	-0.3741	-0.0012
2^+	2800[a]	3134	-334	0.604×10^2	$\pi 1g_{7/2}^{-1}\text{-}2d_{5/2}^{-1}$	3024	0.8485	-0.0139
					$(\pi 1g_{7/2})^{-2}$	3226	-0.4830	0.0097
5^-	2824[b]	3002	-178	0.189×10^9	$\pi 1h_{11/2}\text{-}2d_{5/2}^{-1}$	3444	0.8009	-0.0498
					$\nu 2f_{7/2}\text{-}2d_{3/2}^{-1}$	3530	-0.3407	0.0398
4^+	2887[a]	3183	-299	0.369×10^6	$\pi 1g_{7/2}^{-1}\text{-}2d_{5/2}^{-1}$	3024	-0.6857	0.0179
					$(\pi 1g_{7/2})^{-2}$	3226	0.6297	-0.0031
7^-	3136[b]	3394	-274	0.127×10^{12}	$\pi 1h_{11/2}\text{-}2d_{5/2}^{-1}$	3444	-0.9872	0.0065
8^-	3376[b]	3594	-214	0.290×10^{14}	$\pi 1h_{11/2}\text{-}2d_{5/2}^{-1}$	3444	-0.8694	0.0176
					$\pi 1h_{11/2}\text{-}1g_{7/2}^{-1}$	3645	0.4934	0.0035
9^-	3461[b]	3803	-343	0.429×10^{15}	$\pi 1h_{11/2}\text{-}1g_{7/2}^{-1}$	3645	0.9947	-0.0519
8^-	3518[b]	3663	-143	1.00×10^{13}	$\pi 1h_{11/2}\text{-}2d_{5/2}^{-1}$	3444	-0.8680	0.0074
					$\pi 1h_{11/2}\text{-}1g_{7/2}^{-1}$	3645	-0.4933	0.0179

Table 14: Excitation energies and transition probabilities of the low-lying states in $^{148}_{66}Dy_{82}$

J^π	E_{exp} [a] (keV)	E_{th} (keV)	$E_{exp}-E_{th}$ (keV)	B-value ($0^+ \to J^\pi$)	main config.	ε_{2qp} (keV)	X	Y
2^+	1678	1919	-241	0.497×10^4	$\nu 2f_{7/2}\text{-}1h_{11/2}^{-1}$	4230	-0.5468	-0.1943
					$\pi 2d_{3/2}\text{-}1g_{7/2}^{-1}$	3831	-0.5199	-0.1455
					$\pi 3s_{1/2}\text{-}2d_{5/2}^{-1}$	3343	-0.3780	-0.0862
					$(\pi 1h_{11/2})^2$	3564	-0.2693	-0.1056
3^-	1688	1798	-110	0.295×10^6	$\pi 1h_{11/2}\text{-}2d_{5/2}^{-1}$	3479	-0.7156	0.2296
					$\nu 2f_{7/2}\text{-}3s_{1/2}^{-1}$	3500	-0.2937	0.0906
5^-	2349	2816	-467	0.191×10^9	$\pi 1h_{11/2}\text{-}2d_{5/2}^{-1}$	3479	0.6353	-0.0611
					$\pi 1h_{11/2}\text{-}3s_{1/2}$	3428	-0.3983	0.0270
4^+	2428	2514	-86	0.933×10^7	$\pi 3s_{1/2}\text{-}1g_{7/2}^{-1}$	3591	0.4585	0.0705
					$\pi 2d_{3/2}\text{-}2d_{5/2}^{-1}$	3583	-0.4156	-0.0758
					$\nu 2f_{7/2}\text{-}1h_{11/2}^{-1}$	4230	-0.3834	-0.0897
					$(\pi 1h_{11/2})^2$	3564	-0.3058	-0.0638
6^+	2733	3227	-494	0.719×10^{10}	$\pi 1g_{7/2}^{-1}\text{-}2d_{5/2}^{-1}$	3641	-0.7528	-0.0351
					$(\pi 1h_{11/2})^2$	3564	-0.4916	-0.0277
7^-	2739	3428	-689	0.153×10^{12}	$\pi 1h_{11/2}\text{-}2d_{5/2}^{-1}$	3479	-0.9832	0.0069
					$\pi 1h_{11/2}\text{-}2d_{3/2}$	3669	0.1197	-0.0066
8^+	2834	3495	-661	0.379×10^{13}	$(\pi 1h_{11/2})^2$	3564	-0.9848	-0.0010
10^+	2920	3546	-626	0.606×10^{16}	$(\pi 1h_{11/2})^2$	3564	0.9912	-0.0023

Table 15: Excitation energies and transition probabilities of the low-lying states in $^{150}_{68}Er_{82}$

J^π	E_{exp} [a] (keV)	E_{th} (keV)	$E_{exp}-E_{th}$ (keV)	B-value ($0^+ \to J^\pi$)	main config.	ε_{2qp} (keV)	X	Y
2^+	1579	1868	-289	0.529×10^4	$\nu 2f_{7/2}\text{-}1h_{11/2}^{-1}$	4230	0.5461	0.2009
					$\pi 2d_{3/2}\text{-}1g_{7/2}^{-1}$	3857	0.5081	0.1520
					$\pi 3s_{1/2}\text{-}2d_{5/2}^{-1}$	3397	0.3549	0.0889
					$\pi 2d_{3/2}\text{-}3s_{1/2}$	3231	0.3240	0.0728
					$(\pi 1h_{11/2})^2$	3410	0.3173	0.1134
(3^-)	1786	2060	-274	0.244×10^6	$\pi 1h_{11/2}\text{-}2d_{5/2}^{-1}$	3588	-0.6925	0.1816
					$\nu 2f_{7/2}\text{-}3s_{1/2}^{-1}$	3500	-0.3068	0.0764
(5^-)	2261	2724	-463	0.866×10^8	$\pi 1h_{11/2}\text{-}3s_{1/2}$	3219	-0.6413	0.0411
					$\pi 1h_{11/2}\text{-}2d_{5/2}^{-1}$	3588	0.4213	-0.0470
6^+	2621	3247	-626	0.498×10^{10}	$(\pi 1h_{11/2})^2$	3410	-0.9209	-0.0123
					$\pi 1g_{7/2}^{-1}\text{-}2d_{5/2}^{-1}$	4023	-0.2444	-0.0317
(7^-)	2633	3383	-750	0.167×10^{12}	$\pi 1h_{11/2}\text{-}2d_{3/2}$	3422	-0.9801	0.0186
(8^+)	2734	3343	-609	0.420×10^{13}	$(\pi 1h_{11/2})^2$	3410	-0.9855	-0.0006
(10^+)	2792	3396	-599	0.675×10^{16}	$(\pi 1h_{11/2})^2$	3410	0.9911	-0.0030

FIGURE CAPTIONS

Figure 1: Occupation probabilities for a) a system of independent particles; b) a system of independent quasiparticles. The action of the pairing correlations permits that some of the particles are excited from the occupied single-particle levels to the unoccupied ones and gives rise to a smeared out particle distribution.

Figure 2: Graphical representation of the perturbative expansion (B.7) of the generalized Green's functions using the usual Feynman rules.

Figure 3: Graphical representation of the matrix elements of the particle-particle interaction $F^{pp}_{\alpha\beta\gamma\delta}$, of the direct matrix elements of the particle-hole $F^{ph}_{\alpha\beta\gamma\delta}$ and of the exchange ones $F^{ph\ exch}_{\alpha\beta\gamma\delta}$, which enter in equations (B.10).

Figure 4: In the left part of the figure we draw the proton single-particle energies obtained from the Woods-Saxon diagonalization for ^{88}Sr. In the middle the corresponding quasiparticle energies ε_{qp} (see caption of Table 7) obtained after the solution of the BCS-equations and to the right the experimental energies taken from (Isa82).

Figure 5: The same as in Fig. 4 for ^{90}Zr. The experimental values are taken from (Wap77,Isa82).

Figure 6: The same as in Fig. 4 for ^{146}Gd. The experimental values are taken from (Klz79).

Figure 7: Experimental low-energy level schemes of the four odd-even nuclei around $^{146}_{64}Gd_{82}$. The data are taken respectively from:

(Wil71,Led82) for $^{145}_{63}Eu$,

(Brd79,Nag81) for $^{145}_{65}Tb$,

(Pak82) for $^{147}_{64}Gd$ and

(Klz79,Klz82,Pii82) for $^{147}_{64}Gd$.

The predominantly single-particle levels are labelled. In ^{147}Tb, the position of the $h_{11/2}$ single-particle state relative to the four positive parity levels shown is not known in detail, but is assumed to be within about $\pm$200 keV of the $1/2^+$ state.

Figure 8: Experimental and theoretical level schemes of the nucleus $^{146}_{64}Gd_{82}$ up to ~ 4 MeV. The second level scheme is calculated in the framework of the QRPA-theory using in addition to a density-dependent zero-range force the contribution of the one-pion and one-rho exchange potential. For the experimental references see caption to Table 10.

Figure 9: Quasiparticle energies E and occupation probabilities v^2, obtained solving the BCS-equations (2.6) and (2.7) using a realistic pairing force F^{pair} (see section 3.3) for the N=82 isotones with $60<Z<68$. The results are given for the proton orbits of the N=4 major shell. The energies are given in MeV and the occupation probabilities are dimensionless.

Figure 10: Comparison between the experimental (dashed line) and the calculated (full line) excitation energies for the even-even nuclei ^{142}Nd, ^{144}Sm, ^{146}Gd, ^{148}Dy and ^{150}Er. For the experimental references see the captions to Tables 10, 12, 13, 14 and 15. All the measured levels up to about 4 MeV are represented.

Figure 11: Proton and neutron levels for ^{146}Gd near the Fermi surface (for protons see Table 9 and for neutrons Table 4). The dashed line indicates the Fermi surface, which for protons is smeared out due to the pairing correlations. The full and empty circles represent a particle-hole-like and the two half-full circles a quasiparticle-like excitation.

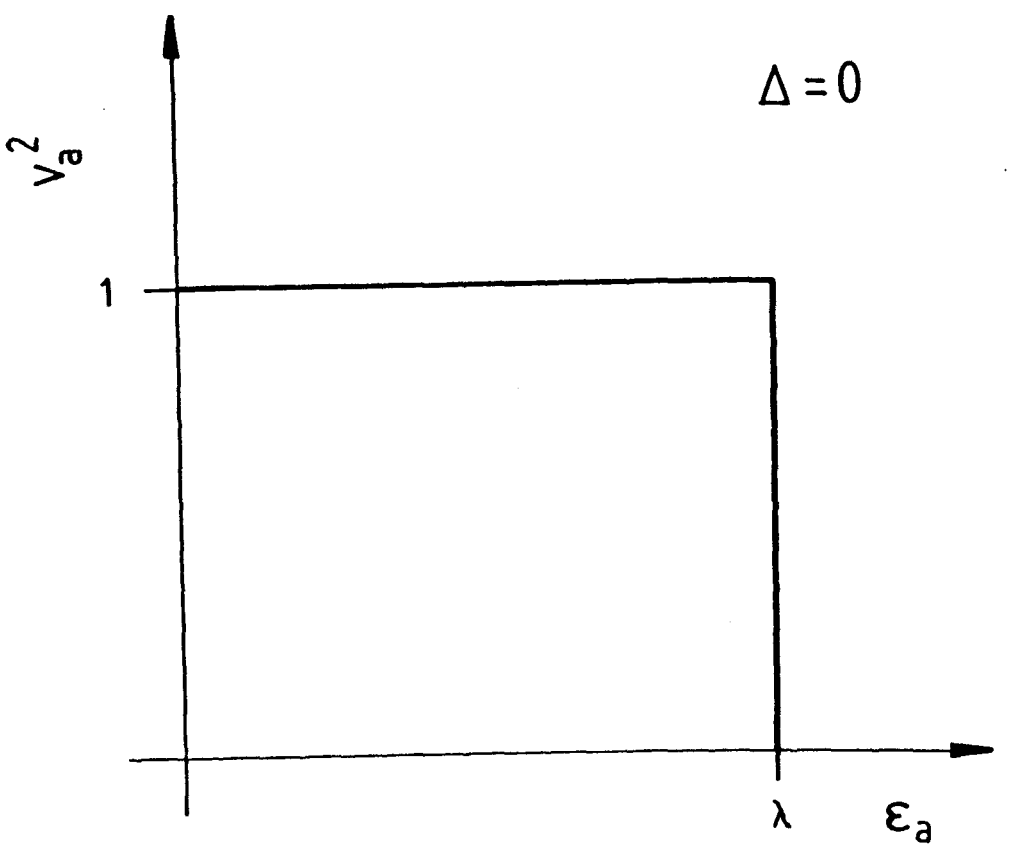

a

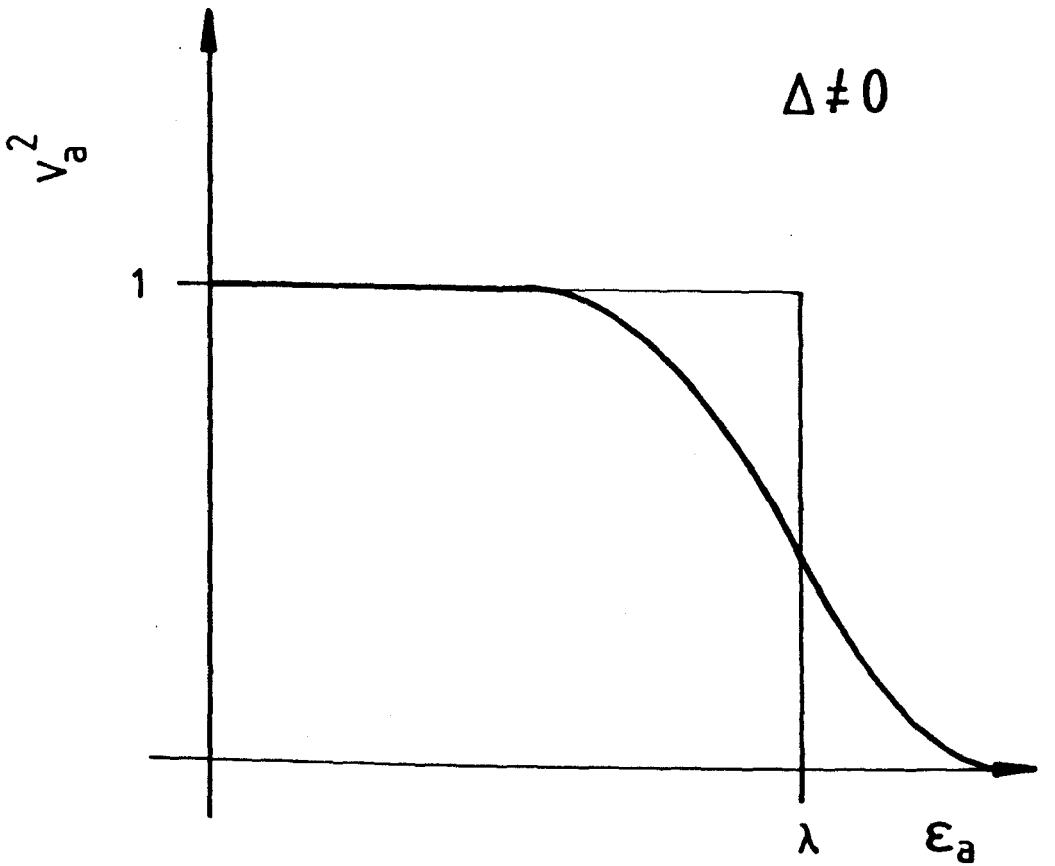

b

Figure 1

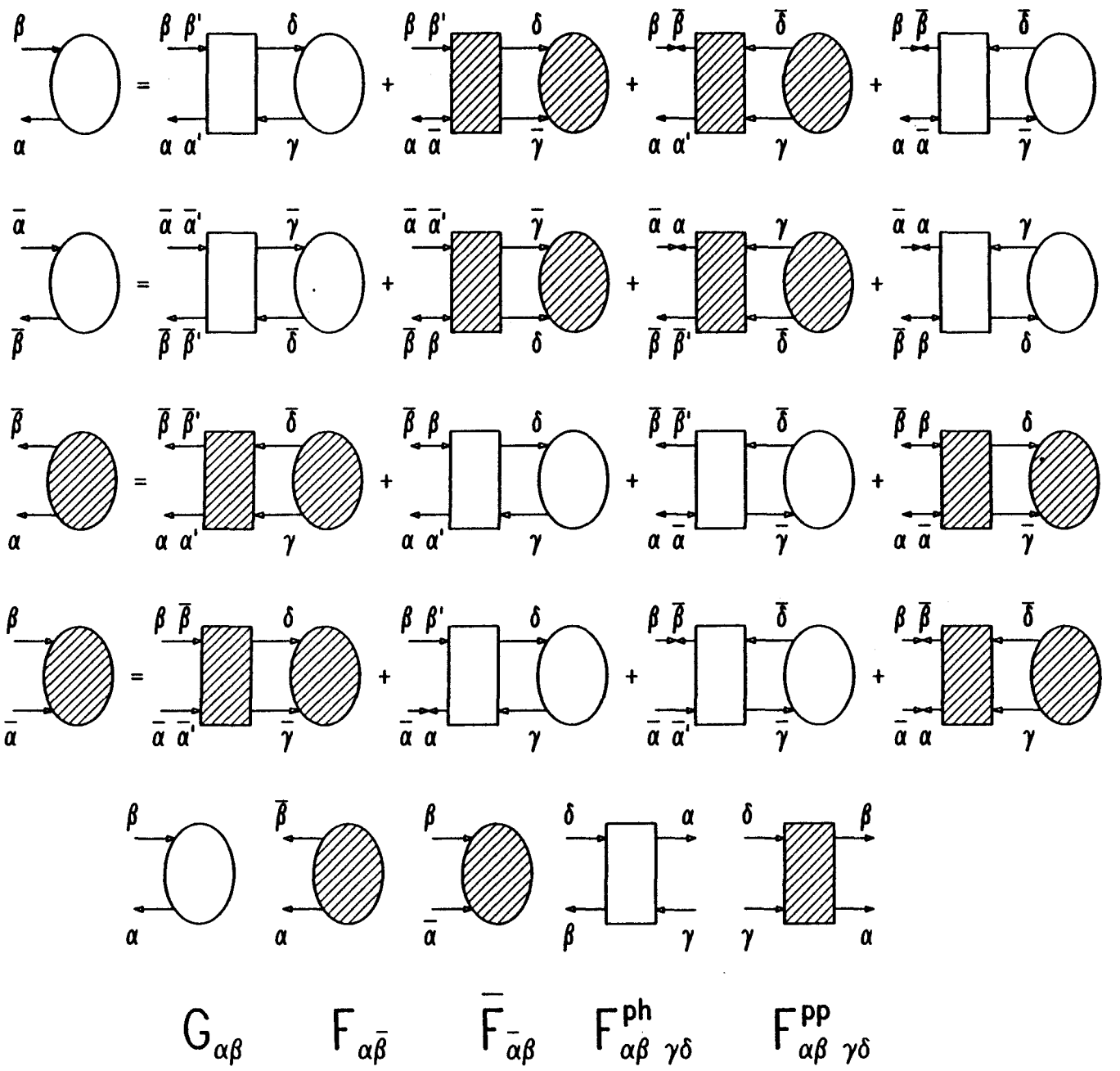

Figure 2

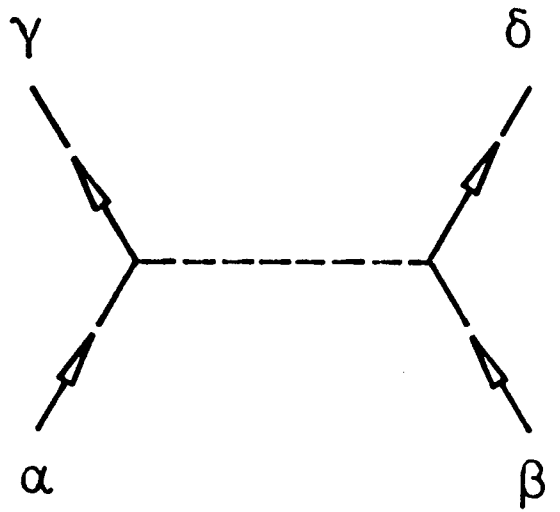

$F^{pp}_{\alpha\beta\ \gamma\delta}$

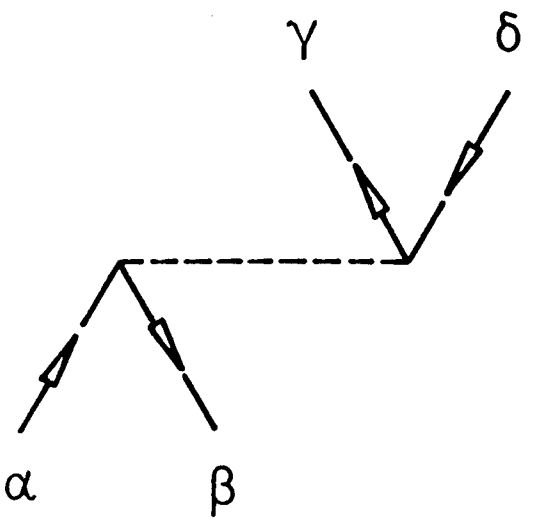

$F^{ph}_{\alpha\beta\ \gamma\delta}$

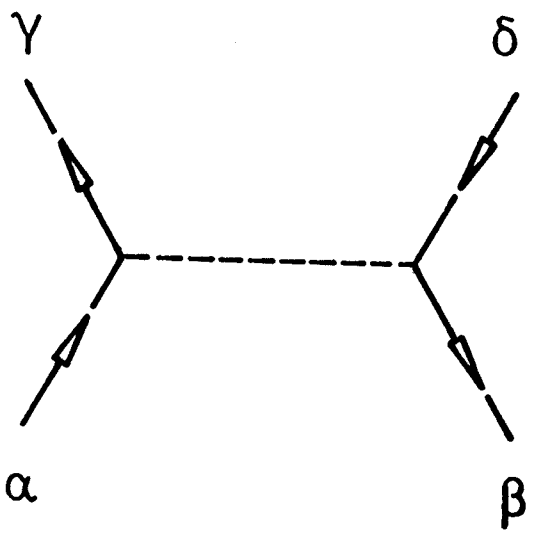

$F^{ph,\,exch}_{\alpha\beta\ \gamma\delta}$

Figure 3

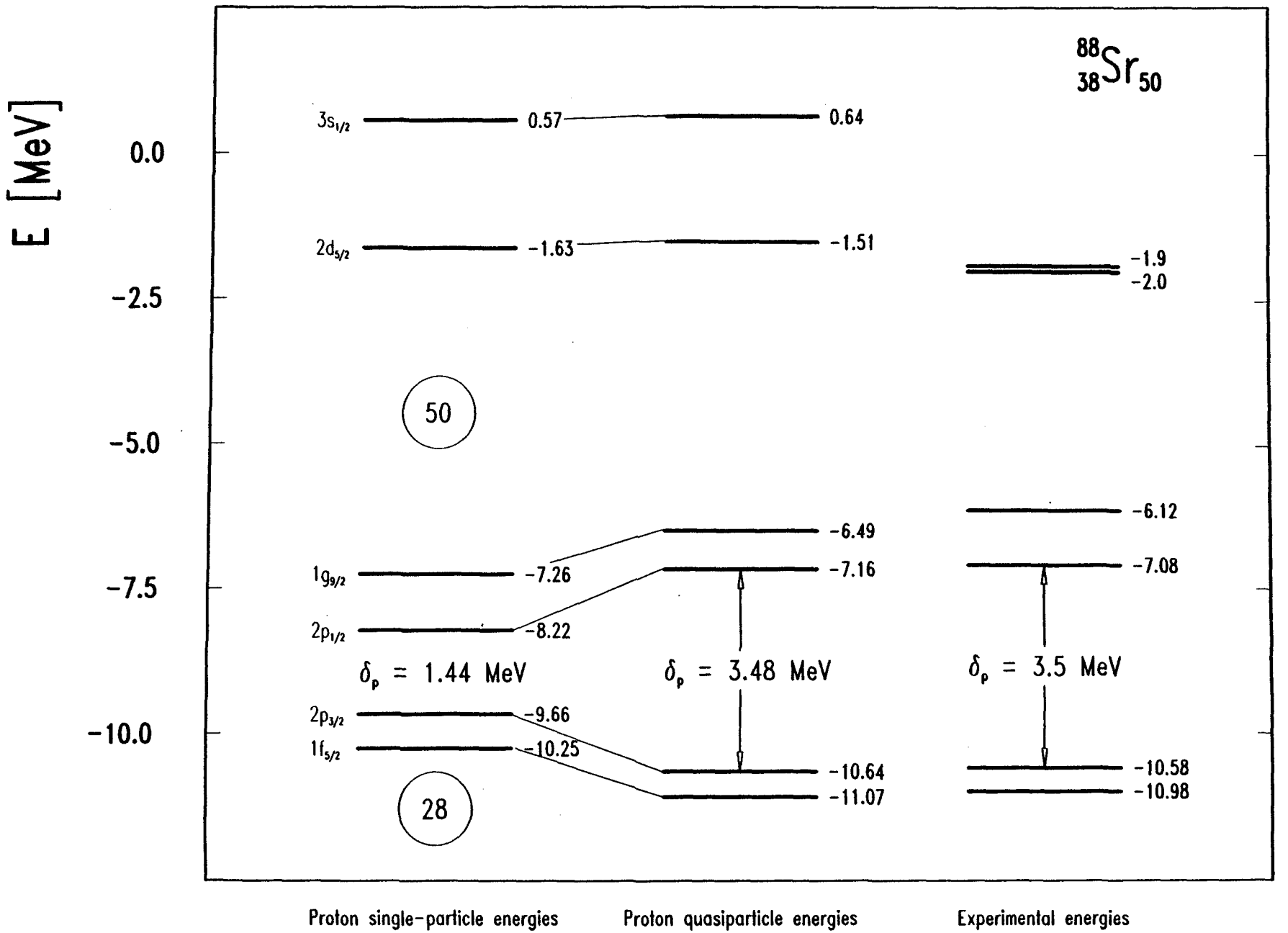
E [MeV]
0.0
-2.5
-5.0
-7.5
-10.0
$^{88}_{38}Sr_{50}$
$3s_{1/2}$
0.57
0.64
$2d_{5/2}$
-1.63
-1.51
-1.9
-2.0
50
-6.12
-6.49
$1g_{9/2}$
-7.26
-7.16
-7.08
$2p_{1/2}$
-8.22
δ_p = 1.44 MeV
δ_p = 3.48 MeV
δ_p = 3.5 MeV
$2p_{3/2}$
-9.66
$1f_{5/2}$
-10.25
-10.64
-11.07
-10.58
-10.98
28
Proton single-particle energies
Proton quasiparticle energies
Experimental energies

Figure 4

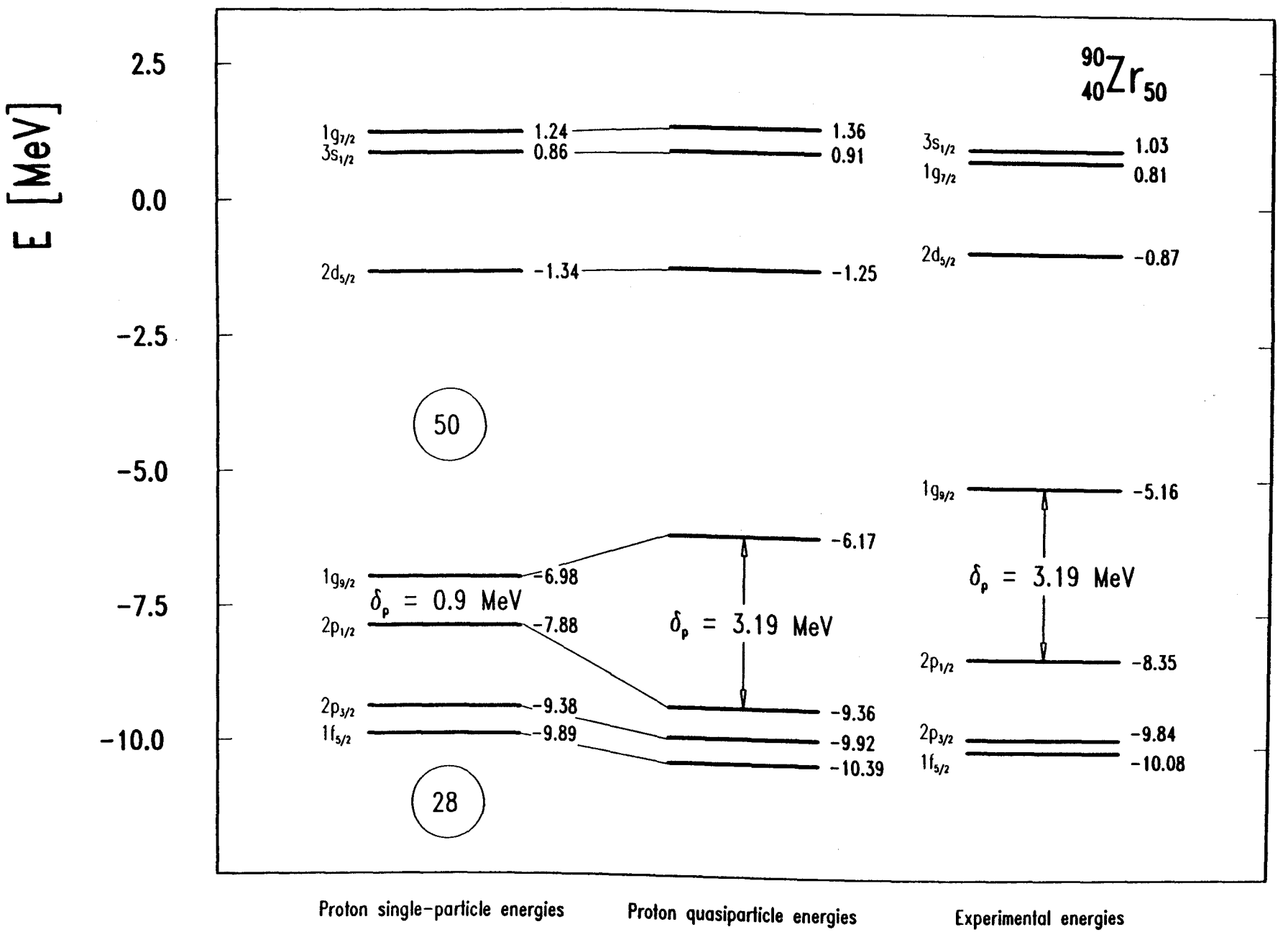
E [MeV]
2.5
0.0
-2.5
-5.0
-7.5
-10.0
$^{90}_{40}Zr_{50}$
$1g_{7/2}$ 1.24
$3s_{1/2}$ 0.86
$2d_{5/2}$ -1.34
50
$1g_{9/2}$ -6.98
$2p_{1/2}$ -7.88
δ_p = 0.9 MeV
$2p_{3/2}$ -9.38
$1f_{5/2}$ -9.89
28
Proton single-particle energies
1.36
0.91
-1.25
-6.17
δ_p = 3.19 MeV
-9.36
-9.92
-10.39
Proton quasiparticle energies
$3s_{1/2}$ 1.03
$1g_{7/2}$ 0.81
$2d_{5/2}$ -0.87
$1g_{9/2}$ -5.16
δ_p = 3.19 MeV
$2p_{1/2}$ -8.35
$2p_{3/2}$ -9.84
$1f_{5/2}$ -10.08
Experimental energies

Figure 5

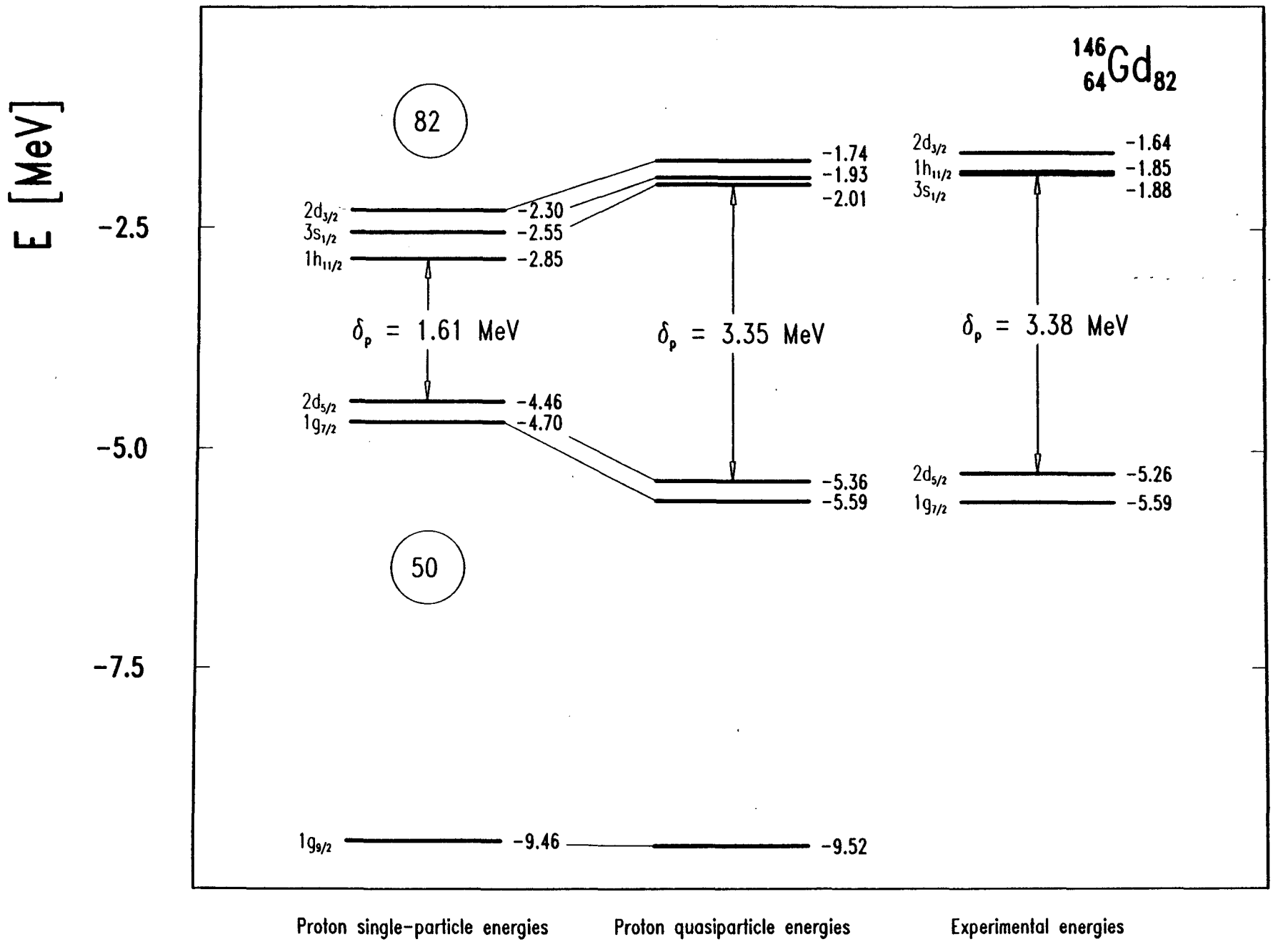
E [MeV]
-2.5
-5.0
-7.5
$^{146}_{64}Gd_{82}$
82
50
$2d_{3/2}$
$3s_{1/2}$
$1h_{11/2}$
$2d_{5/2}$
$1g_{7/2}$
$1g_{9/2}$
-2.30
-2.55
-2.85
-4.46
-4.70
-9.46
δ_p = 1.61 MeV
-1.74
-1.93
-2.01
-5.36
-5.59
-9.52
δ_p = 3.35 MeV
-1.64
-1.85
-1.88
-5.26
-5.59
δ_p = 3.38 MeV
Proton single-particle energies
Proton quasiparticle energies
Experimental energies

Figure 6

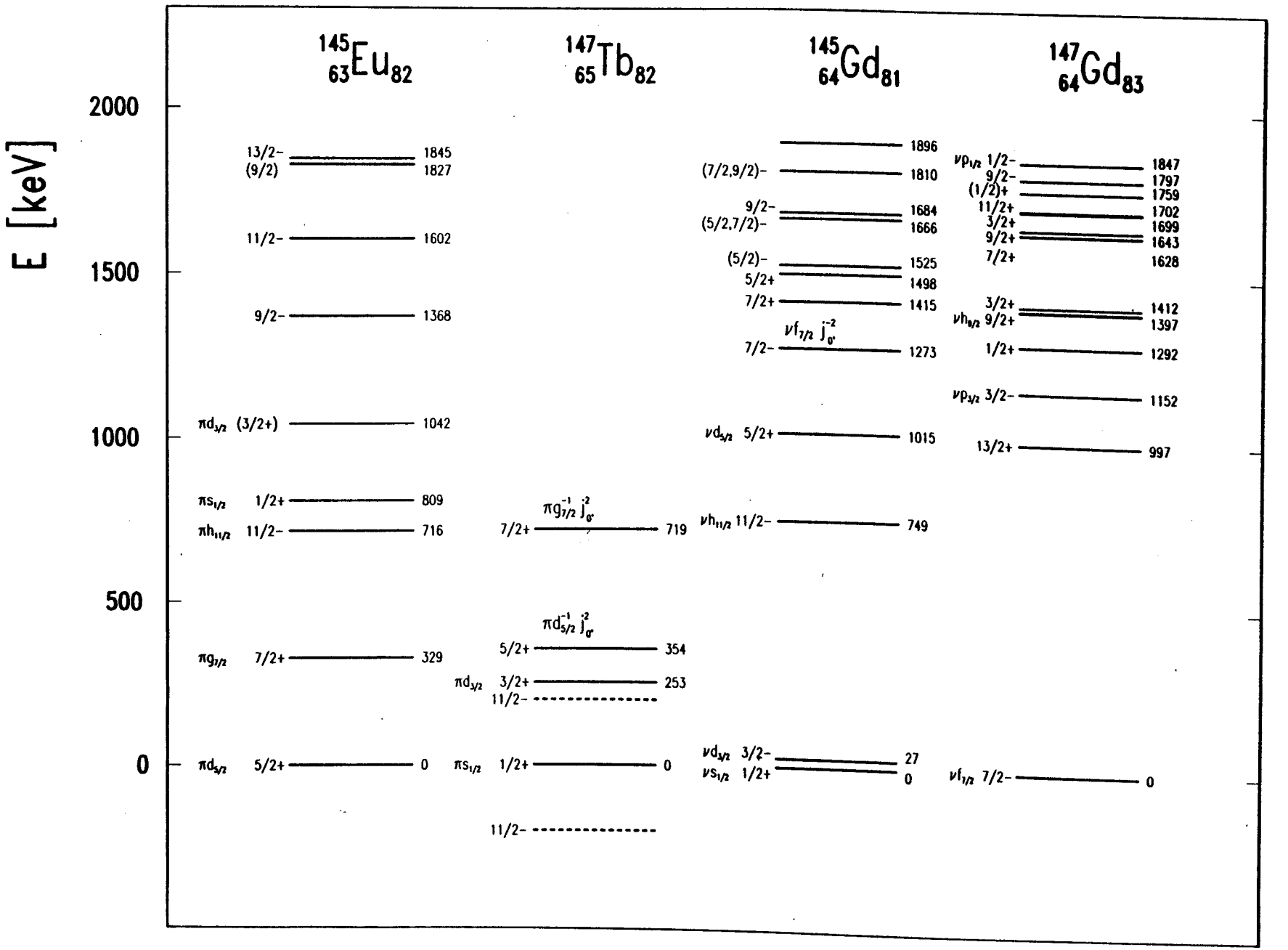
E [keV]
2000
1500
1000
500
0
$^{145}_{63}Eu_{82}$
13/2- 1845
(9/2) 1827
11/2- 1602
9/2- 1368
πd3/2 (3/2+) 1042
πs1/2 1/2+ 809
πh11/2 11/2- 716
πg7/2 7/2+ 329
πd5/2 5/2+ 0
$^{147}_{65}Tb_{82}$
πg7/2^-1 j^2 0+
7/2+ 719
πd5/2^-1 j^2 0+
5/2+ 354
πd3/2 3/2+ 253
11/2- ----------
πs1/2 1/2+ 0
11/2- ----------
$^{145}_{64}Gd_{81}$
1896
(7/2,9/2)- 1810
9/2- 1684
(5/2,7/2)- 1666
(5/2)- 1525
5/2+ 1498
7/2+ 1415
νf7/2 j^-2 0+
7/2- 1273
νd5/2 5/2+ 1015
νh11/2 11/2- 749
νd3/2 3/2- 27
νs1/2 1/2+ 0
$^{147}_{64}Gd_{83}$
νp1/2 1/2- 1847
9/2- 1797
(1/2)+ 1759
11/2+ 1702
3/2+ 1699
9/2+ 1643
7/2+ 1628
3/2+ 1412
νh9/2 9/2+ 1397
1/2+ 1292
νp3/2 3/2- 1152
13/2+ 997
νf7/2 7/2- 0

Figure 7

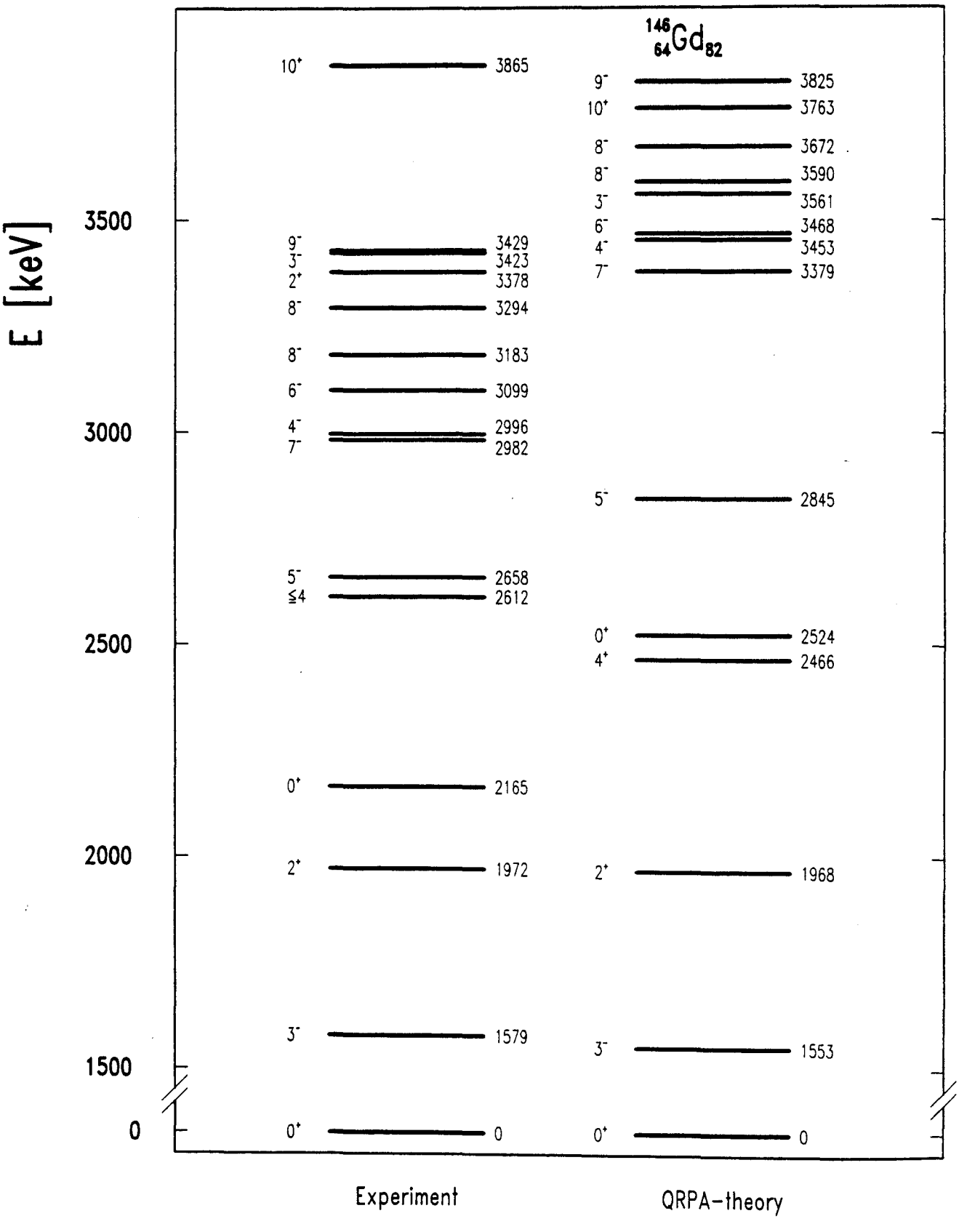
$^{146}_{64}Gd_{82}$
E [keV]
3500
3000
2500
2000
1500
0
10+ 3865
9- 3429
3- 3423
2+ 3378
8- 3294
8- 3183
6- 3099
4- 2996
7- 2982
5- 2658
≦4 2612
0+ 2165
2+ 1972
3- 1579
0+ 0
9- 3825
10+ 3763
8- 3672
8- 3590
3- 3561
6- 3468
4- 3453
7- 3379
5- 2845
0+ 2524
4+ 2466
2+ 1968
3- 1553
0+ 0
Experiment
QRPA-theory

Figure 8

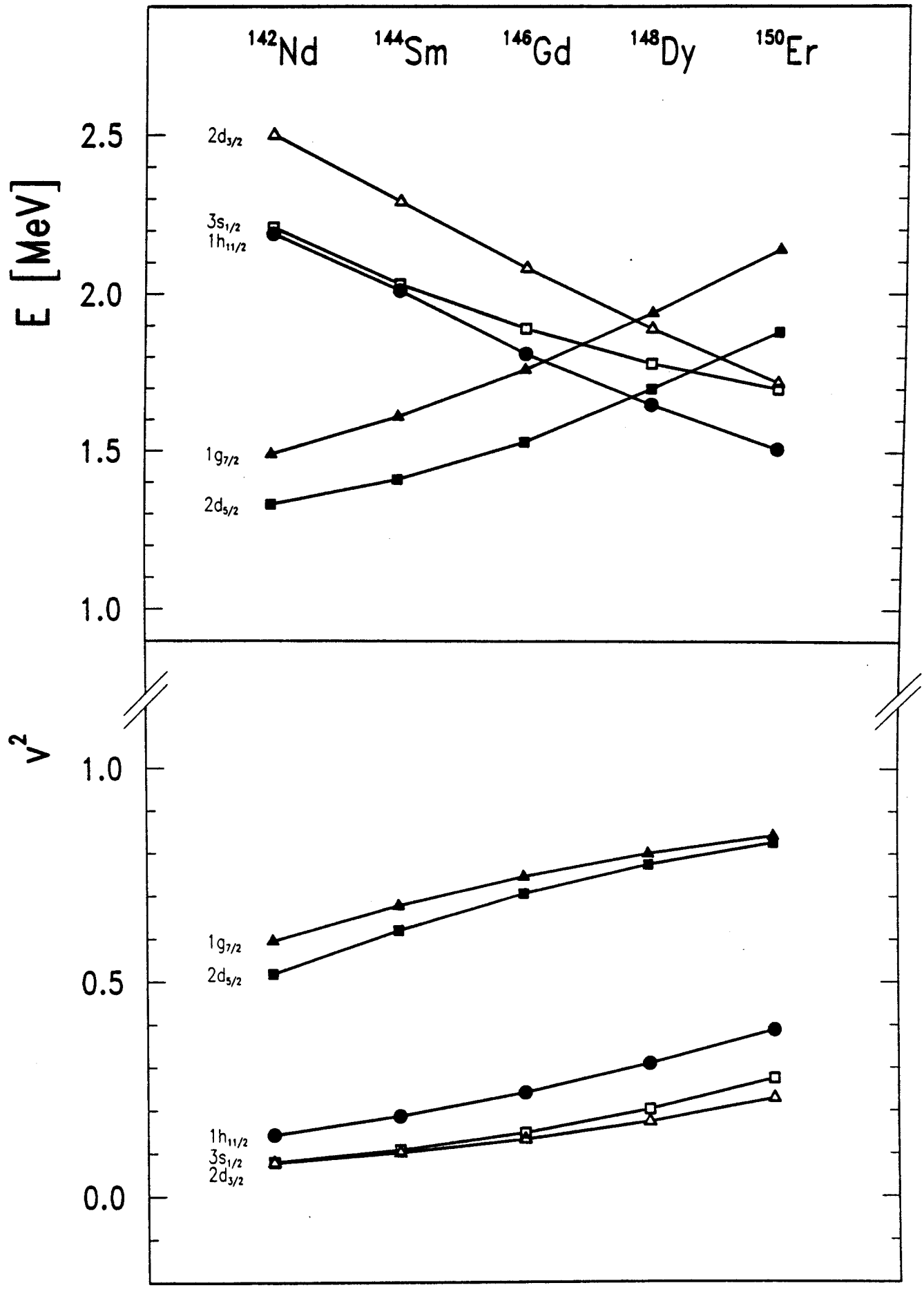
142Nd
144Sm
146Gd
148Dy
150Er
E [MeV]
2.5
2.0
1.5
1.0
2d3/2
3s1/2
1h11/2
1g7/2
2d5/2
v2
1.0
0.5
0.0
1g7/2
2d5/2
1h11/2
3s1/2
2d3/2

Figure 9

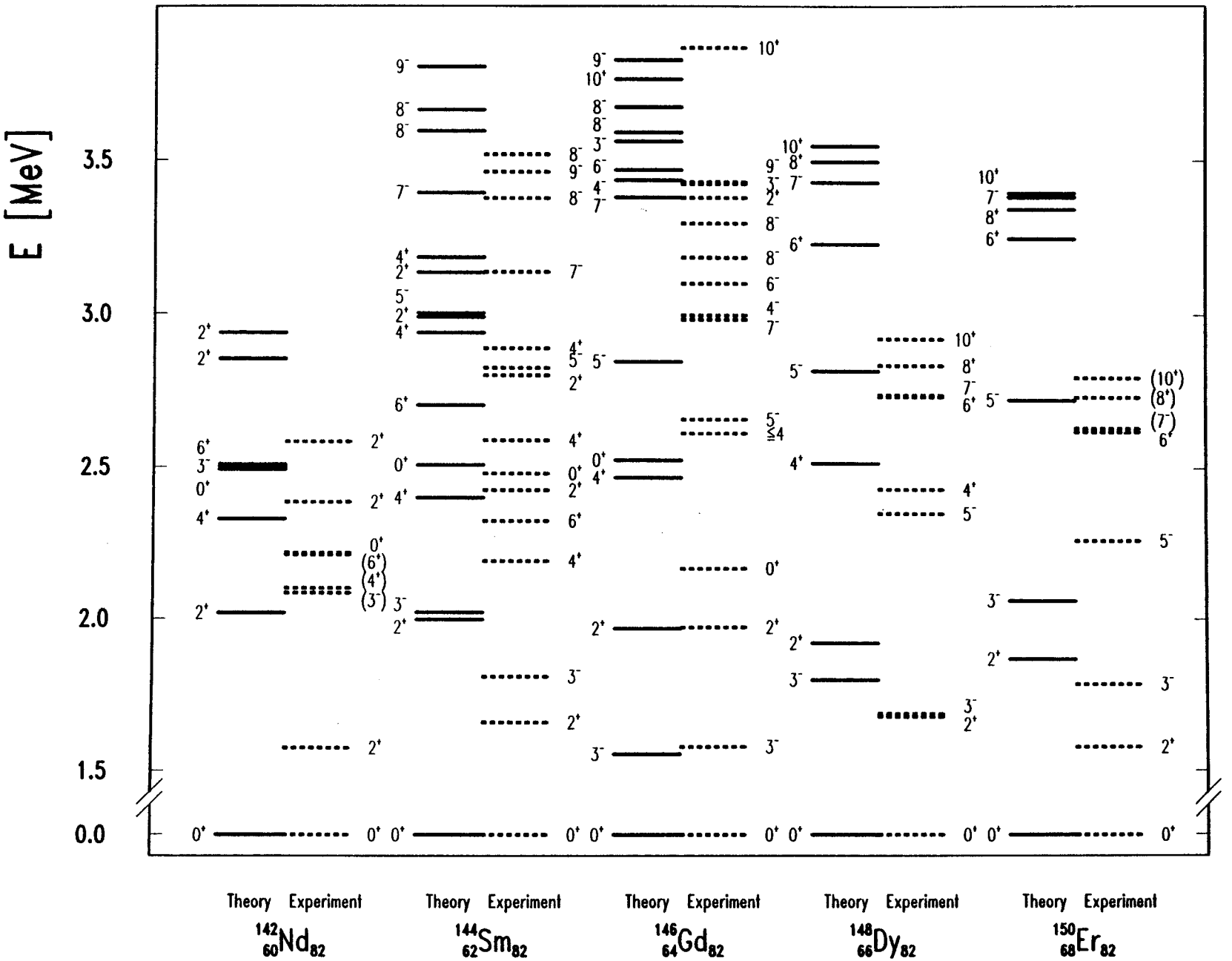
E [MeV]
3.5
3.0
2.5
2.0
1.5
0.0
Theory Experiment
$^{142}_{60}Nd_{82}$
Theory Experiment
$^{144}_{62}Sm_{82}$
Theory Experiment
$^{146}_{64}Gd_{82}$
Theory Experiment
$^{148}_{66}Dy_{82}$
Theory Experiment
$^{150}_{68}Er_{82}$

Figure 10

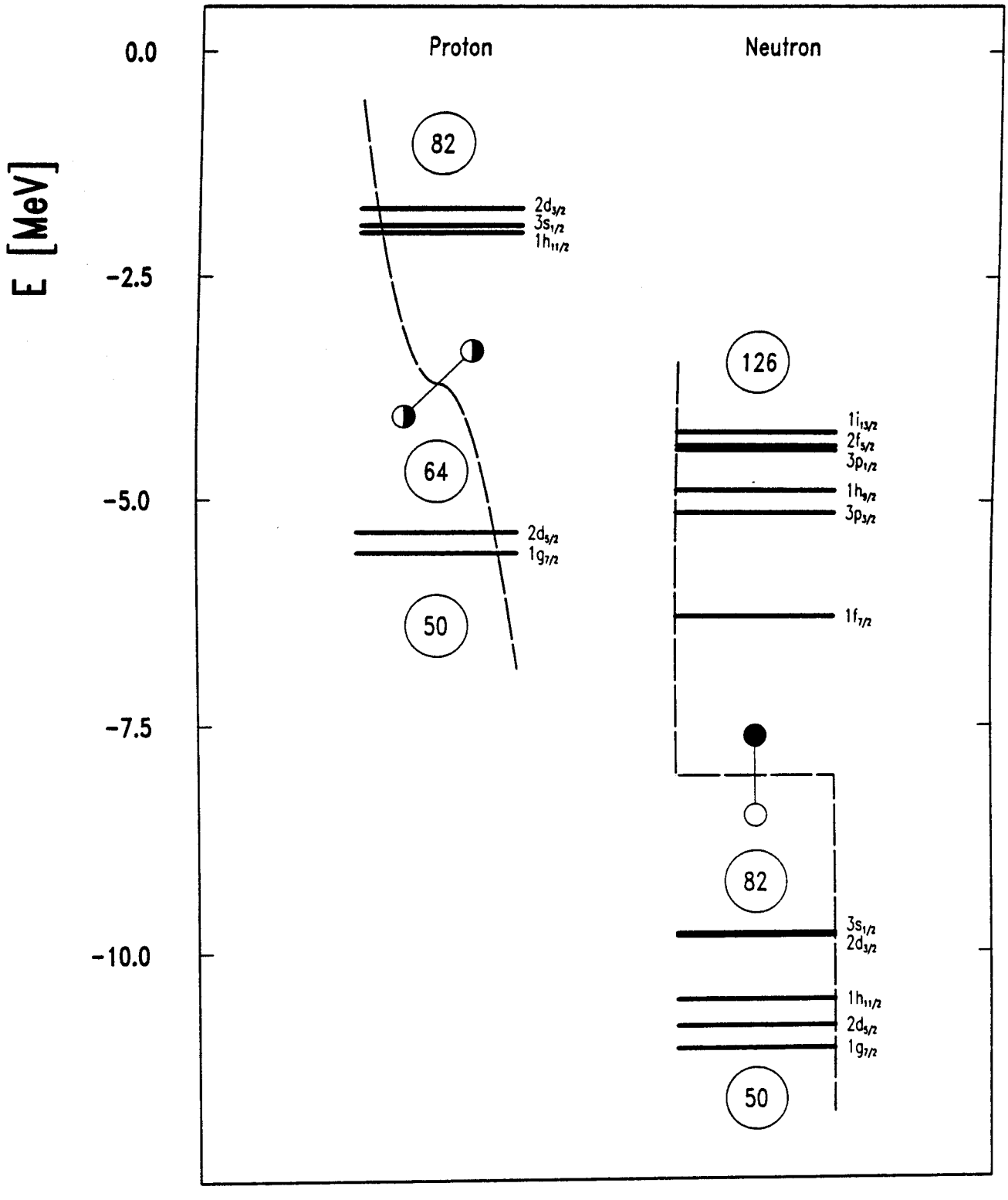
E [MeV]
0.0
-2.5
-5.0
-7.5
-10.0
Proton
Neutron
82
64
50
126
82
50
2d3/2
3s1/2
1h11/2
2d5/2
1g7/2
1i13/2
2f5/2
3p1/2
1h9/2
3p3/2
1f7/2
3s1/2
2d3/2
1h11/2
2d5/2
1g7/2

Figure 11